National Library of Canada
Canadian Theses Service
Ottawa, Canada
K1A 0N4

Bibliothèque nationale du Canada
Services des thèses canadiennes

CANADIAN THESES

THÈSES CANADIENNES

NOTICE

The quality of this microfiche is heavily dependent upon the quality of the original thesis submitted for microfilming. Every effort has been made to ensure the highest quality of reproduction possible.

If pages are missing, contact the university which granted the degree.

Some pages may have indistinct print especially if the original pages were typed with a poor typewriter ribbon or if the university sent us an inferior photocopy.

Previously copyrighted materials (journal articles, published tests, etc.) are not filmed.

Reproduction in full or in part of this film is governed by the Canadian Copyright Act, R.S.C. 1970, c. C-30. Please read the authorization forms which accompany this thesis.

AVIS

La qualité de cette microfiche dépend grandement de la qualité de la thèse soumise au microfilmage. Nous avons tout fait pour assurer une qualité supérieure de reproduction.

S'il manque des pages, veuillez communiquer avec l'université qui a conféré le grade.

La qualité d'impression de certaines pages peut laisser à désirer, surtout si les pages originales ont été dactylographiées à l'aide d'un ruban usé ou si l'université nous a fait parvenir une photocopie de qualité inférieure.

Les documents qui font déjà l'objet d'un droit d'auteur (articles de revue, examens publiés, etc.) ne sont pas microfilmés.

La reproduction, même partielle, de ce microfilm est soumise à la Loi canadienne sur le droit d'auteur, SRC 1970, c. C-30. Veuillez prendre connaissance des formules d'autorisation qui accompagnent cette thèse.

THIS DISSERTATION
HAS BEEN MICROFILMED
EXACTLY AS RECEIVED

LA THÈSE A ÉTÉ
MICROFILMÉE TELLE QUE
NOUS L'AVONS REÇUE

Canada

NL 339 (r. 86/01)

National Library of Canada
Canadian Theses Division
Ottawa, Canada
K1A 0N4

Bibliothèque nationale du Canada
Division des thèses canadiennes

0-315-24757-6

PERMISSION TO MICROFILM — AUTORISATION DE MICROFILMER

• Please print or type — Écrire en lettres moulées ou dactylographier

Full Name of Author — Nom complet de l'auteur

MYSORE, Sudhesh Malliah

Date of Birth — Date de naissance	Country of Birth — Lieu de naissance
Dec. 27, 1956	India

Permanent Address — Résidence fixe

9832-89th Avenue, Edmonton, Alberta. T6E 2S4

Title of Thesis — Titre de la thèse

Analysis and compensation of semiconductor laser nonlinearity for analog video transmission

University — Université

University of Alberta

Degree for which thesis was presented — Grade pour lequel cette thèse fut présentée

Master of Science

Year this degree conferred — Année d'obtention de ce grade	Name of Supervisor — Nom du directeur de thèse
1984	Dr.P.A.Goud Dr.C.G.Englefield

Permission is hereby granted to the NATIONAL LIBRARY OF CANADA to microfilm this thesis and to lend or sell copies of the film.

The author reserves other publication rights, and neither the thesis nor extensive extracts from it may be printed or otherwise reproduced without the author's written permission.

L'autorisation est, par la présente, accordée à la BIBLIOTHÈQUE NATIONALE DU CANADA de microfilmer cette thèse et de prêter ou de vendre des exemplaires du film.

L'auteur se réserve les autres droits de publication; ni la thèse ni de longs extraits de celle-ci ne doivent être imprimés ou autrement reproduits sans l'autorisation écrite de l'auteur.

Date	Signature
August 20, 1984	

NL-91 (4/77)

THE UNIVERSITY OF ALBERTA

ANALYSIS AND COMPENSATION OF SEMICONDUCTOR LASER NONLINEARITY FOR ANALOG VIDEO TRANSMISSION

by

© SUDHESH M. MYSORE

A THESIS

SUBMITTED TO THE FACULTY OF GRADUATE STUDIES AND RESEARCH

IN PARTIAL FULFILMENT OF THE REQUIREMENTS FOR THE DEGREE

OF MASTER OF SCIENCE

DEPARTMENT OF ELECTRICAL ENGINEERING

EDMONTON, ALBERTA

FALL, 1984

THE UNIVERSITY OF ALBERTA

RELEASE FORM

NAME OF AUTHOR SUDHESH M. MYSORE

TITLE OF THESIS ANALYSIS AND COMPENSATION OF SEMICONDUCTOR LASER NONLINEARITY FOR ANALOG VIDEO TRANSMISSION

DEGREE FOR WHICH THESIS WAS PRESENTED MASTER OF SCIENCE

YEAR THIS DEGREE GRANTED FALL, 1984

Permission is hereby granted to THE UNIVERSITY OF ALBERTA LIBRARY to reproduce single copies of this thesis and to lend or sell such copies for private, scholarly or scientific research purposes only.

The author reserves other publication rights, and neither the thesis nor extensive extracts from it may be printed or otherwise reproduced without the author's written permission.

(SIGNED) S. M. M.

PERMANENT ADDRESS:

9832 - 89 Avenue
Edmonton, Alberta
Canada T6E 2S4

DATED August 15 1984

THE UNIVERSITY OF ALBERTA

FACULTY OF GRADUATE STUDIES AND RESEARCH

The undersigned certify that they have read, and recommend to the Faculty of Graduate Studies and Research, for acceptance, a thesis entitled **ANALYSIS AND COMPENSATION OF SEMICONDUCTOR LASER NONLINEARITY FOR ANALOG VIDEO TRANSMISSION** submitted by **SUDHESH M. MYSORE** in partial fulfilment of the requirements for the degree of **MASTER OF SCIENCE.**

R.A. Bond ..... C. Y. Englefield

Supervisor

W. A. Davis .....

R. E. Burt .....

.....

.....

Date 14 August, 1984

To my wife, Geetha

ABSTRACT

Analog video transmission using laser diode transmitters is economically attractive in many short-haul applications. Examples are CATV trunk lines, where multi-channel video transmission using frequency division multiplexing is employed, and teleconferencing, remote monitoring and surveillance, where simple baseband video transmission is usually employed. However, in the 20 or more fiber-optic CATV systems presently operating in North America, a maximum of only 5 or 6 video channels per fiber is transmitted. This limit is due, in great part, to the nonlinearities associated with the use of a laser diode. As well, the picture quality in baseband transmission is degraded because of laser diode nonlinearity at low frequencies.

In this project, opto-electronic feedback compensation and adaptive predistortion techniques were employed to linearise the light-current characteristic of a laser diode. In addition, the transfer characteristics of the compensated laser diode transmitter were found and mathematical techniques involving interpolation of these characteristics by polynomial splines were used to determine the distortion characteristics of the transmitter.

The use of predistortion resulted in a reduction in the second- and third order intermodulation distortion of 15 dB and 11 dB, respectively. Furthermore, these reductions were virtually independent of frequency between 1 MHz and the upper bandwidth of the laser diode transmitter (40 MHz). The use of an adaptive technique maintains the reductions at these levels even if the slope of the laser diode characteristic varies as a result of aging or temperature changes. Employing adaptive predistortion compensation (and taking precautions to reduce distortion caused by modal noise and reflections) can increase the number of video channels that can be transmitted over a single fiber.

The use of opto-electronic feedback and adaptive predistortion simultaneously resulted in a very high degree of linearisation, but over a smaller bandwidth than was the case with predistortion. Reduction in the second- and third order intermodulation distortion of greater than 25 dB and 20 dB, respectively, were obtained for frequencies up to 11 MHz. This technique can be used to improve the picture quality when baseband video transmission is employed.

ACKNOWLEDGEMENTS

I wish to thank Dr. P.A. Goud and Dr. C.G. Englefield for their helpful advice and encouragement throughout the work. My thanks are also extended to Mr. Bert Telder for his expert technical assistance and to my friends and colleagues Rajendra Razdan, Santanu Das and other members of the Optical Communication Group for their helpful discussions and support. Finally, I wish to thank my wife, Geetha Krishnan, and my brother, Suresh, for being of invaluable help in so many ways and for assisting me with the word processing.

Table of Contents

Chapter Page

I. INTRODUCTION 1

A. Historical Background 1

B. Fiber Optic Applications and Field Trials 2

Telephony Applications 3

Video Applications 5

Integrated Distribution 9

Computers 11

Other Applications 12

C. Analog Video Transmission 12

Digital Versus Analog Transmission 12

Analog Modulation Formats 16

Multichannel Video Transmission 17

Linearity Considerations 19

D. Thesis Objectives 23

E. Thesis Organization 24

II. SEMICONDUCTOR LASERS 26

A. Historical Notes 26

B. Laser Structures 27

Homostructure Laser 27

Heterostructure Lasers 30

Double Heterostructure Stripe Lasers 31

C. Threshold Gain and Current Density 33

D. Laser modes 36

Longitudinal Modes 36

Lateral and Transverse Modes 38

E. Nonlinearity of the Light-Current Characteristic 41

Mode Competition Effects 41

Self-focusing Phenomena 42

Shifts in the Lasing Filament 43

Wide-stripe Lasers 43

Narrow-stripe Lasers 44

Gain Saturation 44

Harmonic Distortion Resulting from Junction Heating 45

F. Modulation Behavior 47

General Rate equations 48

Small Signal Modulation 49

Relaxation Oscillations 49

Frequency Response 51

III. REVIEW OF NON-LINEARITY COMPENSATION TECHNIQUES ..54

A. Preemphasis 54

B. Opto-electronic Feedback 55

C. Phase Shift Modulation 58

D. Predistortion 61

Shunt Predistortion 61

Predistortion for Differential Gain Correction 63

Predistortion for Differential Phase Correction 65

E. Quasi-Feedforward Compensation 65

F. Optical Feedforward Compensation 70

G. Adaptive Predistortion 70

H. Summary 75

IV. LASER DIODE TRANSMITTER DESIGN 77

A. Description of the Laser Diode Transmitter 77

B. Distortion Analysis 81

C. Experimental Performance 84

V. OPTO-ELECTRONIC FEEDBACK COMPENSATION 89

A. Effect of Negative Feedback on Distortion 89

B. Description of an Opto-Electronic Feedback Experiment 94

Nyquist Plot 98

Improvements in Intermodulation Distortion 100

C. An Improved Feedback Scheme 101

Nyquist Plot 105

Improvements in Intermodulation Distortion 105

D. Summary 113

VI. DETERMINATION OF LASER DIODE CHARACTERISTICS 115

A. Static Light-Current Characteristic 115

B. Dynamic Light-Current Characteristic 117

C. Summary 127

VII. ANALYSIS OF LASER DIODE DISTORTION 129

A. Single Polynomial Model 130

Formulas for Intermodulation Distortion ...130

Distortion versus Bias Current 133

B. Polynomial Spline Model 140

Formulas for Intermodulation Distortion ...140

Distortion Versus Bias Current 145

Distortion Versus Modulation Current 148

C. Summary 149

VIII. A PREDISTORTION COMPENSATION TECHNIQUE 153

A. Description of the Predistortion Technique ...153

B. Predicted Improvements in Intermodulation Distortion 157

C. Observed Improvements in Intermodulation Distortion 163

D. Summary 171

IX. AN ADAPTIVE PREDISTORTION STRATEGY 174

A. Introduction 175

Compensating for Threshold Current Changes 176

Compensating for Changes in Quantum Efficiency 178

B. Description of Adaptive Predistortion Circuitry 179

C. Experimental Results 181

D. Simultaneous Use of Adaptive Predistortion and Opto-Electronic Feedback 189

E. Summary 195

X. SUMMARY AND DISCUSSION 198

BIBLIOGRAPHY 209

APPENDIX I-IM DISTORTION VERSUS LD BIAS CURRENT 219

APPENDIX II-POLYNOMIAL SPLINE MODEL 221

APPENDIX III-IM DISTORTION OF PREDISTORTED TRANSMITTER ..222

LIST OF FIGURES

Figure		Page
2.1	(a)A broad-contact homojunction laser. (b)A double heterostructure laser. (c)An oxide insulated stripe geometry laser	28
2.2	Frequency response of laser diode.	53
3.1	Preemphasis characteristic to improve baseband linearity.	56
3.2	Phase shift modulation technique.	59
3.3	Simple shunt predistortion.	62
3.4	Differential gain compensation.	64
3.5	Differential phase compensation.	66
3.6	Quasi-feedforward compensation.	68
3.7	Optical feedforward compensation.	71
3.8	Adaptive predistortion technique.	73
4.1	Schematic diagram of the laser diode transmitter.	79
4.2	Calculated plot of the slope dIC_1/dV_{1d} as a function of IC_1.	83
4.3	Observed IM distortion as a function of modulation current.	86
4.4	Variation of $IM(f_2-f_1)$ with frequency f_1.	87
5.1	Idealized feedback configuration.	90
5.2	Block diagram of the first opto-electronic feedback scheme investigated.	95
5.3	Nyquist diagram of the first feedback amplifier.	99
5.4	Calculated and observed reductions in IM distortion as a function of frequency f_1.	102
5.5	Block diagram of the second opto-electronic feedback scheme.	104
5.6	Nyquist diagram of the second feedback amplifier.	106
5.7	IM distortions (a)without opto-electronic feedback, and (b)with opto-electronic feedback.	107
5.8	Calculated and observed reduction in IM distortion as a function of frequency f_1.	108
5.9	Variation of $\Delta IM(f_2-f_1)$ and $\Delta IM(2f_2-f_1)$ with Δf.	110
5.10	Plot of $\Delta IM(f_2-f_1)$ versus LD modulation current.	112
6.1	Static light-current characteristic of laser diode.	116
6.2	Circuit used to determine the dynamic characteristic of the laser diode.	118
6.3	The error voltage waveform for a LD modulation frequency of (a)350 kHz and (b)15 kHz.	121

6.4 Percentage deviation of the dynamic LD characteristic from that of a linear characteristic at modulation frequencies of 15 kHz and 350 kHz. 123
6.5 Static and dynamic light-current characteristics of laser diode. 124
6.6 Sublinearity of the static and dynamic light-current characteristics in the high radiance region. 125
7.1 Calculated and observed values of $IM(f_2-f_1)$ as a function of LD bias current. 135
7.2 Calculated and observed values of $IM(2f_2-f_1)$ as a function of LD bias current. 136
7.3 Observed values of IM distortions versus frequency. 138
7.4 Calculated values of $IM(f_2-f_1)$ using a polynomial spline model and the observed values. 146
7.5 Calculated values of $IM(2f_2-f_1)$ using a polynomial spline model. 147
7.6 Calculated and observed values of $IM(f_2-f_1)$ as a function of LD modulation current. 150
7.7 Calculated and observed values of $IM(2f_2-f_1)$ as a function of LD modulation current. 151
8.1 Schematic of laser diode transmitter with predistortion. 155
8.2 Calculated predistortion current $I\rho(x)$ for several values of Re. 158
8.3 Calculated laser diode current $I_d(x)$ illustrating the superlinearity due to predistortion. 159
8.4 Transfer characteristics of compensated LD transmitter for several values of Re. 161
8.5 Predicted improvements in IM distortions as a function of Re. 162
8.6 Calculated and observed values of $\Delta IM(f_2-f_1)$ due to predistortion. 164
8.7 Calculated and observed values of $\Delta IM(2f_2-f_1)$ due to predistortion. 165
8.8 Observed values of IM reductions versus LD modulation current. 167
8.9 IM distortion (a)without predistortion and (b)with predistortion. 168
8.10 Observed variations of $\Delta IM(f_2-f_1)$ and $\Delta IM(2f_2-f_1)$ with frequency f_1. 170
9.1 A linearised laser diode transmitter using adaptive predistortion. 180
9.2 Adaptive predistortion circuitry. 182
9.3 Second order IM improvement as a function of Re (a)with adaptive feedback and (b)without adaptive feedback. 185
9.4 Third order IM improvement as a function of

Re (a)with adaptive feedback and (b) without adaptive feedback. 186
9.5 IM improvements as a function of percentage variation in slope. 188
9.6 A linearised transmitter using both opto-electronic feedback and adaptive predistortion 191
9.7 Third order IM distortion (a)with no linearisation and (b)with opto-electronic feedback and adaptive predistortion. 193
9.8 IM improvements as a function of frequency when both opto-electronic feedback and adaptive predistortion are used. 194

I. INTRODUCTION

A. Historical Background

The use of optical signals for communication can be traced back to the times of antiquity. The techniques used have ranged from the primitive fire signals employed by the armies of the Roman Empire to the optical telegraph invented by C. Chappe in 1791 [1]. The optical telegraph found widespread use in Europe for more than 60 years and resulted in the development of a binary coded decimal system by A. Edelcrantz [1]. Even today signal lamps are sometimes used for Morse code communication between ships.

Just over a hundred years ago, Alexander Graham Bell experimented with the optical transmission of speech using a "photophone" [2]. The photophone did not reach commercial fruition, however, due to the absence of the necessary electro-optical technology and also due to the rapid development of radio systems. During World War II, several of the countries involved used photophones. Their development received an impetus from advances in gas and solid-state laser technology in the early 1960s. However, the transmission medium was still the atmosphere and, as in the 18th and the 19th centuries, the weather was found to be a limiting factor. Reliable transmission dictated the need for an optical waveguide.

The concept of a dielectric waveguide for the propagation of radio waves had been analysed as early as 1910 by D. Hondros and P. Debye [3]. However, the loss at optical frequencies in the available materials was far too high for application in communication systems. In 1966, K.C. Kao and G.A. Hockham [4] recognized the reason for the high loss and speculated that sufficiently low loss fibers could be produced by the use of ultra-pure glasses. They were proved correct in 1970 when F. P. Kapron et al. [5] reported a quartz fiber with an attenuation of about 20 dB/km. This has been followed by a decade of explosive development during which attenuation figures went down and bandwidths went up. In addition, the need for light sources compatible with optical fibers resulted in the rapid development of semiconductor light sources. Examples of recent achievements include fibers with a loss of less than 0.2 dB/km, laser diodes with a threshold current of a few milliamperes, and experimental systems that operate at several hundred Mbits/s over repeater spans greater than 100 km [6].

B. Fiber Optic Applications and Field Trials

The advantages and special features of fiber optics which makes it atractive in a wide range of applications are:

-Very low attenuation

-Large bandwidth/capacity

-Immunity to electromagnetic interference and crosstalk (better security)

-Immunity to lightning and electromagnetic pulses

-Potential low cost (due to abundance of silica)

-Relatively insensitive to temperature chahges

-High tensile strength

-Low weight (aircraft applications)

-Smaller bending radius than coaxial cable

-Small size (relieves congestion in ducts)

-No problem with ground loops.

Some disadvantages of optical fibers are:

-Problems with source-fiber coupling (especially with single mode fiber)

-Difficulties in cabling, splicing, and connectors

-Inability to conduct current for powering repeaters

-Radiation damage in radioactive environments.

The attractive features of fiber optics have led to its application in many different areas.

Telephony Applications

The most extensive application of fiber optics is in the telephone industry. The rapid advances in the mid 1970's set the stage for a series of field experiments and early

applications throughout Japan [7],[8], Europe [9],[10], and North America [11]-[15]. Because of the ready availability of advanced digital switching, multiplexing, and transmission technology, optical fiber systems for telephony application will use digital modulation formats almost exclusively.

The telephone transmission network can be roughly divided into three levels; the local loop plant, short haul interoffice trunks, and long distance toll trunks. Of the more than 50,000 kilometers of fiber now installed in the United States more than 20,000 km is the Western Electric Company's 44.7 Mbit/s "FT3" metropolitan (short and medium haul) telephone trunk transmission system [11].

In December 1978, for the first time in North America, service was brought into regular subscriber's homes over individual fiber optic loops connected to the telephone network in Yorkville, Ontario. The integrated fiber optic system providing voice, video, and data was installed by Northern Telecom [12].

The steady improvement in fiber performance and associated technologies has led Western Electric to develop higher capacity long-haul lightwave transmission systems for metropolitan and intercity applications. In January 1980, plans for a 90 Mbits/s "FT3C" system in the North East corridor (Boston-New York-Washington) were announced. The capacity of these FT3C installations can eventually be tripled by the use of wavelength division multiplexing (WDM)

at wavelengths of 0.825 um, 0.875 um, and 1.3 um [13]. In 1980 and 1981, a DS4 rate (274 Mbit/s) fiber optic trunking system was installed in Calgary, Alberta for Alberta Government Telephones. The 52 kilometer entrance link connecting the Calgary central office to a remote radio relay site is still the highest bit rate operational fiber optic telephone link in North America [14].

Second generation systems are now being developed that will surpass existing long-haul transmission systems in cost effectiveness, taking advantage of long wave-length single-mode optical fiber technology. A 400 Mbit/s field trial is under way with the eventual goal of utilizing Gbit/s transmission and WDM technology in order to achieve full use of single-mode fibers [15].

Video Applications

The scarcity of radio bandwidth and the high loss and cost of coaxial cables has hampered the growth of video transmission applications. The large bandwidth and low cost of fiber optics offers an ideal medium for video. Some of the principal fiber optic video applications are outlined below.

Broadcast Links

Broadcast applications typically involve only 1 or 2 TV channels and require extremely high quality performance because of the need for tandem connection through many

facilities. Video loops (VL) are used to carry network television signals from studios to the television operating centers (TOC) and to the broadcast transmitter. Video entrance links (VEL) provide connections via radio sites or satellite earth stations to the cross-country network.

Fiber optics holds the promise of overcoming the problems of high cost, poor stability and expensive maintenance that characterize coaxial and shielded pair (16 PEVL) systems for such applications. An example is the optical fiber system installed in Lake Placid for use during the Winter Olympic Games of 1980. VLs were installed between the broadcast center and the ice arena (where the ice-skating events and the championship hockey games were televised) and between the broadcast center and the stands where the opening ceremonies took place. Because of the short transmission distances involved, digital transmission, which requires costly video CODECs, was not used. Rather, the video signals were transmitted using a FM/IM (frequency modulation/intensity modulation) scheme. It is noteworthy that video signals carried on coax along a 3.2 km route (between the broadcast center and the ice arena) required manual equalization when the temperature changed; lightwave channels along the same route were unaffected by temperature [16].

CATV

Conventional community antenna television (CATV) systems have architectures similar to a tree. At the origin of the system, known as the head end, TV signals are brought in via radio or satellite. From this point multiple-channel TV signals are transmitted to remote locations in the community over trunk coaxial cables that are typically 5/8 to 1 inch in diameter with solid aluminum outer sheaths. Amplifiers are periodically required on these cables, at intervals of 2000 ft or less. Signals branch off from the trunk cables at these amplifier locations. These branches are known as feeder cables. They are typically 1/2 inch in diameter and also have a solid aluminum outer conductor. Individual subscribers are in turn fed from the feeder cables by lines known as drop cables. The drop cable is usually a flexible coaxial cable with a braided aluminum outer conductor such as the standard RG-59 cable. Up to 64 video channels can be transmitted over a cable system such as this using an VSB/FDM format.

Fiber optics is already finding applications in the trunking portion of the CATV network. The driving factor for its entry was the fact that the lower transmission losses in fibers permitted a greater area of coverage. The coverage of CATV systems is limited by the accumulation of noise from the cascaded amplifiers that drive the system. After approximately 27 to 30 amplifiers, the signal quality is rendered unsatisfactory for viewing. Use of fibers permits

the traditional 2000 ft repeater spacing to be extended to over 12,000 ft. Other benefits of using optical fibers for the trunking portion are that the cables are smaller and lighter; maintenance costs are lower due to the absence of lightning pick-up and longitudinal sheath currents; there are no problems with EMI or ground loops; and capital investment and operating costs are potentially lower. For these reasons more than 20 fiber optic CATV trunking systems have already been installed in the U.S. during the past six years [17],[18].

Over the past year fiber optics has made a strong entry into the subscriber distribution portion of CATV systems also. The advantage of using fiber in the subscriber portion is that it virtually eliminates the three biggest problems faced by CATV operators in urban areas: damage to increasingly expensive set-top converters, theft of signals by tampering with cables, and degradation of signal quality because of electromagnetic interference picked up by coaxial cables. Rather than simply replace drop cable with fiber, a new fiber distribution concept has emerged which delivers a single TV channel at a time on a switched basis upon subscriber demand. An example of such a system is the "Mini-hub system" developed by Times Fiber Communications, Inc., for use in high-rise apartments [19]. Use of the mini-hub, accessible only to the CATV company, means that the only part of the system under the customer's control is a digital keypad, which costs about one-tenth as much as

present set-top converters. The small differential cost for the optical link can be justified by the elimination of signal theft alone.

In the eighties fiber optics will penetrate further into CATV systems from both the trunk end and the subscriber distribution end. The increasing demand for more channels and two-way interactive services will serve to accelerate this trend.

Integrated Distribution

Integrated distribution of telephony, data, and video services to a large number of homes in a "wired city" is a scenario of the future communications network. The economic advantages of an integrated optical fiber system become evident considering that an optical subscriber line can replace, in the future, all the individual subscriber lines currently used for telephones, data terminal equipment, telex, teletext, and cable television. Fiber optics is ideally suited to this application because it provides a low-cost broadband medium.

Services which could be provided include:

-Telephony

-CATV

-Pay-TV

-Bidirectional videophone

-FM stereo

-Electronic mail

-Electronic funds transfer

-Facsimile

-Videotex

-Teletex

-Alarms (fire, burglar, medical)

Field trials of fiber optic broad-band integrated systems have been carried out at various places throughout the world: Yorkville (1978) [12] and Elie (1981) [20] in Canada, Berlin (1980) in West Germany [21], Higashi Ikama (1980) in Japan [22], Milton Keynes (1981) in England [23], and Biarritz (1982) in France [24],[25].

In all the field trials, analog transmission is employed for video and broadcast FM while speech and data signals are transmitted digitally using time division multiplexing (TDM). In the Japanese field trial, a baseband video signal, a voice signal and a data signal are frequency division multiplexed and converted into intensity modulated signals.

In the French trial, each subscriber is able to receive bidirectional videophone service, two simultaneous television programs, selected by the viewer out of a possible fifteen, twelve high quality FM stereo radio programs, and miscellaneous narrowband data. Video signals are transmitted using a frequency modulation format rather than by baseband modulation as this offers better protection against system nonlinearities.

In the centrally switched integrated service offered at Elie, Manitoba, each subscriber can choose two out of a possible nine TV channels, seven FM radio channels, and a number of new services such as Telidon-type videotex, teletex, data channels, and security and fire alarm. The modulation format of the video signalas is again FM/IM as in Biarritz.

In the Milton Keynes system television signals are transmitted using pulse frequency modulation (PFM), also known as "square wave FM". A pulse-frequency modulated signal is essentially a frequency modulated square-wave carrier. The carrier frequency used is 25 MHz and the peak frequency deviation is 5 MHz allowing a maximum input signal bandwidth of 10 MHz - more than sufficient for the standard 6 MHz European TV signal.

The advent of centrally switched broadband distribution will mean that TV can serve different sectors of population in small groups instead of en masse. This will promote better and more meaningful programming. There will be many new service-oriented industries arising from the wired city concept. Its introduction will allow the broadband technology to be exploited to its fullest.

Computers

EMI, ground loops, and lightning are major problems for computer systems. Fiber optics can eliminate these problems while offering increased data rates and distances. Excellent

transmission security and reduction in the space occupied by cables in mainframe installations also makes the use of fibers attractive.

Other Applications

The insulating nature of optical fibers makes them useful for telemetry and control of high voltage systems and for control links along transmission lines. Its resistance to tapping and immunity from EMI and EMP has resulted in many military applications also. It is also replacing mechanical linkages and copper wires in aircrafts; weight savings of as much as 90% can be achieved compared to conventional systems.

C. Analog Video Transmission

Digital Versus Analog Transmission

In analog video transmission, noise and nonlinear distortion accumulates at each repeater until the signal quality is rendered unsuitable for viewing. In digital transmission, on the other hand, no additional noise is introduced at a repeater, only the original quantization noise due to the analog to digital conversion exists. This means that system performance is virtually independent of length. Thus a digital format is preferred for long-haul fiber optic video transmission. However, the advantages of digital transmission are achieved at the expense of

bandwidth expansion and the requirement for complex and often costly video CODECs. For these reasons, analog modulation appears economically attractive for local TV distribution. This is especially the case with multi-channel video transmission, where multiplexing and demultiplexing costs are significantly lower for analog modulation.

The bit rate for eight bit pulse code modulation (PCM) sampled at the Nyquist rate is 68 Mbit/s for a video signal with 4.25 MHz bandwidth. It is reported, however, that to prevent undesirable color effects when reproducing large uniform areas of saturated color, the sampling frequency should be locked to a multiple of the chroma subcarrier frequency [26],[27]. Consequently the sampling rate should be three times the frequency of the color subcarrier. The bit rate for eight bit PCM sampled at three times the color subcarrier is 85.6 Mbit/s for NTSC and 106.4 Mbit/s for PAL. Digital transmission tends to concentrate on the bit rates used for telephony such as 34, 70, and 140 Mbit/s in Europe and 45 and 90 Mbit/s in North America. Hence a PCM video signal would be transmitted at a bit rate of 140 Mbit/s in Europe and 90 Mbit/s in North America.

While PCM has the advantage of requiring relatively simple A/D and D/A converters, it has the disadvantage of requiring a very high bit rate. It is generally desirable to aim at a lower bit rate by reducing the redundancy in the transmitted signal. The easiest way to reduce the redundancy in a digitally encoded TV signal is to use differential

pulse code modulation [28]-[30].

In DPCM, redundancy reduction is achieved by encoding only the difference between the current sample amplitude and a predicted amplitude value estimated from past samples. DPCM is applicable if the signal, on the average, changes only a little from sample to sample. This is true for the luminance and chrominance signals but not for the composite signal where the color subcarrier is present. This problem is overcome using a form of DPCM called n-T prediction [28].

The bit rate for five-bit DPCM of this type is 53.5 Mbit/s for NTSC and 66.5 Mbit/s for PAL. The latter figure is attractive for European systems since it can be transmitted at the 70 Mbit/s standard. In North America, however, further measures are needed to reach the DS-3 (44.7 Mbit/s) rate. The measures used are nearly always some variety of a more complex coding system called entropy coding [31]. The use of such a scheme can reduce the bit rate to 20 percent below that of five-bit DPCM or to just below 45 Mbit/s for an NTSC signal. DPCM and entropy coding both introduce quantizing errors that are signal dependent. The quality assessment of the reconstructed picture is necessarily subjective since objective measurements of the impairments introduced by coding schemes do not yet exist.

Complex coding schemes relying on reduction of frame-to frame redundancy, i.e., interframe coding, have been developed that require bit rates as low as 10 Mbit/s or lower [31]. However, they have been developed for video

telephony applications such as videophone and teleconferencing, where the picture shows the head and shoulders of a talking person who does not move too much or too fast. Such schemes cannot be used with a TV picture since it frequently changes completely from one moment to the next. Achieving bit rates less than 45 Mbit/s with broadcast TV signals will therefore require redundancy reduction within a frame, i.e., intraframe coding. These schemes are extremely expensive and picture quality assessments have yet to be made.

Consider a short-haul CATV trunk line that is required to carry 20 or more TV signals. If digital transmission at the FT3C (90 Mbit/s) rate is used then 10 or more fibers will be required. It has been assumed that some form of entropy coding has been used so that two TV signals can be multiplexed on each fiber. Each of these fibers will also require complex CODECs and multiplexers at the transmit and receive ends. It may be more economically attractive in this situation to use analog transmission as this would eliminate the need for the costly CODECs, reduce the number of fibers required, and reduce the cost of multiplexing the signals.

Analog transmission data is also required in a variety of demanding telemetry and sensing systems where digitization is not practicable due to environmental, cost, or bandwidth requirements [32]. An example is the transmission of diagnostic data from a nuclear test site. Some of the data signals require bandwidths so high (from

hundreds of megahertz to over a gigahertz) that the signals cannot be digitized even by the fastest A/D converters available unless complex parallel sampling techniques are used.

Analog Modulation Formats

Three basic modulation formats, all based on composite color TV signals, have been examined in recent publications on single and multi-channel analog video transmission [33]-[43].

The two simplest schemes are baseband (BB) and vestigial sideband (VSB) modulation. Direct intensity modulation with a composite baseband signal (BB/IM) requires the least amount of bandwidth. However, baseband transmission is susceptible to nonlinear distortion and to interference from a variety of sources. In addition, the baseband scheme does not allow for the multiplexing of more than one video signal.

Intensity modulation with a conventional vestigial sideband TV signal (VSB/IM) is a direct copy of the formats used now for TV distribution by radio and by coaxial cable. As a result, it is very convenient for CATV applications. Although it requires a slightly larger bandwidth, it is also more tolerant of nonlinearities than baseband transmission and it allows for the frequency division multiplexing of many channels. A disadvantage of the VSB format is that, because of the picture carrier, it has a lower SNR than does

baseband modulation. In fact, it can be shown [28] that

$$\text{SNR (BB)} = \text{SNR (VSB)} + 12 \text{ dB} \qquad (1.1)$$

which shows that a baseband signal utilizes a channel 12 dB better than does a VSB signal.

The most attractive modulation format is frequency modulation (FM/IM). Frequency modulation offers very high signal to noise ratios and the greatest tolerance of nonlinear distortion, but at the expense of increased bandwidth. The improvement in SNR offered by FM depends on the peak frequency deviation. It can be shown [44] that

$$\text{SNR (FM)} = \text{SNR (BB)} + 20.6\text{dB} + 20\log(\Delta F/B) \qquad (1.2)$$

where ΔF is the peak frequency deviation and B is the video bandwidth (4.2 MHz). Thus a peak frequency deviation of 4 MHz (8 MHz) will result in a 20 dB (26 dB) advantage in SNR over baseband modulation.

Multichannel Video Transmission

In multichannel video transmission using VSB, care must be taken to design an optimum frequency band allocation so as to minimize the effect of intermodulation distortion [45]. Multichannel transmission by FM-FDM/IM, however, has been shown to be far less sensitive to intermodulation distortion [42],[43] and has been realized in commercial

CATV systems [18].

In a Bell Northern Research experiment, a 1.3 um LED was used to transmit three video channels by FM-FDM/IM over a 9.5 km long optical fiber. It was reported that no discernible degradation in the video quality was observed even when the LED was modulated at 100% and the second- and third order harmonic distortion was -22 and -31 dB, respectively [42]. The three video channels were modulated by carrier frequencies of 30, 50, and 70 MHz, respectively and the peak frequency deviation was 8 MHz. It is usually more advantageous to use laser diodes rather than LEDs in multichannel analog video transmission. This is because laser diodes have a much larger modulation bandwidth and couple at least an order of magnitude more light into an optical fiber than LEDs. The latter point is particularly important for multichannel analog transmission since the number of channels that can be transmitted is limited by the available optical power [30],[34]. This is so since, as the number of channels increases, the signal power per channel decreases while the noise remains unchanged. Hence the SNR decreases by 6 dB if the number of channels is doubled.

A formula for the SNR at the output of an avalanche photodiode (APD) receiver has been derived for the case of N standard NTSC TV signals transmitted by VSB-FDM/IM [34]. The only noise sources considered are the quantum noise, the dark current noise and the thermal noise in the optical receiver. The expression for the signal to noise ratio is of

the form

$$SNR = a(P/N)^2/(bP+c) \qquad (1.3)$$

where N is the number of TV channels, P is the average received optical power and a, b, and c are receiver parameters (such as load resistance, APD dark current, avalanche gain, etc.). The SNR is inversely proportional to the square of the number of multiplexed channels and hence sets a limit to the number of channels that can be transmitted.

For a fixed value of SNR, it can be seen from equation (1.3) that the received optical power must increase as the number of transmitted channels increases. By assuming typical values for the receiver parameters and the use of a laser diode with a 1 mW light output, the maximum repeaterless transmission distance can be calculated. These calculations show that, for the minimum Department of Communication Standards defined in Broadcast Procedure-23 for CATV systems, more than 20 channels can be delivered over a distance of 8 km [34].

Linearity Considerations

The fiber trunks in the 20 or more fiber-optic CATV systems operating in North America presently can transmit a maximum of only 5 or 6 video channels per fiber [17]. Thus up to 10 fibers and their associated laser diodes and

photodetectors are required to replace a single coaxial cable capable of transmitting up to 64 video channels. The limit of 5-6 video channels per fiber is much less than that imposed by SNR considerations only. Rather, this limit is due to modal noise, modal distortion, distortion due to reflections, and the nonlinearity of the laser diode (LD) itself. Eliminating or minimizing these effects will mean that more video channels will be transmitted over future fiber trunks.

Modal noise is the random amplitude modulation of an optical signal as it passes a point of speckle-selective loss. Modal distortion arises in analog systems because current modulation of a LD also modulates the emission frequency. This effect modulates the mode-selective loss, resulting in nonlinear distortion [46]. Both these problems can be virtually eliminated by the use of single-mode fiber or the use of a less coherent, multi-mode laser diode [47].

When part of the LD light output is reflected back from the fiber end face, coupling lenses, or connectors, the LD output begins to fluctuate at frequencies that are multiples of the reciprocal round trip time. This degrades the linearity of the LD [48]. The use of an optical isolator between the LD snd the fiber can reduce feedback to a tolerable level [49].

The nonlinearity in the light-current characteristic of laser diodes is a limiting factor in the number of video channels that can be transmitted by analog multiplex

systems. During the last decade, improved fabrication techniques, device structures and geometries have had success in producing laser diodes with linear light responses [50]-[54]. Highly linear laser diodes were used to achieve intermodulation distortion less than -65 dB in a recent study on multichannel TV transmission [35]. It was reported, however, that of the many lasers tested only a small number were found which exhibited sufficiently linear light-current characteristics to be useful for multi-channel analog TV transmission.

As a result, many circuit techniques that compensate for the intrinsic nonlinearity of the light sources have been investigated in the last several years [55]-[67]. These techniques include the use of preemphasis, opto-electronic feedback, phase-shift modulation, predistortion, and various forms of feedforward. Only a few of these linearization techniques are feasible for use with laser diodess due to such factors as cost, the difficulty of obtaining two well matched LDs, or the sensitivity of the LD characteristic to temperature and aging.

The linearity of a laser diode and associated driver circuitry is most easily determined by measurement of the intermodulation distortion. This is easily done by applying a two-tone signal to the LD driver and measuring the levels of the intermodulation products at the output of the optical receiver on a spectrum analyzer. In general, it is not possible to characterize a nonlinear device using a two-tone

test signal. Rather, a test signal possessing a spectrum covering the entire bandwidth of interest should be used. However, as will be discussed in Section 2.6, a laser diode possesses a simple nonlinearity without memory for frequencies up to approximately 200 MHz. The nonlinearity of such a device is frequency independent and a two-tone test can indeed be used to characterize the nonlinearity over this range of frequencies. The BP-23 standard sets -53 dB as the allowable level of intermodulation distortion for a CATV system.

In analog video transmission, the effect of nonlinearities can also be described in terms of the "differential gain" and "differential phase" of the system. The differential gain (DG) is defined as the variation in amplitude of the 3.58 MHz color subcarrier when the amplitude of the luminance signal is varied from blanking to reference-white level. The differential phase (DP) is defined as the variation in phase of the color subcarrier as the level of the luminance signal is varied from blanking to reference white. The effect of differential gain is a distortion in the color saturation of the picture whereas differential phase results in a distortion in the hue of the colors. Harmonic distortion can be derived directly from DG and DP values whereas only the worst values of DG and DP can be found if the harmonic distortion levels are known [68]. Performance requirements for CATV trunks are 9% for DG and 2° for DP.

D. Thesis Objectives

The main objective of this thesis is to demonstrate that compensation techniques, namely opto-electronic feedback and adaptive predistortion, can be employed to linearise the light-current characteristic of a laser diode over bandwidths sufficiently large to make them useful for analog video transmission. In addition, the dynamic light-current characteristic of the laser diode is to be found and used to characterize the distortion properties of the laser diode.

More explicitly, the goals are:

1. To construct a highly linear laser diode driver.
2. To determine the dynamic light-current characteristic of a LD.
3. To determine the distortion characteristics of the LD by performing a polynomial-spline interpolation of the LD dynamic characteristic.
4. To linearise the LD transmitter using opto-electronic feedback at video frequencies.
5. To demonstrate a novel adaptive predistortion scheme to achieve linearisation over large bandwidths.
6. To use the interpolation techniques developed to predict the effectiveness of the adaptive predistortion technique.

E. Thesis Organization

The remaining chapters of the thesis are organized as follows:

Chapter II is a review of semiconductor lasers. The areas of laser modes, rate equations, LD nonlinearity, and LD modulation are briefly examined.

Chapter III is a review of the many compensation techniques that have been studied over the past several years with the aim of linearising light sources.

Chapter IV deals with the construction of a very linear analog LD driver.

Chapter V deals with the result of an opto-electronic feedback experiment at video frequencies. Nyquist diagrams are used to predict the stability of the feedback amplifiers.

In Chapter VI, the static and dynamic light-current characteristics of the laser diode are found.

In Chapter VII, the dynamic LD characteristic is approximated by a polynomial-spline model. This model is used to calculate the IM distortion as a function of the LD bias current and the LD modulation current. These values are then compared with the measured IM distortion.

Chapter VIII describes a novel predistortion technique. The effect of predistortion is to linearise the transfer characteristic of the LD transmitter over a large bandwidth. By using the polynomial-spline model, the improvements in IM distortion are calculated. These are then compared with the

actual improvements in distortion.

In Chapter IX, the predistortion technique of the previous chapter is made adaptive. Through the use of a low frequency feedback loop, changes in the slope of the LD light-current characteristic are adaptively compensated for by the predistortion circuitry. In addition, both opto-electronic feedback and adaptive predistortion are used together to achieve very large reductions in IM distortion.

Chapter X presents an overall summary and discussion of the thesis.

II. SEMICONDUCTOR LASERS

From a humble beginning as a simple p-n junction two decades ago, the semiconductor laser has evolved into a variety of sophisticated opto-electronic devices adapted for a myriad of exciting applications. The tremendous amount of research carried out to-date has led to a more thorough understanding of quantum electronics and has also resulted in advances in semiconductor technology. Semiconductor laser technology now shows signs of approaching maturity. While more research than ever is being done in this area, new papers deal more with improved technological realizations than with new fundamental insights.

The area of semiconductor laser devices in optical communication has been extensively dealt with in many books [69]-[74]. In this chapter a necessarily brief review of fundamental concepts in this area is presented.

A. Historical Notes

The concept of obtaining stimulated emission of photons by recombination of carriers across a p-n junction was first suggested by Basov *et al.* [75] in 1961. A year later, coherent light emission from GaAs p-n junctions was demonstrated by several groups in the U.S. Only two years before this the first gas laser had been demonstrated, and a year previous to this the first laser of any type - a ruby laser had been constructed. Despite having its origin at

around the same time as other types of lasers, semiconductor lasers are only now approaching maturity after a relatively long period of development.

For a given degree of inversion, stimulated emission in semiconductors is more intense than other laser materials. The early broad-contact p-n junctions, called homostructures, required large currents and could not be operated continuously at room temperature. These were replaced in 1969 by heterostructures containing several semiconductor layers of different compositions. This had the revolutionary impact of transforming the semiconductor laser from a laboratory device operating at cryogenic temperatures into a practical and efficient device capable of operating CW at room temperature. Another significant impetus to semiconductor laser technology was the advent of fiber optics in the 1970's and the realization that the semiconductor laser could be used as a high speed optical source in fiber optic communication systems.

B. Laser Structures

Homostructure Laser

The first laser structure that was fabricated was the broad-contact laser such as the one shown in Fig. 2.1(a). It consisted of a rectangular chip of GaAs into which a planar p-n junction was diffused. Such lasers are easy to fabricate and are still used today for rapid evaluation of crystal

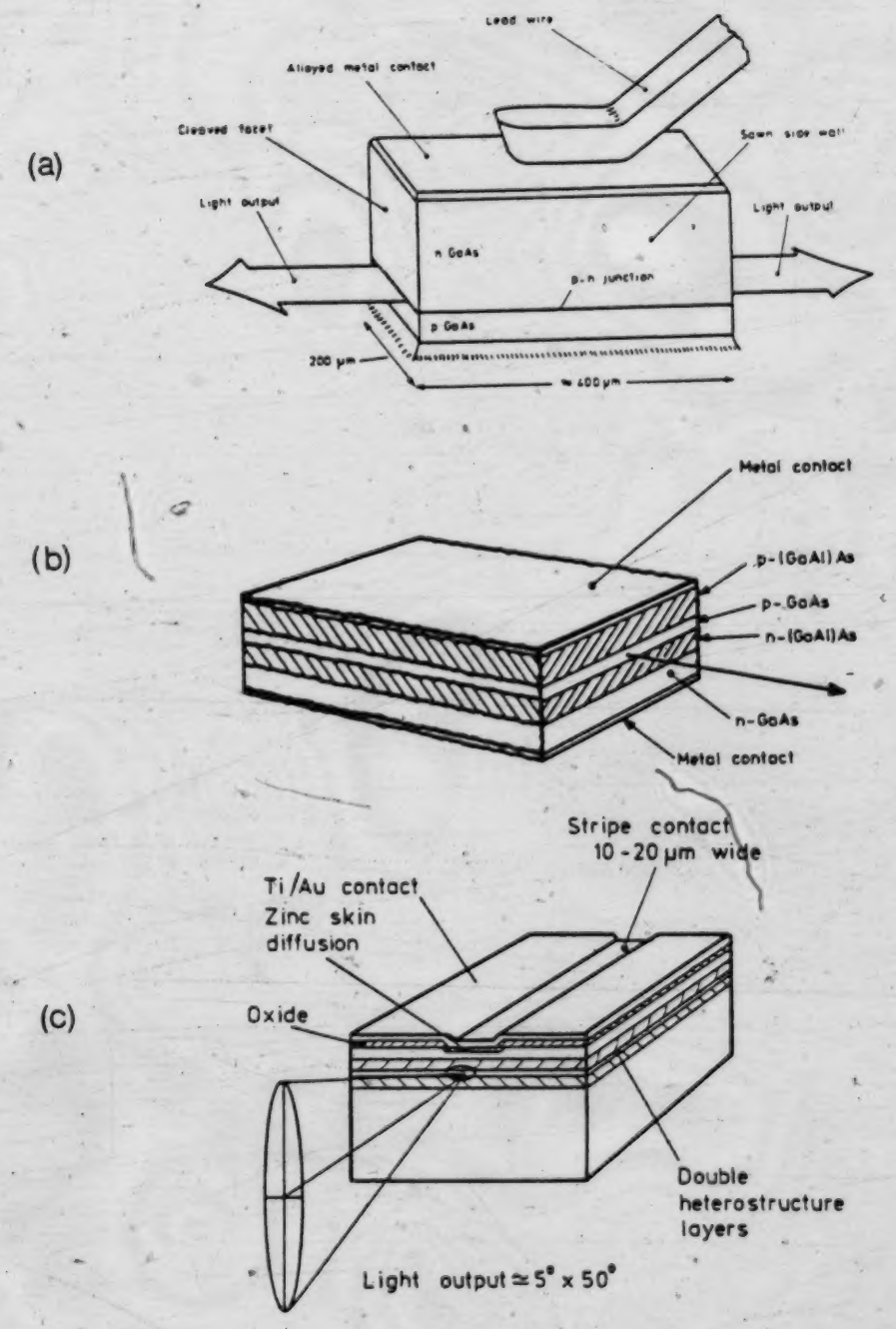

Figure 2.1 (a)A broad-contact homojunction laser. (b)A double heterostructure laser. (c)An oxide insulated stripe geometry laser.

quality.

The passage of current through the diode causes minority carriers, particularly electrons, to be injected across the p-n junction into a region approximately a diffusion length thick where they combine with the majority carriers. Stimulated emission starts to occur in this region when the current density is raised to a sufficient level. The cleaved end faces of the chip are partially reflective due to the high refractive index of GaAs and they form a Fabry-Perot resonator. This resonator is excited into laser oscillation, approximately over the thickness of the diffusion region, when the current is raised above a certain value known as "threshold". As a consequence of the high rate of stimulated emission possible in semiconductors, the length of the Fabry-Perot resonator may be made much smaller than in other types of lasers; a length between 200μm and 1000μm being typical.

The injected carrier density needed to reach threshold for laser action is about $10^{18}/cm^3$. A disadvantage of the broad-contact laser is its very high threshold current density, lying in the range 50-100 kA/cm^2 at room temperature. This translates into a threshold current of more than 10 A for a typical broad-contact laser. The required current density is so high (a) because the inversion region is not precisely defined but tails away in the direction in which carriers diffuse, and (b) because the stimulated light is not satisfactorily confined to the

region where inversion is created.

Heterostructure Lasers

Both of the above shortcomings of the homojunction laser were overcome by incorporating into the device, on each side of the GaAs inversion layer, an additional layer composed of a semiconductor with a higher band-gap as shown in Fig. 2.1(b). Such multilayer laser structures are called heterostructures.

These structures provide means of confining both the injected carriers and light within the active layer. The injected carriers are confined by the potential barriers that exist at the higher band-gap interface and the light is confined by the waveguide formed by the higher refractive index of the lower band-gap layer. The inverse relation between band-gap and refractive index is observed in most of the III/V mixed semiconductors. The specific advantages of the heterostructure are (a) that an optical waveguide is created, (b) that the active region is made very thin, and (c) that the carrier concentration is much more uniform. The development of heterostructure lasers led to very large reductions in the threshold current densities at room temperature; a value as low as 1 kA/cm^3 is now common.

Various heterostructure geometries have been developed for optimizing different aspects of laser performance. By varying the number and dimensions of the different layers it is possible to obtain, for example, either high peak-power,

low threshold current, reduced divergence of the optical output, or better mode stability.

Double Heterostructure Stripe Lasers

Of all the heterostructure geometries, the one best suited for optical communication is the double heterostructure stripe laser. In stripe lasers the injected carriers and light are confined not only in the direction perpendicular to the junction (in the 'transverse' direction) but also in the plane of the junction (in the 'lateral' direction). This is done by confining the current to a narrow stripe aligned along the axis of the laser. A simple oxide insulating stripe laser is shown in Fig. 2.1(c). A narrow stripe opening is etched into an insulating silicon dioxide layer so that the metal contact is restricted to this area. Therefore lateral confinement of the light and injected carriers is obtained.

A stripe geometry laser is advantageous for the following reasons:

1) By making the stripe width less than the fiber core diameter, good coupling of the radiation into optical fibers can be obtained.

2) Threshold current is decreased due to the smaller volume of the active region.

3) The number of permitted lateral modes can be controlled.

4) Single filament operation and stable fundamental lateral mode emission can be obtained by making the stripe widths less than 15 μm.

5) Elimination of most of the junction perimeter from the surface results in a decreased degradation rate.

6) The thermal resistance of the diode is reduced because the active region is embedded in a larger inactive semiconductor medium.

7) A smaller active diode area makes it easier to obtain a reasonably defect-free area.

A disadvantage of the stripe geometry laser is that its power output is less than that of broad-contact lasers because of the smaller volume of the active region. Still, power output of approximately 10 mW can be obtained.

The past few years have seen the development of a large number of stripe geometry structures. A few of these are the mesa stripe, the buried heterostructure stripe, the hetero-isolation stripe, the striped substrate, and the Zn-diffused planar stripe lasers. All of these have threshold currents of less than approximately 100 mA and can be operated CW at room temperature. The purpose of many of these special fabrication processes is to improve the linearity of the light-current characteristics.

C. Threshold Gain and Current Density

Let "g" represent the optical gain per cm provided by stimulated emission in the inverted region of the semiconductor. The photon flux per unit area, F, then grows exponentially as the optical wavefront travels axially along the laser:

$$F(z) = F_0 \exp(gz) \tag{2.1}$$

where z is in the direction of propagation.

The gain depends on the degree of population inversion in the active region, which in turn depends on the value of the injected current density, J. In general, there is no simple relation between gain and injected current density. However, in the lightly doped material used in double heterostructure lasers it is observed that there is a superlinear dependence of gain on current at very low values of current density and a sublinear dependence at very high values of current density. For current densities between these extremes the gain is found to vary linearly with the current density. Over a considerable range of gain (from 20 to 500 cm $^{-1}$)this relationship is of the form

$$g = A(J - J_0) \tag{2.2}$$

where the current intercept J_0 and the gradient A depend on temperature. J_0 is the current density at which the gain

becomes positive and varies approximately with temperature as $T^{3/2}$. The gradient A is of the order of 0.045 cm/A at room temperature and varies with temperature approximately as T^{-1}.

The gain increases with increasing current density until a point is reached when it is sufficient to cancel out the optical loss due to such processes as scattering, diffraction, and free-carrier absorption. At this point laser oscillation begins. Let α denote the optical loss per cm. Then the condition that the round-trip optical gain due to stimulated emission be equal to the fractional loss of energy is expressed by the equation

$$\exp(2gL) = (1/r_1r_2)\exp(2\alpha L) \tag{2.3}$$

where L is the axial length of the laser cavity and r_1 and r_2 are the reflectivities of the end mirrors.

The threshold gain g_t is therefore given by

$$g_t = \alpha + (1/2L)\ln(1/r_1r_2) \tag{2.4}$$

The reflectivity for normal incidence of a plane wave on a dielectric-air interface is given by

$$r_1 = r_2 = (n-1)/(n+1) \tag{2.5}$$

where n, the refractive index of GaAs, is equal to 3.5. For

a laser of length L = 300μm, for example, the loss due to the reflectivities of the mirrors is approximately 20cm^{-1}. In addition, the absorption loss in GaAs has a value of about 10cm^{-1}. Therefore the threshold gain in this example is approximately 30cm^{-1}.

The threshold gain g_t usually lies in the region where the gain-current relationship is linear (i.e., between 20 and 500 cm^{-}). Hence the threshold current density J_t can be obtained from equations (2.2) and (2.4):

$$J_t = J_0 + (1/A)[\alpha + (1/2L)\ln(1/r_1r_2)] \qquad (2.6)$$

The threshold current J_t is strongly dependent on temperature because of the temperature dependence of the gain-current relationship. It is found empirically that the threshold current density of many laser diodes increases exponentially with temperature

$$J_t = J_{t0} \exp(T/T_0) \qquad (2.7)$$

where the value of T_0 and the range of validity of the equation varies. The temperature coefficient of the threshold current density can be found by differentiating equation (2.7) with respect to temperature:

$$(1/dT)(dJ_t/J_t) = T_0^{-1} \qquad (2.8)$$

The value of T_0 has been observed to lie in the range from 40° to 200° K. The temperature coefficient of the threshold current thus lies between 0.5%/°K and 2.5%/°K.

D. Laser modes

Longitudinal Modes

Below threshold, a semiconductor laser has a broad spontaneous emission spectrum with a width of 30-40 nm. This is because the recombinations occur between holes and electrons having a spread of energies. Above threshold, however, the spectral width becomes less than 3 nm. This is due to the discrimination exerted by the gain spectrum (width about 40 nm). The gain spectrum exhibits a sharp peak so that only for wavelengths in a narrow spectral region (width about 3 nm) will the optical gain be large enough for lasing to occur. In addition, only discrete wavelengths in the region will satisfy the condition for laser oscillation. This condition is that an integral number of half-wavelengths must fit in the laser cavity:

$$(\lambda/2n)q = L \tag{2.9}$$

where q is an integer. For $\lambda = 0.85\mu m$, $n = 3.5$, and $L = 300\mu m$, q has a value of approximately 2470. When q changes by 1, another wavelength at which laser oscillation can occur is found by using equation (2.9). The spacing between

two adjacent permitted wavelengths is found by differentiating equation (2.9)

$$dq = (2L/\lambda)\,[(dn/d\lambda) - (n/\lambda)]\,d\lambda \qquad (2.10)$$

The spacing between adjacent modes, $d\lambda$, is found by taking $dq = 1$ in equation (2.10):

$$d\lambda = -\lambda^2/[2L(n - \lambda\, dn/d\lambda)] \qquad (2.11)$$

For the same values as in the previous example, the mode spacing is found to be 0.34 nm. Therefore a laser oscillator having a cavity length L much larger than the emission wavelength operates in a large number of propagating modes, each having a slightly different wavelength. These are called the *longitudinal modes* of the laser.

Since the spectral width of the region where lasing can occur is about 3 nm and the mode spacing is between 0.2 and 0.3 nm, a typical multi-longitudinal mode semiconductor laser will emit a central line surrounded by up to a dozen other spectral lines. For long distance communication at very high bit rates a semiconductor laser with a single mode emission spectra is desired to minimize pulse spreading due to material dispersion in the fiber.

Several techniques for obtaining single longitudinal mode lasers have been devised [76]. In the simplest of these the cavity length is reduced to 50μm, about one sixth the

usual length. From equation (2.11) it can be seen that the effect of this is to increase the mode spacing to about 2 nm. Since the spectral width of the gain spectrum is roughly of the same magnitude, the result is that the laser oscillates in a single longitudinal mode. The spectral width of a mode is determined by the Q value of the resonator. It can be shown that the linewidth is inversely proportional to the power output in the mode and is less than 0.1 nm for a typical singlemode laser of this type.

Much smaller linewidths can be obtained from other types of single mode lasers. *Coupled-cavity lasers* have two laser cavities; laser oscillation occurs at only that wavelength which can resonate in both cavities. In *injection locked lasers*, a multimode laser is forced to oscillate in a single longitudinal mode by using a single wavelength source as an external driver. In the *frequency selective feedback* approach, exceedingly small linewidths are obtained by incorporating a diffraction grating somewhere in the light path. Examples of lasers using this technique are the distributed feedback laser and the distributed Bragg reflector laser.

Lateral and Transverse Modes

A three dimensional rectangular optical resonator can, in general, support a large number of resonant modes. These modes can be indexed in terms of the number of complete half wave periods existing in the three spatial directions. The

number of half wave periods in a dielectric waveguide resonator is non-integral and hence the index is conventionally taken as the nearest integer below the actual value. Thus each mode can be indexed by a three-index code of the form mnq where q applies in the axial direction, m applies in the lateral direction (perpendicular to the junction plane), and n applies to the transverse direction (perpendicular to the other two directions).

The longitudinal mode number q is large (about 2470) as mentioned earlier but m and n may have values from zero upwards. A mode for which m is equal to zero is called a *fundamental lateral mode*; similarly, a mode for which n is equal to zero is called a *fundamental transverse mode*.

The far-field radiation pattern of a fundamental lateral mode consists of a single lobe in the direction perpendicular to the junction. Higher order lateral modes result in a far-field pattern with multiple lobes which are undesirable for fiber coupling, Therefore it is desired that only the fundamental lateral mode is excited. This is normally done by restricting the thickness of the laser junction to a size where only one half-period of the wave can be accomodated. This thickness lies in the range 0.5-2μm, depending on the properties of the heterostructure waveguide.

In the transverse direction, the sides of the laser diode are normally nonreflective which favors the excitation of the fundamental transverse mode only. However, there is

usually some weak form of optical confinement at the sides; hence, in practice, lasers wider than 20-30μm exhibit low order transverse modes(n>0) with thresholds not much higher than that of the fundamental mode (n = 0). Thus, while fundamental lateral mode operation may be obtained near threshold, higher order modes may be generated with increasing current. These higher order transverse modes exhibit multi-lobed far-field patterns in the direction parallel to the junction.

The higher order transverse modes are undesirable not only because they make coupling into fibers difficult but also because mode competition effects with increasing current results in nonlinearity in the light-current characteristic. Single transverse mode laser operation can be obtained by making the difference between the propagation losses of the fundamental and higher order modes as large as possible. A simple way to do this is to restrict the stripe width to very small values of 1-2μm, although this is at the expense of a lower power output from the device. Another approach is to incorporate regions in the device that produce a greater absorption loss for higher order transverse modes than for the fundamental one. Schemes involving buried channels [77], constricted active region thickness [78], and angled contacts [79] have been proposed for this purpose.

E. Nonlinearity of the Light-Current Characteristic

Many papers have dealt with the nonlinearity of the light/current characteristics of stripe lasers and techniques to improve the linearity [50]-[54],[80]-[82]. It has generally been found that the light/current characteristics of stripe lasers beyond threshold are nonlinear. The nonlinearity is greatest for stripe widths between 10 and 20μm. A variety of light/current nonlinearities are found in this range. In most cases, some form of a "kink" appears at an output level of between 2 and 10 mW. This consists of a point of inflection in the light/current curve where the output may temporarily level off or even fall. Kinks are caused by mode competition effects, the formation of lasing filaments due to self-focusing, and shifts in the filament away from the center of the stripe.

Mode Competition Effects

In an ideal laser, the injected carrier concentration is clamped at its threshold value for laser diode currents larger than the threshold current. Consequently, all the current that exceeds the threshold level produces stimulated emission. The external quantum efficiency η, which is the ratio of the increase in emitted photons to the increase in injected electrons, is thus constant above the threshold and the light/current curve exhibits a constant slope in this region.

It is observed, however, that the excitation of a higher order transverse mode with increasing laser diode current can be accompanied by an inflection point on the light/current characteristic. In the neighbourhood of the inflection point, the slope is observed to first decrease and then increase again. The cause of the decrease in slope is the gradual saturation in the emission of the fundamental mode in a current range still below the threshold of the higher order mode. As the higher order mode "turns on" and becomes dominant, the slope increases once again. Accompanying the mode change is an increase in noise in the optical output; such noise enhancement is observed whenever threshold is reached by any mode.

Self-focusing Phenomena

A different type of nonlinearity, where the slope first increases and then decreases, is caused by self-focusing of the laser beam. Self-focusing is a phenomena in which the lasing beam interacts with the medium through which it propagates in such a way as to provide its own optical waveguide. This process results in the formation of a lasing filament contained in the self -induced dielectric waveguide. As the current is increased, the optical guiding becomes stronger and the filament contracts in width. The effect of this self-focusing phenomenon on the light-current curve is to increase the slope in the current range over which the focusing is first initiated, followed by a region

of decreased slope where the filament narrows and the spontaneous output increases.

Shifts in the Lasing Filament

Yet another type of nonlinearity results if the lasing filament is displaced from the center of the stripe. Such displacements can occur if the gain profile becomes asymmetric about the center of the laser diode. Such a shift is accompanied by a saturation or even a dip, in the light-current characteristic because of the deterioration in the coupling between the lasing filament and the injected carriers.

Wide-stripe Lasers

The nonlinearity of the light/current characteristic is strongly dependent on the width of the stripe. As the width of the laser is increased beyond 25-35 μm the kinks straighten out and eventually disappear. This is because many transverse modes are excited thus producing a smooth transition from one mode to the next. However, the multi-lobed far-field pattern of such a wide-stripe laser makes it unsuitable for fiber optic communication.

Stripe lasers with stripe widths between 10 and 20 μm are especially likely to have kinks in their light-current characteristic. This is probably because over this range of widths the lasing mode switches from being gain-guided to being self-focused and small changes in parameters can have

a large effect on the laser behavior.

Narrow-stripe Lasers

It has been observed, however, that reducing the stripe width to 8μm or less prevents the appearance of kinks over the normal operating range of current [83]. The power level at which the first kink occurs increases rapidly as the stripe is narrowed, from around 2 mW at 10μm width to over 100 mW at 2μm width.

Gain Saturation

Laser diodes with a kink-free light/current characteristic and operating only in the fundamental lateral and transverse modes are now commonly available. Although the characteristics are kink-free, this does not mean that they are completely free of nonlinearities. In fact, some degree of saturation in the power output is always seen at higher current levels. Since the optical intensity is greatest at the ends of the laser, the stimulated emission is also greatest at these points, and the higher recombination rate reduces the injected carrier concentration and the optical gain. Saturation sets in and eventually, at sufficiently high powers, the saturation becomes complete and the gain adjusts itself so that the stimulated emission rate is everywhere equal to the carrier injection rate. Light is generated uniformly throughout the the bulk of the laser rather than more strongly near the end

faces as is the case just above the threshold.

This results in a lowering of the differential quantum efficiency since the light, on the average, suffers optical absorption over a greater length before it exits from the end faces. As a result, the light/current characteristic of even a relatively linear laser diode will have some degree of sublinearity in the high radiance region.

The mechanisms contributing to harmonic distortion in LEDs have been investigated theoretically in detail [83]. Such is not the case with semiconductor lasers. However, the distortion properties of laser diodes have been predicted to a certain degree through the numerical solution of the rate equations [84]-[86]. In these techniques, time-varying quantities in the rate equations are replaced by their Fourier series representation resulting in a infinite set of simultaneous differential equations. These equations are then solved using iterative methods.

Harmonic Distortion Resulting from Junction Heating

Modulation at low frequencies can result in thermally induced nonlinearities. Assuming no other nonlinearity causing mechanisms in the laser diode, the relationship between the output power P and the drive current I above threshold is given by

$$P = (\eta h\nu/e)\,(I-I_t) \qquad (2.12)$$

where $h\nu$ is the photon energy, e is the electron charge, η is the external differential quantum efficiency, and I_t the threshold current. Although the power-current relationship seems perfectly linear, nonlinearities result when junction heating causes the value of I_t to become time dependent. The threshold current as a function of the temperature change ΔT is given by

$$I_t = I_{t,0} \exp(\Delta T/T_0) \tag{2.13}$$

for some constant T_0. The temperature rise ΔT above the heat sink temperature is given by

$$\Delta T = K(VI + RI^2) \tag{2.14}$$

where K is the thermal resistance, V is the junction voltage, and R is the series resistance of the diode.

The power-current relationship is thus given by

$$P = (\eta h\nu) \left[I - I_{t,0} \exp[K(VI+RI^2)/T_0] \right] \tag{2.15}$$

For a sinusoidal drive current equation (2.15) can be expanded in a Fourier series to give the harmonic components in the power output. The amount of distortion present depends on the frequency of the driving current. A major role is played by the thermal time constant τ

$$\tau = KC \qquad (2.16)$$

where C is the heat capacity which can be estimated from the volume of the active region and the specific heat capacity of the material. Typical diodes have thermal time constants of about a microsecond. The characteristic frequency of the effects of junction heating is given by

$$f_o = (2\pi\tau)^{-1} \qquad (2.17)$$

This frequency is on the order of a megahertz. For modulation frequencies below f_o, the period of the driving current signal equals or exceeds the thermal time constant and there is significant temperature fluctuation of the active region. For modulation frequencies above f_o, the temperature fluctuations are insignificant and so is the nonlinearity due to junction heating.

F. Modulation Behavior

Semiconductor lasers respond much more rapidly to changes in the pump power than do other types of lasers. Their light output can be modulated directly and efficiently by varying the diode current to produce pulses at bit rates of several Gbits/sec, making them very suitable for application to communication systems. This is a consequence of the short time constant associated with the carrier injection and also of the high excitation rate which allows

a small optical cavity to be used. However, current modulation is a complicated process which involves both the carrier and photon population.

General Rate equations

The following system of nonlinear coupled differential equations describes the interaction between the density of stimulated photons N_1 and the injected election density N_2

$$dN_1/dt = g(N_2-N_0)N_1 - (N_1/\tau_1) \quad (2.18)$$

$$dN_2/dt = (J/ed) - (N_2/\tau_2) - g(N_2-N_0)N_1 \quad (2.19)$$

where

τ_1 = photon lifetime

τ_2 = spontaneous carrier lifetime

d = width of recombination region

J = current density

e = electron charge

g = slope of gain-current relation

N_0 = intercept of gain-current relation

These equations are appropriate for laser diodes under the following simplifying assumptions: (1) the laser is operating in a *single mode* above threshold, (2) the lasing cavity has a homogeneous population inversion, and (3) the optical gain G is linearly related to the injected carrier density by $G = g(N_2-N_0)$.

Small Signal Modulation

The small-signal modulation of laser diodes can be analysed by making the substitutions

$$\begin{aligned} N_1(t) &= N_1 + n_1(t) \\ N_2(t) &= N_2 + n_2(t) \\ J(t) &= J + j(t) \end{aligned} \tag{2.20}$$

in (2.18) and (2.19). The quantities N_1 N_2 and J now represent the average values of the photon density, carrier density, and current density, respectively. Also, $n_1(t)$, $n_2(t)$, and $j(t)$ represent the small signal variations in these three quantities. Equations (2.18) and (2.19) then become

$$dn_1/dt = gN_1n_2 \tag{2.21}$$

$$dn_2/dt = -n_2(\tau_1^{-1}+gN_1) - g(N_2-N_0) + j(t)/ed \tag{2.22}$$

where terms such as $n_1(t)n_2(t)$ have been set to zero because of the small-signal assumption.

Relaxation Oscillations

Equations (2.21) and (2.22) are a system of *linear* coupled equations and hence can be replaced by the following pair of second order, *uncoupled*, equations

$$n_1''(t) + \gamma n_1'(t) + \omega_1^2 n_1(t) = (1/ed)gN_1j(t) \tag{2.23}$$

$$n_2''(t) + \gamma n_2'(t) + \omega_1^2 n_2(t) = (1/ed)j'(t) \qquad (2.24)$$

where

$$\omega_1^2 = (\tau_1\tau_2)^{-1} (g\tau_1 N_0+1) [(J/J_t)-1]$$

$$\gamma = \tau_2^{-1} + \tau_1\omega_0^2$$

$$J_t = (edN_2/\tau_2)$$

Solutions for $n_1(t)$ and $n_2(t)$ are of the form $\exp(-\gamma/2 \pm j\omega_0)t$. The term $\exp(-\gamma/2)t$ is a damping term while the term $\exp(\pm j\omega_0 t)$ represents an oscillation behavior at the *natural resonant frequency* ω_0, where

$$\omega_0^2 = \omega_1^2 - (\gamma^2/4)$$
$$\simeq (\tau_1\tau_2)^{-1} [(J/J_t)-1] \qquad (2.25)$$

The approximations $N_2 >> N_0$ and $\tau_2 >> \tau_1$ have been made in the derivation of equation (2.25).

This natural resonance of the electron and photon populations is responsible for the phenomenon known as *relaxation oscillations*. When a step function of current is applied which takes the current beyond threshold there is a delay in the optical response, and the injected carrier concentration rises to a level beyond its equilibrium level. The photon concentration then increases exponentially with time to a value higher than its equilibrium value. The resulting high optical fields deplete the carrier concentration and in turn the photon concentration below their steady state values, allowing the carrier

concentration to build up again. This process then repeats itself giving rise to exponentially decaying oscillations in the carrier and photon concentration variations. The frequency of oscillations are given by ω_o and the carrier concentration variation is advanced in phase by approximately a quarter cycle compared with the photon density. Up to 15 ns can elapse before a steady state is reached.

Frequency Response

The natural resonance of the electron and photon populations also affects the sinusoidal modulation, distortion, and noise characteristics of the laser. The frequency characteristics of the laser diode can be found by using equations (2.23) and (2.24). A harmonic time dependence of the drive current is assumed

$$j(t) = j_o \exp(j\omega t) \tag{2.26}$$

where the notation is as in equation (2.20).

Frequency information can be conveniently described by the diode transfer function $H(\omega)$, defined as the ratio of the small-signal photon density n_1 to the small-signal current drive j at an angular frequency ω. Solving equations (2.23) and (2.24) for n_1, the transfer function is obtained

$$H(\omega) = \tau_2 N_1 / [\tau_2 N_1 - \tau_1 \tau_2^2 \omega^2 + j\omega\tau_1\tau_2(N_1+1)] \tag{2.27}$$

Fig. 2.2 shows the amplitude response $|H(f)|^2$ when τ_1 = 1ps and τ_2 = 2ns. The frequency response has been normalised by taking the average photon density, N_1, to be equal to 1.

It can be seen that the response of the laser diode to sinusoidal modulation of the current varies little with frequency over most of the frequency range up to resonance, but experiences an enhancement at the resonance frequency itself by a factor of more than 10. The response rapidly diminishes above the resonance frequency. Photon quantum noise, electron shot noise, and harmonic distortion are similarly enhanced in the resonance band.

When a laser diode is sinusoidally modulated, it has been observed [84] that the harmonic distortion is independent of frequency for modulation frequencies between several MHz and approximately 200 MHz. For modulation frequencies higher than this, the higher order harmonics of the modulation signal approach the resonance band and an enhancement in the harmonic distortion is observed. 69t for frequencies between a few MHz and about 200 MHz the laser diode exhibits a nonlinearity without memory (i.e., the distortion characteristics are frequency independent).

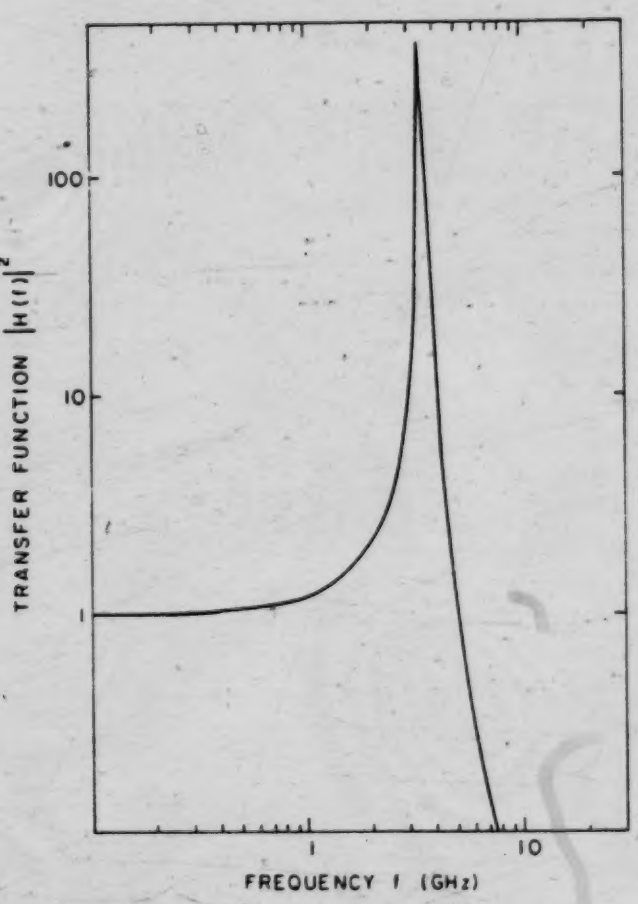

Figure 2.2 Typical frequency response of laser diode.

III. REVIEW OF NON-LINEARITY COMPENSATION TECHNIQUES

Due to the stringent linearity specifications imposed on repeatered video transmission lines, much research has been done over the last decade on the problem of improving the linearity of optical sources. Two avenues of investigation have been pursued. First, improved fabrication techniques, device structures and geometries have had some success [50]-[54] in producing light sources with a more linear response. Secondly, circuit techniques have been used to compensate for the inherent non-linearity of the light sources.

Compensation techniques that have been investigated include preemphasis, opto-electronic feedback, phase shift modulation, predistortion, quasi-feedforward, and optical feedforward [55]-[67].

A. Preemphasis

A simple linearising technique for laser diode transmitters was demonstrated by K. Asatasi in 1980 [55]. This technique compensates for the nonlinearity caused by active layer heating at frequencies less than a few tens of kilohertz. The 15.75 KHz horizontal sync frequency in a TV signal falls in this frequency range and hence contributes to the nonlinearity.

The compensation technique consists of preemphasizing the laser diode drive current using a preemphasis circuit

inserted between the signal source and diode driver. A deemphasis circuit placed after the optical receiver restores the preemphasised signal to its original form.

The preemphasis characteristic adopted is shown in Fig. 3.1. Frequencies lower than 100 KHz are attenuated 9 dB relative to frequencies above 1 MHz. This preemphasis reduces the magnitude of the 15.75 KHz horizontal sync frequency to one third of its original magnitude. A 9 dB reduction in the harmonic distortion is reported.

An advantage of this scheme is its simplicity; the preemphasis and deemphasis circuits are built using only resistors and capacitors. A disadvantage is that it is only effective in the transmission of baseband signals; little distortion improvements would be obtained with wideband signals.

B. Opto-electronic Feedback

The opto-electronic feedback method involves the use of a monitoring photodiode and a feedback network to provide negative electrical feedback to the drive circuitry. The nature of the signal changes from electrical to optical and then back to electrical as it travels around the feedback loop; hence the name, opto-electronic feedback. Sampling of the optical output can be done using a tee coupler in the output fiber or, as is more usual, a photodiode packaged along with the source can be used to monitor the output of the rear facet.

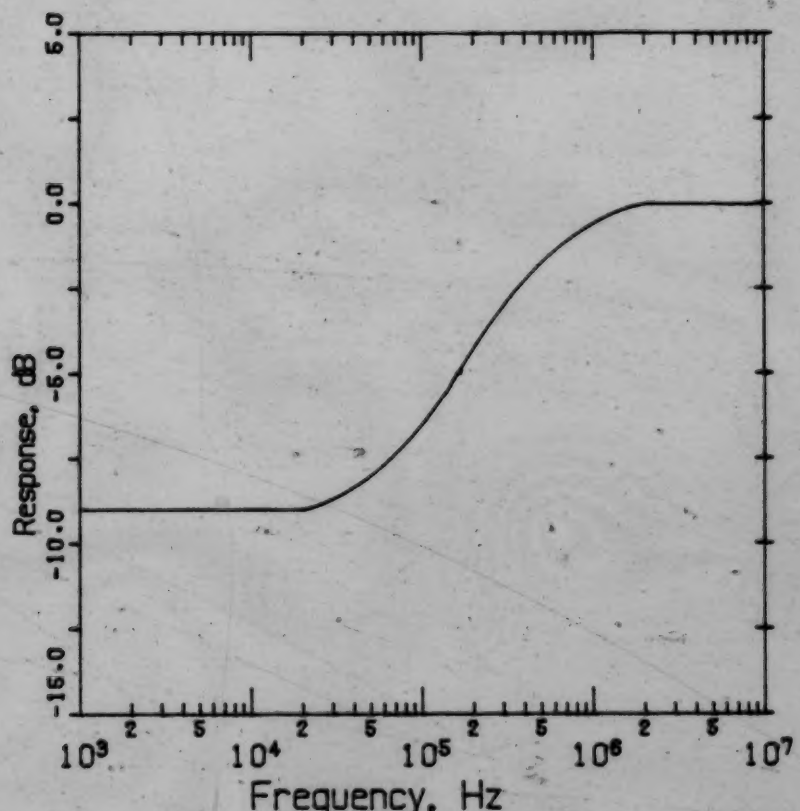

Figure 3.1 Preemphasis characteristic to improve baseband linearity.

Application of this technique to wideband transmission is difficult because of the high gain - bandwidth requirements and the small phase shifts required for stability. It has also been pointed out that improvements in third order distortion may be poor, especially for video signals, since these contain complex cross-modulation terms as well as third harmonic components [87].

It has been reported that up to 20 dB reduction of second harmonic distortion was obtained using optoelectronic feedback in a single channel TV transmission experiment [56]. In the same experiment, opto-electronic feedback has also been used in conjunction with the preemphasis technique previously described to reduce the differential gain from greater than 10% to less than 2%. In another experiment involving single channel color TV transmission, 12 dB and 4 dB improvements in second and third order harmonic distortion, respectively, were reported [57].

Opto-electronic feedback has also been employed to reduce laser noise and distortion induced by reflected light [58]. Light reflected from the fiber end face back into the laser diode is known to degrade linearity and SNR in analog video transmission [48]. By deliberately reflecting light back into the laser diode and then applying opto-electronic feedback, it was demonstrated that the degradation of DG, DP, and SNR caused by this self- coupling could be eliminated. The DG/DP of the analog video transmitter employing the opto-electronic feedback was reduced to 2% and

2° from 25% and 10°, respectively.

In summary, opto-electronic feedback has proved useful for single-channel TV transmission. It can also compensate for the nonlinearity of the drive circuitry as well as laser diode nonlinearity caused by reflected light. A disadvantage is that its usefulness for wideband transmission is questionable. As well, when the optical output is monitored using a built-in photodiode, problems may arise due to mistracking of the front and rear facet light output. Improvements in fabrication technology will largely eliminate this problem.

C. Phase Shift Modulation

A phase shift modulation technique for the selected cancellation of harmonic components of any order was demonstrated in 1977 [59]. Consider two LED transmitters whose optical outputs are summed in an optical tee coupler as shown in Fig. 3.2. If the two LEDs have matched light/current characteristics then the outputs of the two LEDs can be written as

$$L_1 = a_1 A \cos(wt) + (a_2 A^2/2)\cos(2wt) + a_2 A^2/2$$
$$L_2 = a_1 A \cos(wt+\phi) + (a_2 A^2/2)\cos 2(wt+\phi) + a_2 A^2/2 \qquad (3.1)$$

where a_1 and a_2 are constants characterising the LEDs, and A and w are the amplitude and frequency of the modulation signal. The sum of the two optical outputs is given by

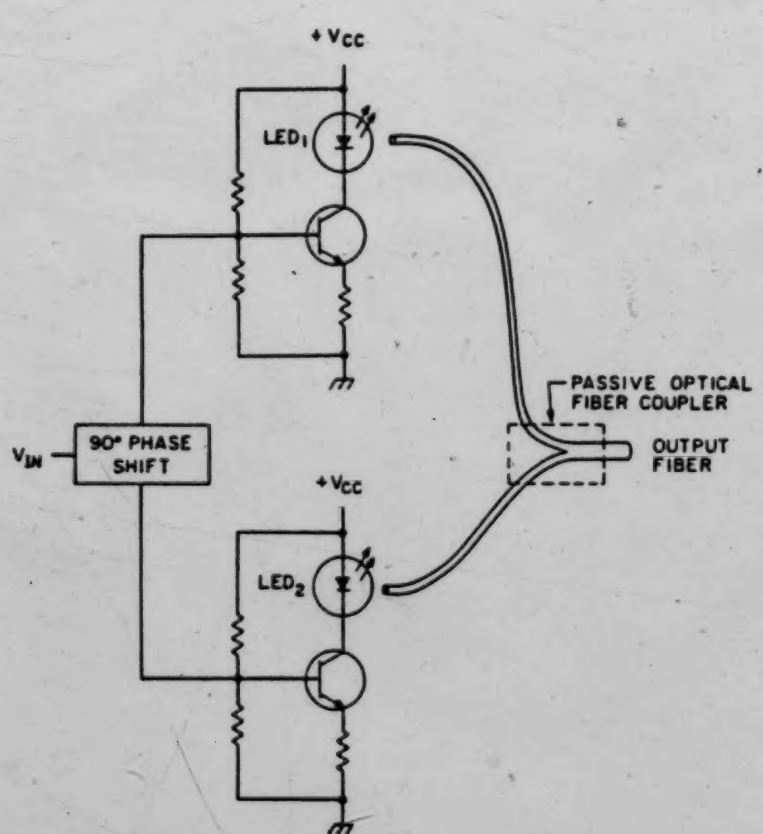

Figure 3.2 Phase shift modulation technique.

$$L_1+L_2 = 2a_1A\cos(\phi/2)\cos(wt+\phi/2) + a_2A^2\cos(\phi)\cos(2wt+\phi) + a_2A^2 \qquad (3.2)$$

It can be seen that for $\phi=90°$ the amplitude of the second harmonic term, $a_2A^2\cos(\phi)$, is equal to zero. A 25 dB improvement in the second order distortion at 3.1 MHz for a figure of -60 dB was reported. A twin-contact stripe LED was used to obtain matched LEDs.

Performing a similar calculation on the nth order term shows that the n'th order distortion is cancelled when the phase angle between the two modulation signals is equal to $180°/n$. Simultaneous cancellation of both second- and third order distortion can thus be achieved by using an additional pair of matched LEDs. This occurs if the modulation signals within each pair are out of phase by 90° (to eliminate second order distortion) and the signal phase shift between the pairs is 60° (to then eliminate third order distortion).

In spite of its effectiveness in cancelling several harmonic components simultaneously, the phase shift modulation technique has several disadvantages. In the cancellation of second order distortion, for example, there is a 3 dB power penalty due to the presence of the term $\cos(\phi)$ in the amplitude of the fundamental term. In addition precisely matched sources, high quality tee couplers, and identical coupling between the sources into the fibers are all necessary to achieve an effective distortion reduction with this technique.

D. Predistortion

Predistortion is a direct compensation technique that requires no additional optical devices. In this scheme, complementary distortion is introduced into the input signal so that it cancels as nearly as possible the distortion introduced by the optical source and associated driver circuitry. The result, ideally, is a transmission path completely free of distortion.

Shunt Predistortion

A simple predistortion technique that alters the LED or laser current in response to the signal amplitude is shown in Fig. 3.3. The series diode-resistor combination placed in parallel across the LED has the effect of shunting a larger fraction of the total current around the LED at low drive levels and vice versa at high drive levels. Thus the negative curvature of the LED or laser characteristic in the high radiance region is compensated by greater drive. The use of a germanium diode and resistor in parallel with a Burrus LED was found to extend the range of drive current for a given level of output linearity by nearly 50% [60].

Resistor R provides some degree of control over the amount of additional drive provided in the high radiance region. However, it is not possible to simultaneously control the magnitude of the additional drive and the region of the LED or laser characteristic over which the additional drive is applied.

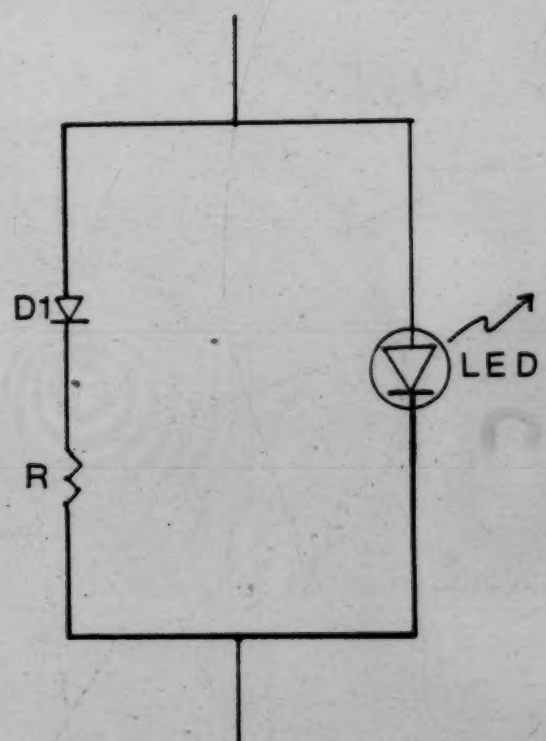

Figure 3.3 Simple shunt predistortion.

Predistortion for Differential Gain Correction

A similar scheme that affects the slope of the amplifier transfer characteristic at various points was demonstrated by K. Asatani and T. Kimura in 1977 [61],[62]. A differential gain correction circuit, shown in Fig. 3.4, is placed before the source driver. At low drive levels all diodes are conducting, the total emitter resistance is small, and hence the gain of the circuit is high. As the drive level increases, the diodes stop conducting one by one and the gain decreases correspondingly. The bias voltages V_i determine where in the amplifier's transfer characteristic the associated resistors R_i affect the gain. By reversing the diode directions, the gain can be made to progressively increase as the drive level increases.

By using several such diodes in appropriate directions and varying the bias and resistance values, arbitrary nonlinearities in the amplifier's transfer characteristic can be compensated. Due to the exponential nonlinearity of the switching diodes, the compensated characteristic is free of discontinuities at the points where the diodes switch on or off.

The authors of this scheme were able to obtain a reduction in DG from 12.5% to less than 1% using a compensating circuit with three diodes. The corresponding amount of second order and third order harmonic distortion improvements was calculated to be 22 dB and 23 dB, respectively.

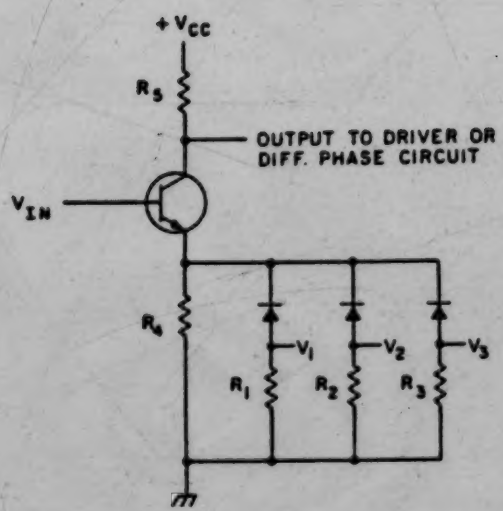

Figure 3.4 Differential gain compensation.

Predistortion for Differential Phase Correction

The authors of the differential gain compensation technique have also reported a scheme for differential phase compensation using predistortion [61],[63]. The phase correction circuitry is shown in Fig. 3.5.

The circuit provides a phase lead at frequency f of

$$\phi = 2\tan^{-1}(2fCR)^{-1} \qquad (3.3)$$

where R is the effective resistance of the shunt combination of R_1, R_2, and R_3. As the input level increases the diodes turn on in succession, hence R and the phase lead decrease. If an increase in phase is required with increasing luminance signal then the diode directions should be reversed. A three diode compensating network with appropriate bias and resistance values was found to reduce the differential phase from 2.8° to less than 1°.

Cascading the differential gain and differential phase compensating circuitry allowed for independent compensation of DG and DP. Simultaneous reductions of DG and DP to below 1% and 1°, respectively, was demonstrated.

E. Quasi-Feedforward Compensation

The authors of the phase shift modulation technique have reported another novel scheme which they label quasi-feedforward compensation [64],[65]. This technique is similar to predistortion in that the input signal is

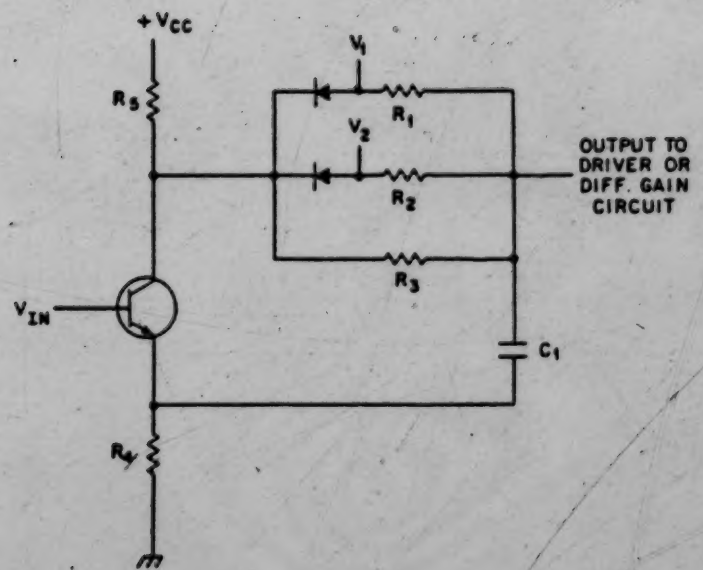

Figure 3.5 Differential phase compensation.

distorted before being fed to the LED driver. However, instead of predistorting the input signal using passive components, the signal is altered using and "error signal" obtained from a reference LED.

The compensation scheme is illustrated in Fig. 3.6. The assumption that the nonlinearity of a LED is free of memory allows one to analyze this nonlinearity using a polynomial expansion of its light/current characteristic. Suppose the light/current characteristics of the two LEDs, expanded to three terms, is given by

$$L_1 = a_1S + a_2S^2 + a_3S^3$$
$$L_2 = b_1S + b_2S^2 + b_3S^3 \qquad (3.4)$$

Define Δ to be the nonlinear portion of the LED characteristic:

$$\Delta = a_2S^2 + a_3S^3 \qquad (3.5)$$

The drive signal of LED2 is equal to $(\alpha S-\beta\Delta)$, where α and β are gain parameters that can be varied. Replacing S by $(\alpha S-\beta\Delta)$ in the expression for L_2 gives the overall transfer characteristic. Truncated to three terms this characteristic is given by:

$$L_2 = c_1S + c_2S^2 + c_3S^3 \qquad (3.6)$$

where

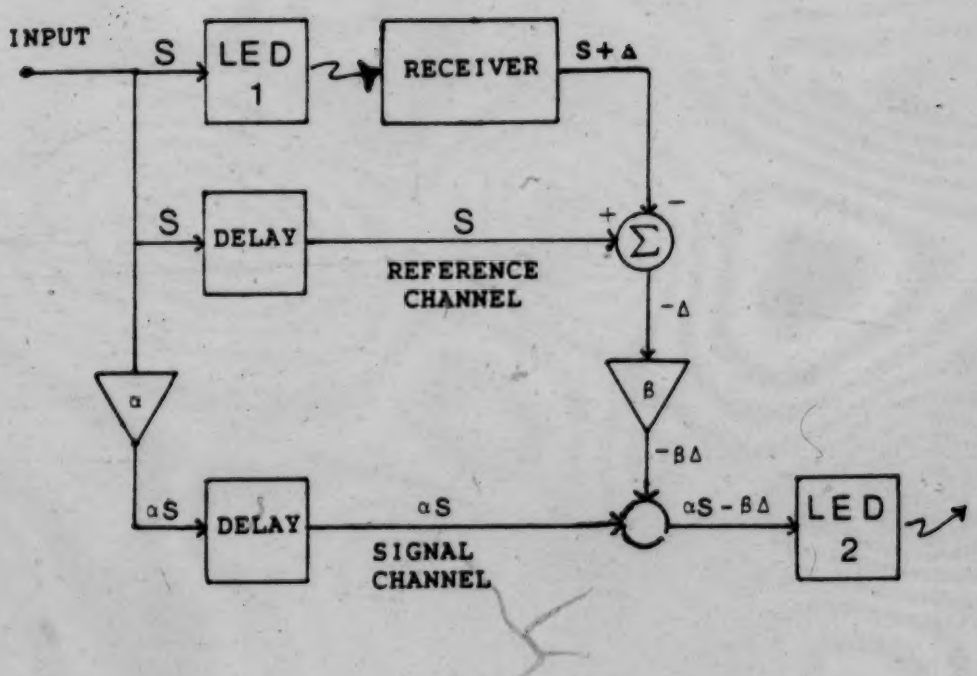

Figure 3.6 Quasi-feedforward compensation.

$$c_1 = \alpha b_1 a_1$$

$$c_2 = \alpha^2 b_2 - \beta a_2 b_1$$

$$c_3 = \alpha^3 b_3 - \beta a_3 b_1 - 2\alpha\beta b_2 a_2$$

It can be seen from equation 3.6 that the second order distortion in the output is eliminated when the gain β is equal to

$$\beta = (\alpha^2 b_2)/(a_2 b_1) \tag{3.7}$$

and the third order distortion is eliminated provided the gain α is equal to

$$\alpha = (b_1 b_2 a_3)/(a_2 b_1 b_3 - 2a_2 b_2^2) \tag{3.8}$$

With this technique a reduction in the second- and third order intermodulation distortion of 35 dB and 20 dB, respectively, were obtained in a three-tone test. To achieve this degree of effectiveness, very precise time delays (obtained by using lengths of coaxial cable) and amplifiers with very flat amplitude and phase response over the frequency range of interest were required. In addition, implementation of this technique is easier when the characteristics of the two optical sources are closely matched.

F. Optical Feedforward Compensation

The optical feedforward compensation scheme shown in Fig. 3.7, is a variation of a well known electrical feedforward counterpart [66]. As in the quasi-feedforward compensation scheme, distortion compensation using feedforward is achieved through the isolation of the distortion produced by the optical source and a subsequent injection of an error signal back into the circuit. The difference between the two schemes is that injection of the error signal occurs in the optical domain in the feedforward scheme. Also, a single LED is used for both signal transmission and error monitoring in the feedforward technique.

Although the two LEDs used in this scheme need not be closely matched, requirements for efficient and stable coupling of optical signals in an optical tee coupler can pose practical difficulties.

G. Adaptive Predistortion

The predistortion techniques discussed so far have the problem that they cannot compensate for changes in the LED or laser characteristic. It is especially impractical to use these techniques with laser diode transmitters, since laser characteristics do change significantly as a result of aging or temperature changes. An adaptive predistortion technique demonstrated by Bertelsmeier and Zschunke in 1983 [67] eliminates this problem.

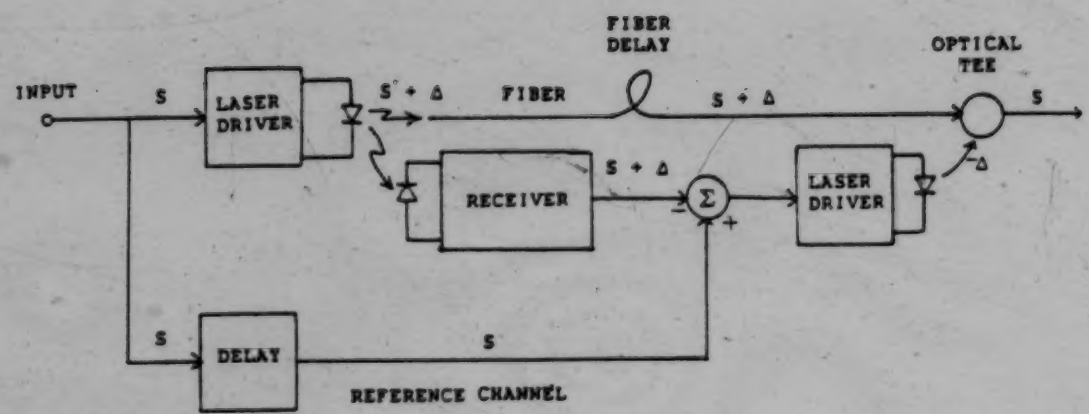

Figure 3.7 Optical feedforward compensation.

A block diagram of this technique is shown in Fig. 3.8. In this technique, second- and third order harmonics of the input signal u_0 are generated (by bridge-type circuits using Schottky diodes) and weighted by the gain coefficients b_2 and b_3. Adding them to the undistorted signal results in the predistorted signal u_1 that drives the optical source:

$$u_1 = b_1u_0 + b_2u_0^2 + b_3u_0^3 \tag{3.9}$$

If the light/current characteristic of the source, approximated by a third degree polynomial, is given by

$$u_2 = a_1u_1 + a_2u_1^2 + a_3u_1^3 \tag{3.10}$$

then the optical output u_2, truncated to three terms, is given by

$$u_2 = c_1u_0 + c_2u_0^2 + c_3u_0^3 \tag{3.11}$$

where

$$c_1 = a_1b_1$$

$$c_2 = a_1b_2 + a_2b_1^2$$

$$c_3 = a_1b_3 + a_3b_1^3$$

The second order distortion can thus be eliminated if the gain coefficient b_2 is equal to

$$b_2 = (-a_2b_1^3)/a_1 \tag{3.12}$$

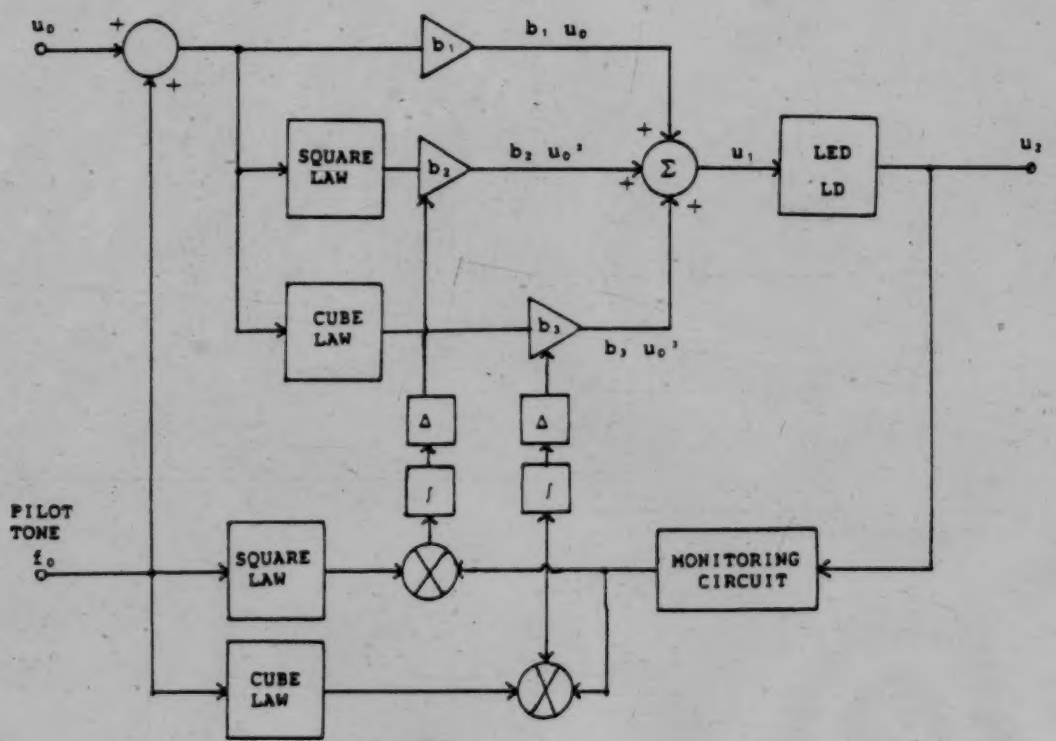

Figure 3.8 Adaptive predistortion technique.

and the third order distortion vanishes if the gain coefficient b_3 is equal to

$$b_3 = (-a_3 b_1^3)/a_1 \qquad (3.13)$$

To correct for changes in the LED or laser characteristic these gain coefficients must be made adjustable. This is done by the addition of a sinusoidal pilot signal of frequency f_0 to the input signal in an unused frequency band. A monitoring photodiode detects the pilot tone and its residual distortion in the output and feeds it back to the adaptive circuitry. Here, the feedback signal is mixed with $2f_0$ and $3f_0$ and then integrated to provide the residual distortion coefficients c_2 and c_3. Error signals obtained by differentiation of c_2 and c_3 are used to adaptively adjust the gain coefficients b_2 and b_3 so as to minimize the residual distortion.

This adaptive adjustment strategy was successfully tested in an experiment using only electrical components. A pilot tone of frequency 5.35 MHz was used. Second and third order intermodulation distortion improvements of 18 dB and 13 dB, respectively, were reported for frequencies between 10 MHz and 130 MHz.

It is feasible, therefore, to use this compensation scheme with laser diode sources for transmission of broadband signals. This is at the expense of increased complexity and more stringent requirements than the other

predistortion techniques. The square and cube law devices must contain insignificant amounts of unwanted harmonics. Also, only very small amplitude and phase deviations in the response of the gain coefficient amplifiers and the square and cube law devices can be tolerated.

H. Summary

Many effective compensation techniques have been developed over the last few years. However, many of these have employed LEDs rather than laser diodes in spite of the higher optical output and smaller spectral width obtainable from the latter devices. In part this is due to the fact that the LEDs have been in use for a longer period of time and hence their technology is more advanced . But it is also a result of additional problems that are encountered in trying to linearise a laser diode transmitter.

Laser diode characteristics are affected to a much greater extent by aging or temperature variations than are the characteristics of LEDs. Only compensation techniques that measure the nonlinearity and correct it in real time such as opto-electronic feedback, feedforward, phase shift modulation or adaptive predistortion would be of practical use with laser diodes. But the feedforward and phase shift modulation schemes require two lasers closely matched in their mode-instability behavior - an almost impossible task. In addition, the cost of laser diodes is much higher than that of LEDs and represent a substantial portion of the

total cost of the transmitter. Hence schemes requiring two laser diodes can almost double the cost of a transmitter placing them at a serious disadvantage.

Techniques such as preemphasis, opto-electronic feedback, and adaptive predistortion are well suited for use with laser diodes. Opto-electronic feedback and preemphasis, however, are useful in the transmission of baseband video signals only. Adaptive predistortion is therefore the most promising linearisation technique for broadband communications.

IV. LASER DIODE TRANSMITTER DESIGN

This chapter is concerned with the design and testing of an analog laser diode transmitter. As this transmitter is to be used for the purpose of testing the opto-electronic feedback technique at video frequencies, the LD transmitter must have a large bandwidth and must allow for the introduction of negative feedback. As well, the total harmonic distortion of the electronic circuitry must be much less than the distortion introduced by the laser diode at all modulation levels of interest.

A. Description of the Laser Diode Transmitter

The laser diode used in this experiment is a single-transverse and multi-longitudinal mode CW GaAlAs DH Stripe laser (Laser Diode Labs Model LCW-10F) operating at 815 nm. It has a threshold current of 70 mA (at 25°C) and a maximum safe current of about 95 mA. The LD driver must bias the LD at a dc current of 85 mA and must be able to modulate the LD over its entire linear range from 75 mA to 95 mA.

Great care must be taken to ensure that the instantaneous LD drive current never exceeds the maximum safe current even if the transmitter is overdriven or breaks into oscillation. Laser diodes are extremely fast devices with rise times typically less than 0.5ns. Even very brief (< 1us) current transients which exceed the maximum rating can cause damage ranging from slight degradation to

catastrophic destruction, depending on the magnitude and duration of the transient. Of the many transmitter configurations tested, the one shown in Fig. 4.1 proved to be superior with respect to linearity considerations as well as the safety of the laser diode. It consists of a differential amplifier utilizing Widlar current sources for biasing. The current sources allow for the precise control of the bias current and modulation depth of the LD. As well, negative electrical feedback is readily facilitated by the presence of the inverting input of the differential amplifier. In addition, this LD transmitter circuit has a low THD figure, excellent stability, and a 3 dB bandwidth of 40 MHz which is more than sufficient to demonstrate linearisation techniques for video transmission.

Transistors Q1 through Q5 are high frequency transistors (2N5943). The reference current, I_{Yo}, is determined by the collector and emitter resistors of Q3 and is given by

$$I_{Yo} = (Vcc_1 - Vee - Vbe_3) / (Rc_3 + Re_3) \qquad (4.1)$$
$$\simeq (40v - 0.65v) / (1.5 + 0.47)K \simeq 20mA$$

Base-emitter voltages are taken to be 0.65V and all base currents are ignored since all transistors have a beta greater than 100. Transistors Q4 and Q5 are Widlar current sources. The collector current, I_1, of Q4 is found by summing voltages around the emitter-base loop of Q3 and Q4,

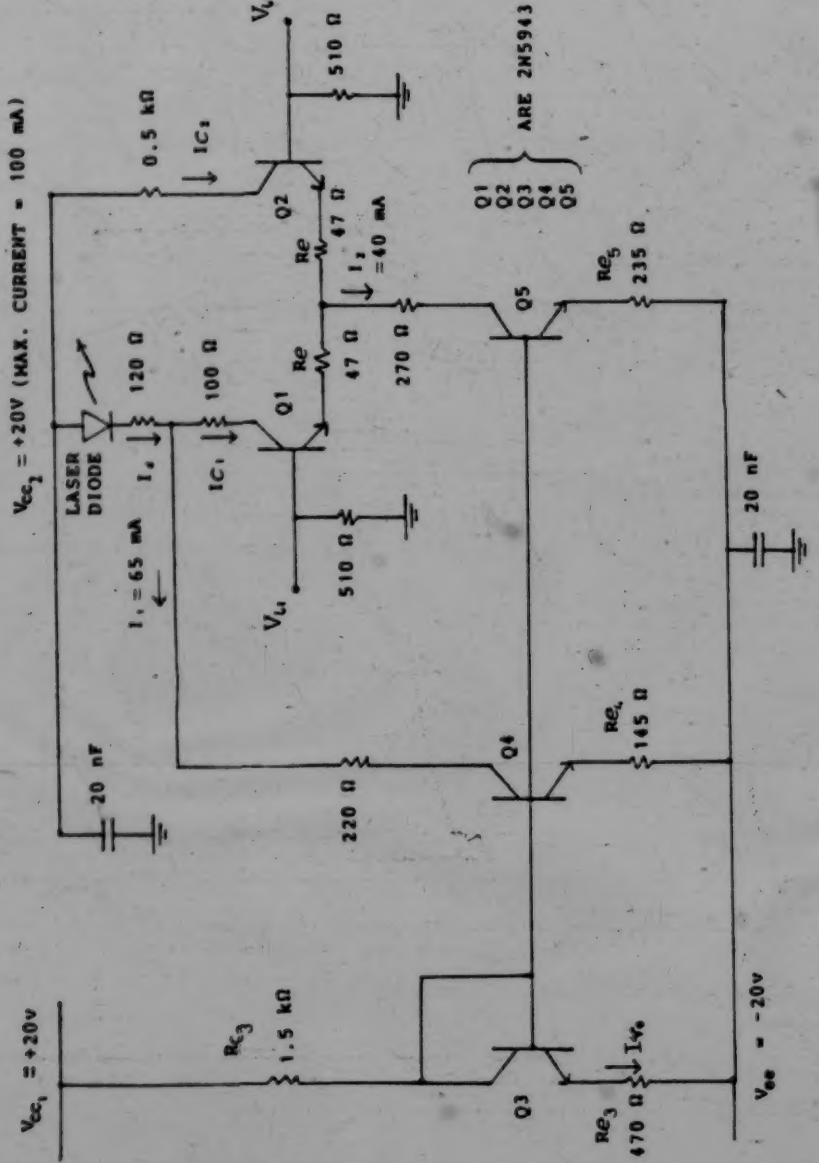

Figure 4.1 Schematic diagram of laser diode transmitter.

$$I_1 \simeq (Re_3/Re_4)\, I_{vo} \qquad (4.2)$$
$$= (0.47K/0.145K)(20mA) \simeq 65mA$$

Thus Q4 draws a constant current of I_1 = 65 mA through the laser diode. Similarly, the collector current of Q5, I_2, is given by

$$I_2 \simeq (Re_3/Re_5)\, I_{vo} \qquad (4.3)$$
$$= (0.47K/0.235K)(20mA) = 40mA$$

Thus Q5 draws a constant current of I_2 = 40 mA through the differential pair Q1-Q2.

Under quiescent conditions (i.e., $V_{i1} = V_{i2} = 0$) and assuming that Q1 and Q2 are a matched pair, then the collector currents of both Q1 and Q2 are identically equal to 20 mA. Hence, the LD quiescent current is equal to $I_1 + (I_2/2)$ = 85 mA. When an input signal, no matter how large, is applied to the differential amplifier, the peak-to-peak current modulation of the LD is always less than or equal to I_2. As backup protection, a crowbar circuit in the positive power supply limits the total LD current to 100 mA.

The collector resistors of Q1, Q2, Q4, and Q5 serve as dropping resistors. That is, they reduce the collector-emitter voltages and hence the power dissipated in these transistors to a permissible level. Their values are such that none of the transistors are driven to saturation even under maximum modulation of the differential amplifier.

The emitter resistors of Q4 and Q5 control the LD bias current and modulation current, respectively. The emitter resistors R_e of Q1 and Q2 improve the distortion performance of the LD transmitter.

B. Distortion Analysis

In this section the linearity of the LD driver circuitry is analyzed from its transfer characteristic. It must be noted that it is the linearity of the circuitry itself that is being examined and not that of the LD light output; thus the output signal in question is the collector current of either Q1 or Q2.

Summing the voltages around the loop containing the base-emitter junctions of Q1 and Q2 gives the result

$$V_{12} + V_t \ln(I_{C_2}/I_{C_1}) + R_e (I_{C_2} - I_{C_1}) = 0 \qquad (4.4)$$

where $V_{12} \equiv (V_{b1} - V_{b2})$ and $V_t = kT/q$ ($\simeq$26mv at 300°K) is the volt equivalent of temperature. If $R_e = 0$ then (4.4) can be easily solved for I_{C_1},

$$I_{C_1} = I_2 / [1 + \exp(-V_{12}/V_t)] \qquad (4.5)$$

where use has been made of the relation $I_{C_2} = I_2 - I_{C_1}$.

If $R_e \neq 0$ then (4.4) is a transcendental equation and a closed form expression for the collector current cannot be obtained. However, (4.4) can be used to obtain the slope,

dIC_1/dV_{1d}, at each point of the transfer characteristic. Differentiating (4.4) with respect to V_{1d} and simplifying,

$$IC_1' = x(1-x)I_2 / [V_t + 2x(1-x)I_2Re] \qquad (4.6)$$

where IC_1' denotes dIC_1/dV_{1d} and the parameter x is equal to the ratio IC_1/I_2.

From (4.6) it can be seen that dIC_1/dV_{1d} is a maximum at x=0.5 and approaches zero as x approaches either 0 or 1. That is, the slope of the transfer characteristic is a maximum at $IC_1 = I_2/2$ (i.e., at $V_{1d} = 0$) and approaches zero as IC_1 approaches either of the limits 0 or I_2. The variation of the slope dIC_1/dV_{1d} with IC_1 is shown in Fig. 4.2.

At $V_{1d} = 0$, the slope is a maximum and is given by

$$IC_1'(0) = [(4V_t/I_2) + 2Re]^{-1} \simeq 0.01S \qquad (4.7)$$

where the values $Re = 47\ \Omega$ and $I_2 = 40$ mA have been used. This is the transimpedance gain of the LD transmitter at the center of its linear region. The range over which the total harmonic distortion of the transmitter circuitry is less than -40dB can be determined approximately by finding two points on the transfer characteristic such that the slope varies by no more than ±1% between these two points. From (4.6) (which is a quadratic equation in x) the two points are found to be $x = 0.5 \pm 0.26$. Hence, the total harmonic

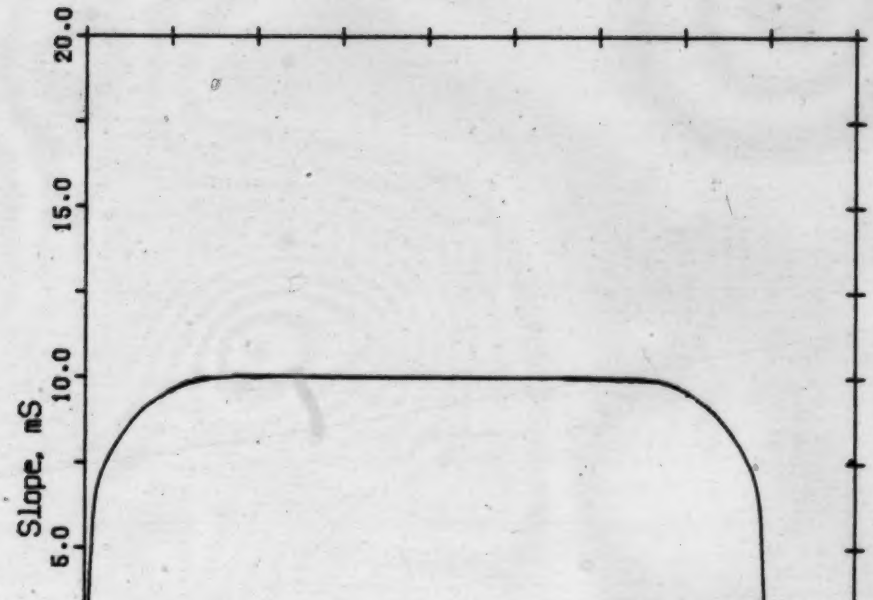

Figure 4.2 Calculated plot of the slope $dIC_1/dV_{1,}$ as a function of IC_1.

distortion introduced by the LD transmitter is less than -40dB as long as the peak-to-peak current modulation of the laser diode is less than $0.52I_2 \simeq 21$ mA.

The drive current of the LD transmitter does not contain distortion terms of all orders since the transfer characteristic is symmetric about the point $I_2/2$. This is because if the amplifier is driven by a sinusoidal signal the drive current, i(t), will possess *half-wave symmetry*. That is, it will satisfy the relation $i(t \pm T/2) = -i(t)$ where T is the period of the signal. It can easily be shown that the Fourier series of such a signal contains only odd order terms.

In conclusion, if emitter resistors Re greater than about 10 Ω are used in the differential amplifier, then the LD transmitter introduces negligible amounts of second order distortion and third order distortion of less than -40dB for peak-to-peak LD current modulation less than $\simeq I_2/2$.

C. Experimental Performance

The linearity of the LD driver circuitry is evaluated in this section. The distortion present in the LD drive current is determined by monitoring the voltage across a resistor (which is in series with the laser diode) using a spectrum analyser. The *intermodulation* distortion in the drive current is measured rather than the *harmonic* distortion since the signal generator itself generates relatively high levels of second order harmonic distortion

(up to -40dB at high input levels and at high frequencies).

A two-tone input signal at closely separated frequenies f_1 and f_2 is used; the amplitudes of the two tones are equal. $IM(f_2-f_1)$ is defined to be the power in the second order intermodulation distortion term at frequency f_2-f_1 divided by the power in either of the fundamental terms. Similarly, $IM(2f_2-f_1)$ denotes the power in the third order intermodulation distortion term at frequency $2f_2-f_1$ divided by the power in a fundamental term. These intermodulation products are not present in the input signal but, rather, are generated by the nonlinearity of the LD transmitter circuitry.

Fig. 4.3 shows the observed values of second and third order IM distortion as a function of the peak-to-peak drive current for an input signal consisting of tones at frequencies f_1 = 5.0 MHz and f_2 = 5.1 MHz. Intermodulation distortion levels below -50dB could not be measured as the distortion would lie beneath the noise floor of the spectrum analyzer in such a case. The results show that second order IM distortion is absent until the amplifier is driven so hard that clipping occurs. The third order IM distortion is less than -40dB for LD drive currents less than 25 mA peak-to-peak. This degree of linearity is sufficient since, as will be seen in a later chapter, the LD nonlinearity is much worse than this.

Finally, the frequency variation of $IM(2f_2-f_1)$ is investigated. With f_2-f_1 kept constant at 0.1 MHz, f_1 is

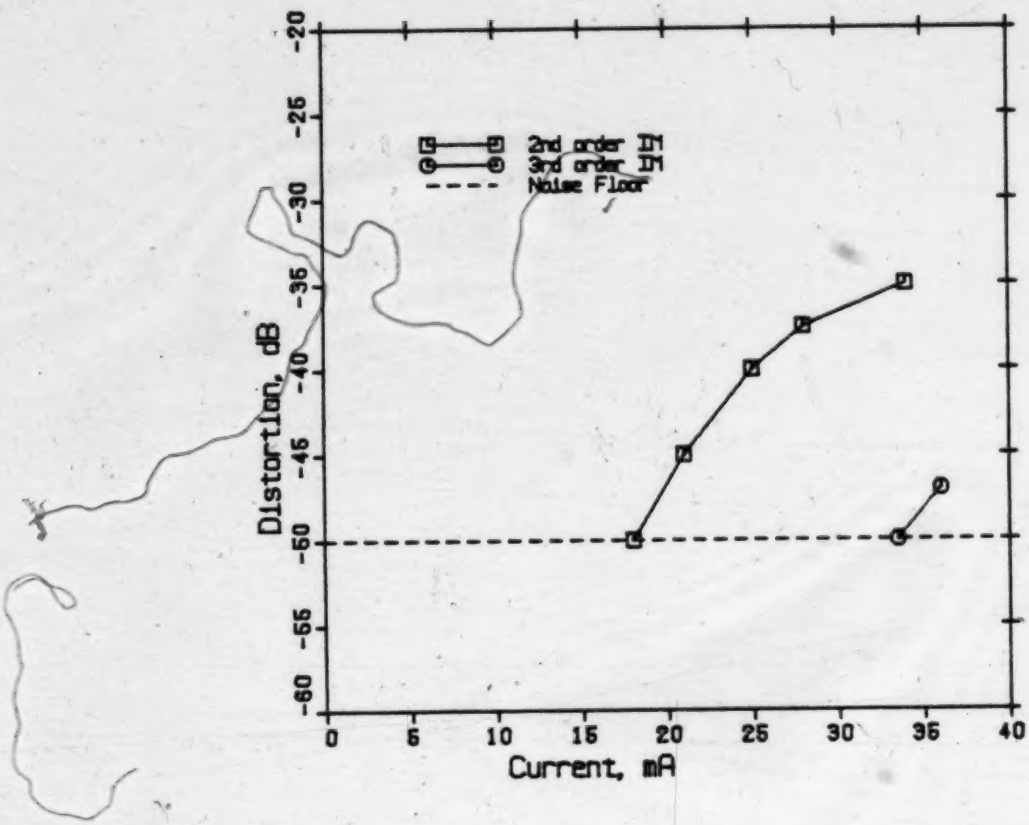

Figure 4.3 Observed intermodulation distortion as a function of peak to peak modulation current.

varied from 1 MHz to 40 MHz, the 3dB bandwidth of the LD transmitter. The observed values of $IM(2f_2-f_1)$, for a drive current of 20 mA peak-to-peak, are shown in Fig. 4.4. The distortion becomes worse for frequencies near the upper 3dB point of the amplifier; however, the distortion remains below -40dB at all frequencies less than 40 MHz.

The LD transmitter can therefore modulate the laser diode at frequencies up to 40 MHz and drive currents up to 25 mA peak-to-peak with the required level of linearity.

V. OPTO-ELECTRONIC FEEDBACK COMPENSATION

In this chapter, the effectiveness of opto-electronic feedback for linearising the light-current characteristic of a laser diode is investigated. The primary focus of this project is on analog video transmission; hence the objective is to devise an opto-electronic feedback technique that results in significant linearisation of the laser diode characteristic over a bandwidth of at least 4.2 MHz. Such a technique would be useful in achieving acceptable levels of distortion when baseband transmission of a video signal is used. As well, if linearisation over a bandwidth of 15 MHz or more can be achieved, then this technique could be used to obtain very low values of intermodulation distortion and noise when the video signal is transmitted using frequency modulation.

Two opto-electronic feedback schemes will be tested. They will be evaluated with respect to the stability of the feedback amplifier and its effectiveness in linearising the LD characteristic. Stability can be determined by plotting the loop gain in the complex plane (i.e., a Nyquist diagram) and determining the phase margin of the feedback amplifier.

A. Effect of Negative Feedback on Distortion

Consider the idealized feedback configuration of Fig. 5.1. The feedback network (which is usually linear and passive) has a transfer function β (usually a real constant)

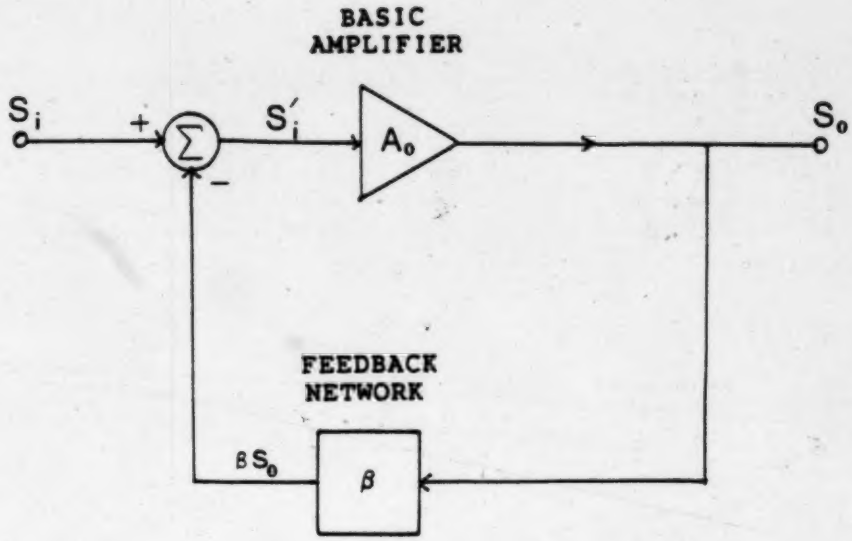

Figure 5.1 Idealized feedback configuration.

and feeds back a signal βS_o to the input differential node. The error signal $S_i' = S_i - \beta S_o$ is then amplified by the basic amplifier with transfer function A_o. The transfer gain A_o must include the loading effect of the feedback network as well as any load present at the output.

From Fig. 5.1 the gain with feedback, or closed-loop gain A, is found:

$$A \equiv S_o/S_i = A_o/(1 + \beta A_o) \qquad (5.1)$$

Differentiating (5.1) with respect to A_o and simplifying gives the following relationship,

$$dA/A = (dA_o/A_o) / (1+\beta A_o) \qquad (5.2)$$

Equation (5.1) suggests that the closed-loop gain is smaller than the open-loop gain by the *desensitivity factor* D, where $D \equiv (1+\beta A_o)$. In addition, equation (5.2) suggests that the percentage variation in the slope of the transfer characteristic is smaller by the factor D for the feedback amplifier than for the basic amplifier. This suggests that feedback has the effect of reducing distortion since distortion is caused by variations in the slope of the basic-amplifier transfer characteristic.

Let $IM(f_2-f_1)$ denote the amount of second order IM distortion in the output of the basic-amplifier at a certain output-signal amplitude. Now introduce feedback and increase

the input signal level so that the output-signal amplitude is maintained at it's previous level. Let $IM(f_2-f_1)'$ denote the amount of second order IM distortion present now at the output. Note that $IM(f_2-f_1)'$ has two components: $IM(f_2-f_1)$, which is present even in the absence of a feedback signal, and $-\beta A IM(f_2-f_1)'$, which is the result of feeding $-\beta IM(f_2-f_1)'$ back to the input. Hence, by the superposition principle,

$$IM(f_2-f_1)' = IM(f_2-f_1) - \beta A\, IM(f_2-f_1)'$$

or

$$IM(f_2-f_1)' = IM(f_2-f_1)/D \qquad (5.3)$$

A similar derivation shows that the third order IM distortion is also reduced by the factor D:

$$IM(2f_2-f_1)' = IM(2f_2-f_1)/D \qquad (5.4)$$

Note that since the principle of superposition has been used in their derivation, (5.3) and (5.4) are valid only in that region where the basic-amplifier is approximately linear. As an extreme example, consider the region of the transfer characteristic where the basic-amplifier starts clipping. The value of the open-loop gain, A_o, is equal to zero in this region and hence the desensitivity factor is equal to 1. Consequently, the use of feedback in this region results in no decrease in distortion. In general, the reduction in distortion resulting from the use of feedback decreases as

the amplifier is driven to saturation.

Equations (5.3) and (5.4) show that both second- and third order IM distortion are reduced by an equal amount when feedback is applied. While this is the case with a simple two-tone input signal, it has been reported [87] that improvements in third order IM distortion may be poor for a video signal since third order IM products contain complex cross-modulation terms.

According to (5.1), feedback reduces the gain of an amplifier by the factor $(1+\beta A_o)$. Thus if $|1+\beta A_o|$ is greater than one the feedback is negative and if $|1+\beta A_o|$ is less than one the feedback is positive. The *loop gain* βA_o is, in general, a complex quantity that varies with frequency. A plot of βA_o in the complex plane from all frequencies from $-\infty$ to $+\infty$ forms a closed curve called the Nyquist diagram.

The criterion for positive or negative feedback can be represented in the complex plane. The equation $|1+\beta A_o| = 1$ represents an unit circle centered at the point $-1+j0$ in the complex βA_o-plane. The feedback is negative for those frequencies where βA_o lies outside this circle, since $|1+\beta A_o| > 1$ at these points. Conversely, the feedback is positive at those frequencies where βA_o lies inside this circle. In this latter case the system can remain stable provided it satisfies Nyquist's criteria. Nyquist's criterion states that a feedback amplifier is stable if and only if its Nyquist diagram does not enclose the point $-1+j0$. It can be shown that Nyquist's criterion is

equivalent to the condition that all poles of the closed-loop transfer gain A lie in the left half-plane.

A feedback amplifier may be stable but yet so close to instability that a slight additional phase shift introduced into the feedback loop results in oscillation. An indication of the stability of a feedback amplifier is its *phase margin*. The phase margin is defined as 180° - $|\arg(\beta A_o)|$ at the frequency at which $|\beta A_o| = 1$. Another indicator of stability is the *gain margin*. This is equal to $20\log(\beta A_o)$ at the frequency at which $\arg(\beta A_o) = 180°$. An amplifier with a phase margin greater than 45° and a gain margin greater than 10 dB is considered to be very stable. Techniques such as pole-zero compensation and dominant-pole compensation are used to stabilize a feedback amplifier but usually with reduced bandwidth as a penalty.

B. Description of an Opto-Electronic Feedback Experiment

The first opto-electronic feedback scheme to be tested employs a simple resistive feedback network. A block diagram of this scheme is shown in Fig. 5.2. The laser diode and LD driver circuitry have been described in the previous chapter.

For linearisation over a wide frequency range, the bandwidth of the negative feedback loop should be as large as possible. Or more precisely, the total time delay in the feedback loop should be minimized. As the laser diode used in this project is packaged with a fiber pigtail one meter

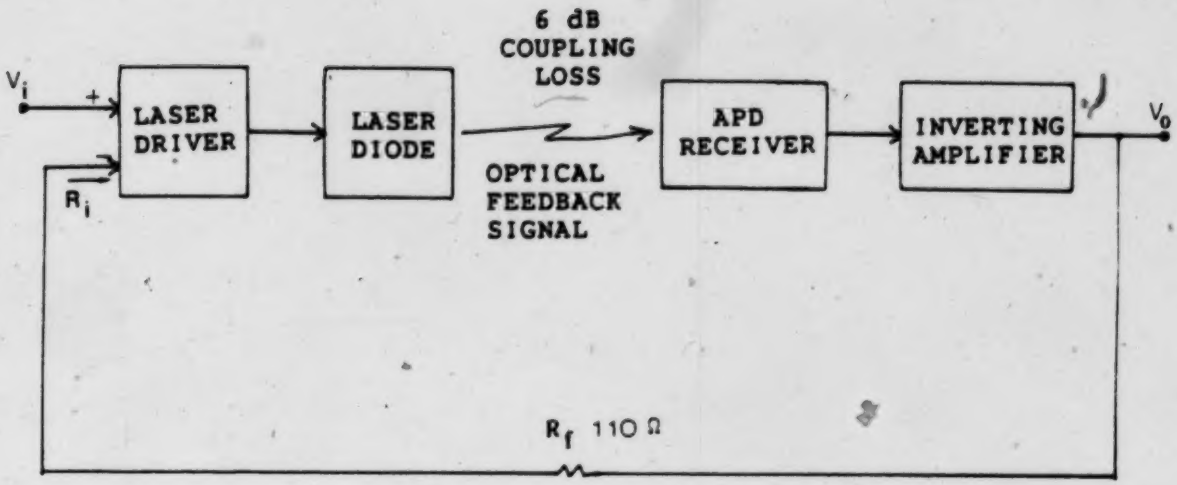

Figure 5.2 Block diagram of the first opto-electronic feedback scheme investigated.

long and does not have a built-in monitoring photodiode, the main factor limiting the bandwidth of the feedback loop is the physical path length of this loop. If the length of the fiber pigtail is minimized and amplifiers with very small phase shifts are employed, however, then linearisation at video frequencies should still be possible.

In practice, the power level of the sampled optical feedback signal should be a small fraction of the total light output of the LD. In this experiment, however, the light output from the fiber pigtail is used directly for the purpose of feedback. Therefore, sampling of the LD light output was simulated by introducing a 8 dB loss in the fiber-optic connector at the end of the fiber pigtail.

The considerable amount of reflected light would degrade the linearity and SNR of a high coherence single mode laser diode. No degradation in the linearity of the multimode laser diode used in the experiment was observed, however. This is because the coherence length of the multimode laser diode is small enough that the reflected light is essentially uncorrelated with the emitted light [48]. Furthermore, it has been demonstrated that opto-electronic feedback can eliminate the degradation in linearity and SNR caused by reflected light [58].

The inverting amplifier in the feedback loop was required to achieve a reasonable loop gain as well as to invert the signal so that the feedback is negative. The amplifier was also needed to drive the spectrum analyzer

which has an input impedance of 50 Ω.

The open loop gain of the "basic-amplifier" is defined by $A_o \equiv V_o/V_i$ with the feedback loop broken. The feedback transfer function β is determined by the resistive network formed by the feedback resistor (110 Ω) and the input impedance of the inverting terminal of the LD driver (510 Ω). Thus β is equal to 0.82.

The maximum loop gain attainable in this configuration is limited by the high input voltage required by the LD driver. For example, for an emitter resistance of R_e = 47 Ω, the LD driver has a transconductance gain of 0.01S. Consequently, an input voltage of approximately 0.5 V peak is required for a 10 mA p-p current modulation of the LD. Since the maximum output of the inverting amplifier is about 1V peak, this limits the open loop voltage gain A_o, and hence the loop gain βA_o, to less than approximately four.

In order to obtain a loop gain as large as possible, the transconductance gain of the LD driver was increased by decreasing the value of the emitter resistance to R_e = 22 Ω from R_e = 47 Ω. For this value of R_e, the low frequency loop gain, $\beta A_o(f=0)$, was measured to be 3.2. While this value of loop gain is low, it has the advantageous effect that the feedback amplifier is stable without the need for any compensation technique.

Nyquist Plot

By determining the complex values of the loop gain $\beta A_o(f)$ as a function of frequency, the Nyquist diagram of the feedback amplifier can be plotted. This allows such factors as the stability of the feedback amplifier and the frequency at which it enters the region of positive feedback to be determined.

By plotting the values of the loop gain in the complex βA_o-plane, the Nyquist diagram shown in Fig. 5.3 was obtained. The magnitude and phase of the loop gain were measured using a vector voltmeter. The Nyquist curve is not complete, since only loop gains corresponding to positive frequencies from 0 to 15 MHz are shown. Nevertheless, the diagram reveals much information. It is seen that the feedback amplifier is stable, since $|\beta A_o|$ is less than 1 when $\arg(\beta A_o)$ equals $-180°$. The Nyquist curve intersects the circle $|1+\beta A_o| = 1$ at a frequency of 11.4 MHz. For frequencies higher than this, the Nyquist curve lies in the region of positive feedback (i.e., $|1+\beta A_o| < 1$). The phase of βA_o equals $-109°$ at the point where the Nyquist curve intersects the circle $|\beta A_o| = 1$. Consequently, the phase margin of the feedback amplifier is equal to 71°. Also, the gain margin is equal to $|20 \log (0.3)| = 10.5$ dB. The feedback amplifier is thus very stable and should prove effective in linearising the LD light output for frequencies up to 11.4 MHz.

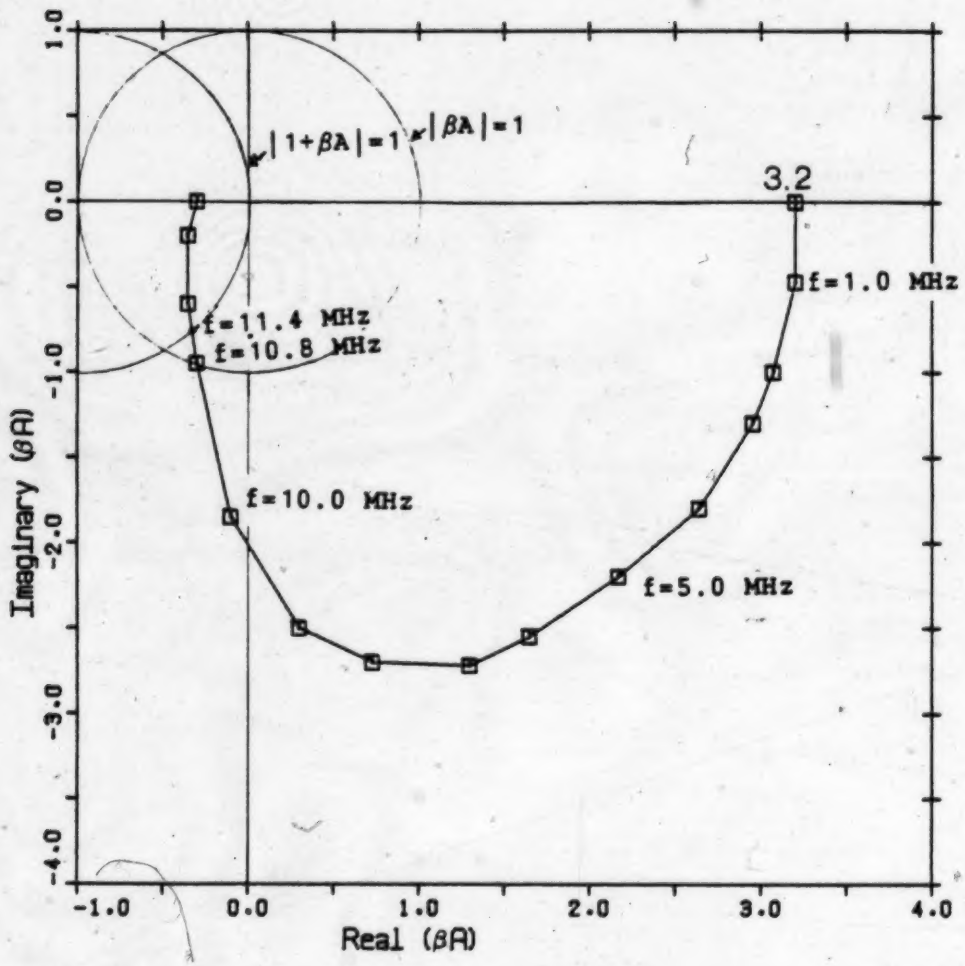

Figure 5.3 Nyquist diagram of the first feedback amplifier.

Improvements in Intermodulation Distortion

Consider a two-tone input signal where the two frequencies are close together. That is, suppose that $f_2 = f_1+\Delta f$, where Δf is small in comparison to f_1. Suppose that the feedback loop in Fig. 5.2 is closed and the input level adjusted so that the output level remains the same as when the feedback loop was open. Let $\Delta IM(f_2-f_1)$ and $\Delta IM(2f_2-f_1)$ denote the reduction (in dB) in the second- and third order intermodulation distortion, respectively, observed at the output of the inverting amplifier when the feedback loop is closed.

According to (5.3) and (5.4), both the second- and third order IM products are reduced by a factor of $|1+\beta A_0(f_1)|$ when feedback is applied. That is, the distortion terms are reduced by

$$\Delta IM(f_2-f_1) = \Delta IM(2f_2-f_1) = 20\log|D(f_1)| \qquad (5.5)$$

where D is the desensitivity factor. As mentioned in section 5.1, the improvements in the IM distortion terms are independent of the output level as long as the LD transmitter is in its linear region of operation.

$|D(f)|$ is equal to the distance between the point $-1+j0$ and the point on the Nyquist plot corresponding to frequency f. Hence it can be found directly from Fig. 5.3. The expected reduction in IM distortion is then given by

equation (5.5). A plot of the calculated reduction in the IM distortion as a function of frequency is shown in Fig. 5.4.

Also shown in Fig. 5.4 are the observed reductions $\Delta IM(f_2-f_1)$ and $\Delta IM(2f_2-f_1)$. The measurements were made for a LD modulation current of 15 mA p-p and a two-tone input signal with a frequency separation of Δf = 0.1 MHz. The reductions in the second- and third order IM distortion are not exactly identical as predicted by (5.5); however, they differ by no more than 1 dB over the frequency range from 0 to 12 MHz.

the reductions in IM distortion decrease with frequency until, at a frequency of 10.8 MHz, there is no improvement seen when feedback is applied. For frequencies above 10.8 MHz, $\Delta IM(f_2-f_1)$ and $\Delta IM(2f_2-f_1)$ are both negative indicating that feedback actually degrades the linearity of the LD transmitter. The feedback amplifier is thus in the region of positive feedback for frequencies above 10.8 MHz. This is in good agreement with the calculated value for this frequency of 11.4 MHz. The observed reductions in IM distortion are also in very good agreement with the values calculated from the Nyquist diagram.

C. An Improved Feedback Scheme

The opto-electronic feedback scheme shown in Fig. 5.2 was effective in reducing IM distortion for frequencies from 0 to 10.8 MHz and gave an improvement of more than 10 dB for frequencies from 0 to 8 MHz. In this section the feedback

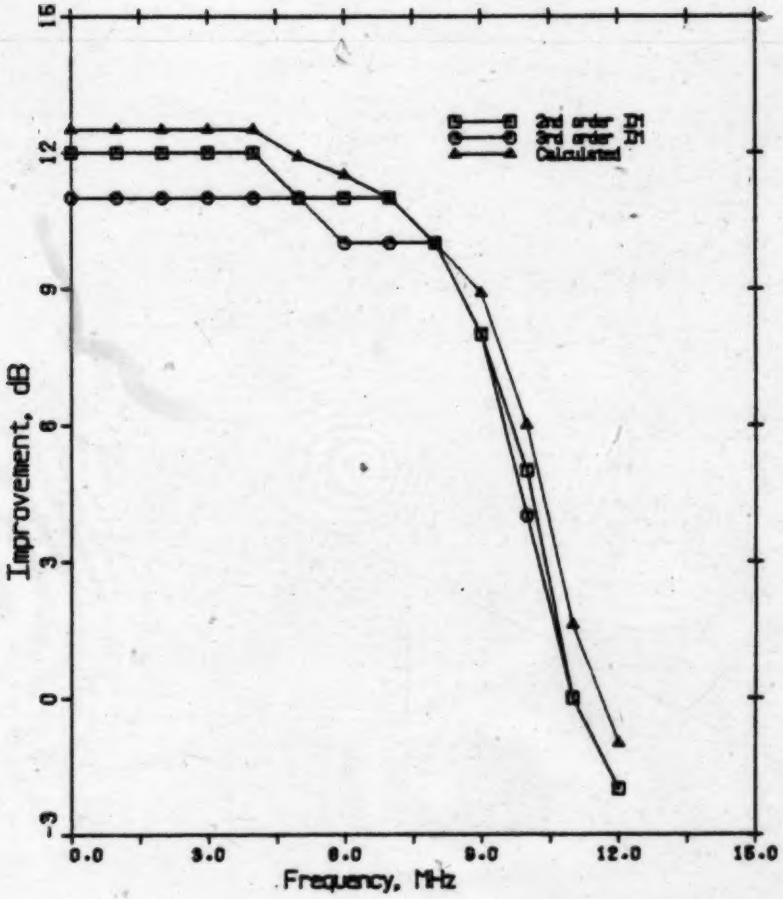

Figure 5.4 Calculated and observed reductions in IM distortions as a function of frequency f, (with Δf=0.1 MHz).

scheme is modified so that a larger reduction in IM distortion is obtained over a wide range of frequencies.

The amount of distortion reduction that could be obtained with the previous scheme was limited by the high input levels required by the LD driver. As well, the range of frequencies over which a reduction in distortion could be obtained was limited by the large phase shift introduced by the HP 461A inverting amplifier into the feedback loop. Both of these problems can be avoided by eliminating the HP 461A amplifier from the feedback loop and placing a wideband amplifier before the LD driver.

A block diagram of the new opto-electronic feedback scheme is shown in Fig. 5.5. The wideband amplifier is a cascade combination of two inexpensive Avantek monolithic amplifiers. The cascade amplifier has a bandwidth greater than 100 MHz and a phase shift that increases very slowly with frequency. By placing this amplifier before the LD driver, a higher loop gain can be achieved than in the previous feedback scheme. However, voltage feedback can no longer be used since the cascade amplifier is not a differential amplifier and has no inverting terminal. Instead, the input current signal and the feedback current signal are summed at the input node.

A simple resistive feedback network can no longer be used as this would allow feedforward of the input signal. Therefore, a buffer amplifier is used to provide the feedback signal. A common-collector amplifying stage serves

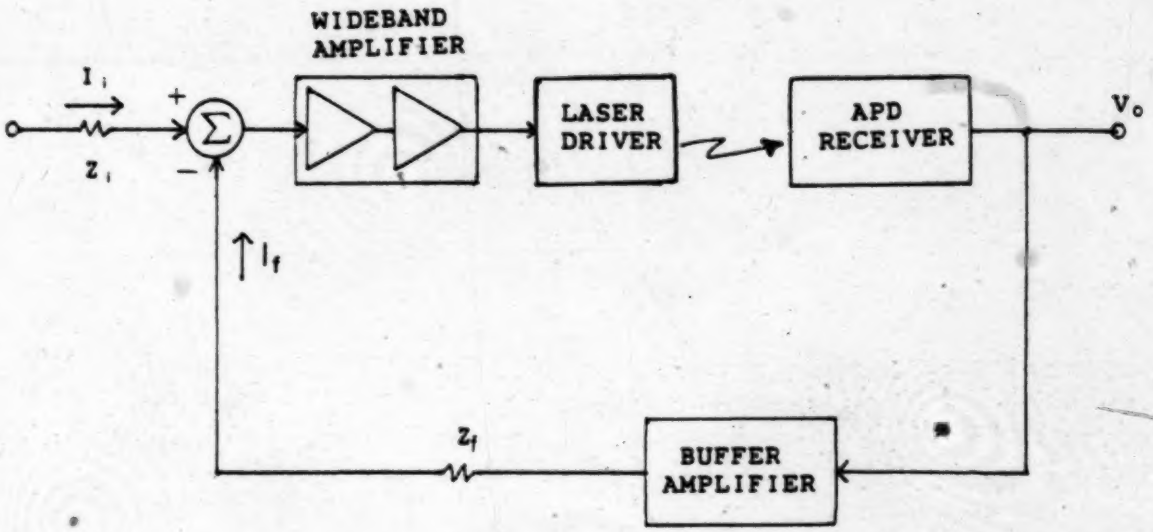

Figure 5.5 Block diagram of the second opto-electronic feedback scheme.

as the buffer amplifier.

Nyquist Plot

A Nyquist plot of this feedback amplifier is shown in Fig. 5.6. The low frequency loop gain is equal to 6.6 as compared to only 3.2 for the first feedback scheme. Another significant difference is that the feedback amplifier does not enter the region of positive feedback until a frequency of 16.8 MHz is reached as compared to 10.8 MHz for the first feedback scheme. The phase margin is equal to 67° and the gain margin is greater than 10 dB. The feedback scheme is therefore very stable.

Improvements in Intermodulation Distortion

The reduction in intermodulation distortion, as observed on the spectrum analyzer, for a two-tone input signal at frequencies f_1 = 7.0 MHz and f_2 = 7.4 MHz and a LD modulation current of 17 mA p-p is shown in Fig. 5.7. The IM distortion without opto-electronic feedback is $IM(f_2-f_1)$ = -26 dB and $IM(2f_2-f_1)$ = -30 dB; when feedback is applied, the IM distortion is reduced to $IM(f_2-f_1)$ = -40 dB and $IM(2f_2-f_1)$ = -43 dB. The improvements in IM distortion is thus $\Delta IM(f_2-f_1)$ = 14 dB and $\Delta IM(2f_2-f_1)$ = 13 dB.

The expected improvements in IM distortion can be calculated theoretically as a function of frequency by measuring $|D(f)|$ from Fig. 5.6. and using equation (5.5). These values are plotted in Fig. 5.8. Also shown in Fig. 5.8

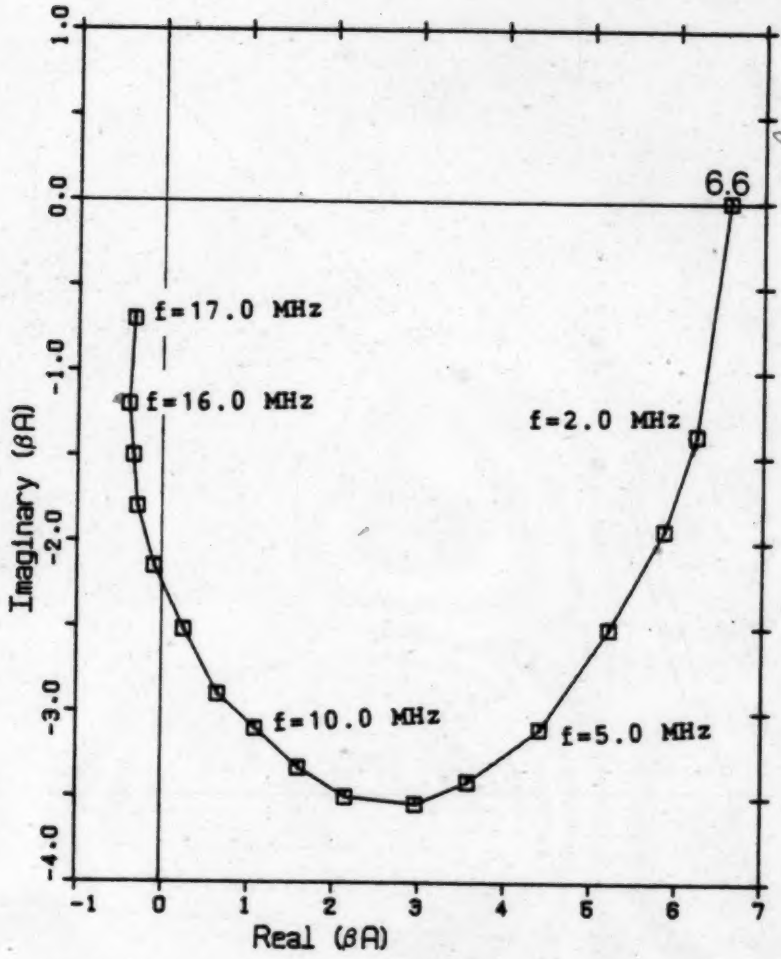

Figure 5.6 Nyquist diagram of the second feedback amplifier.

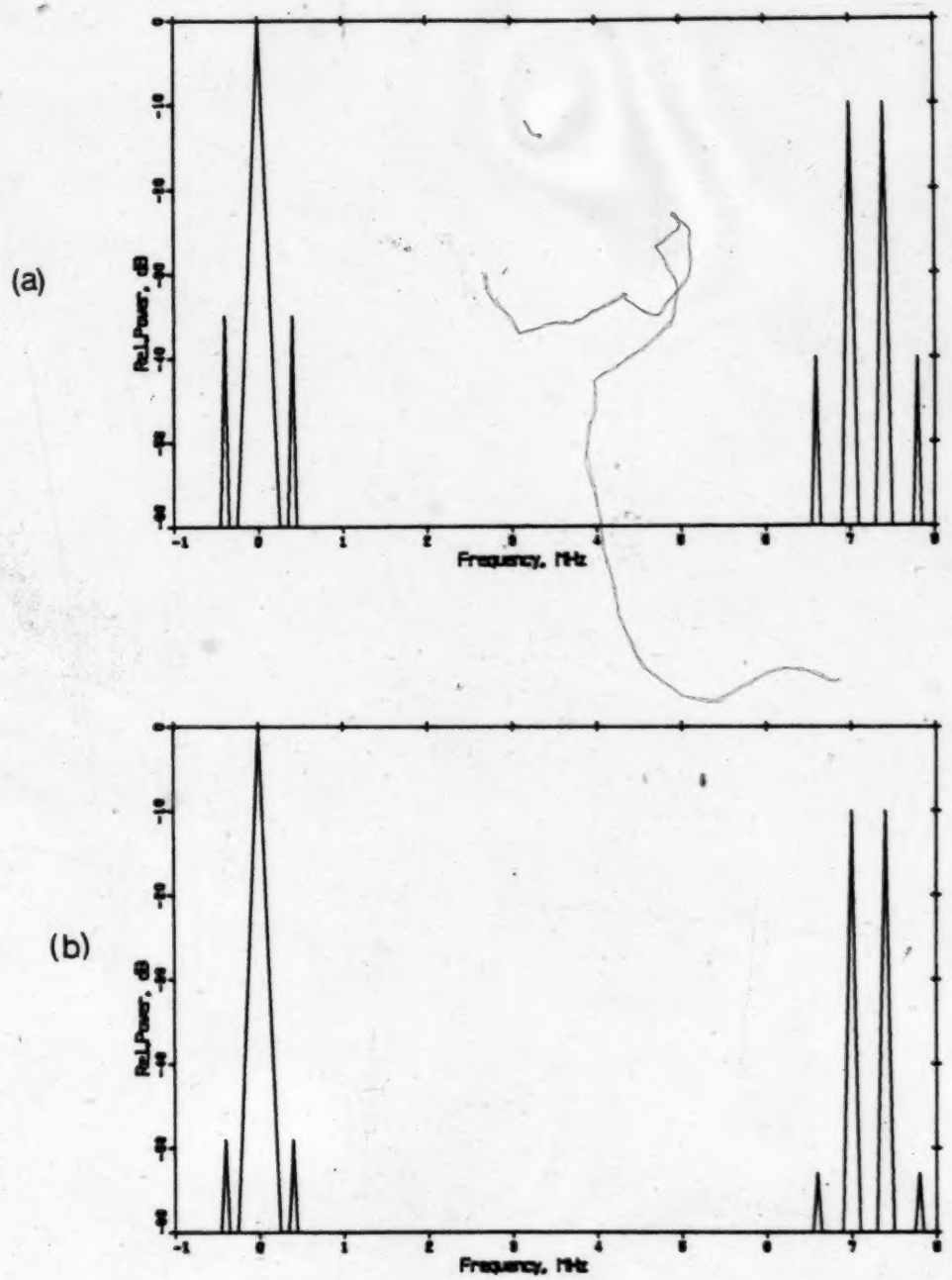

Figure 5.7 Intermodulation distortion present in laser diode output (a) without opto-electronic feedback and (b) with opto-electronic feedback (for a modulation current of 17 mA p-p).

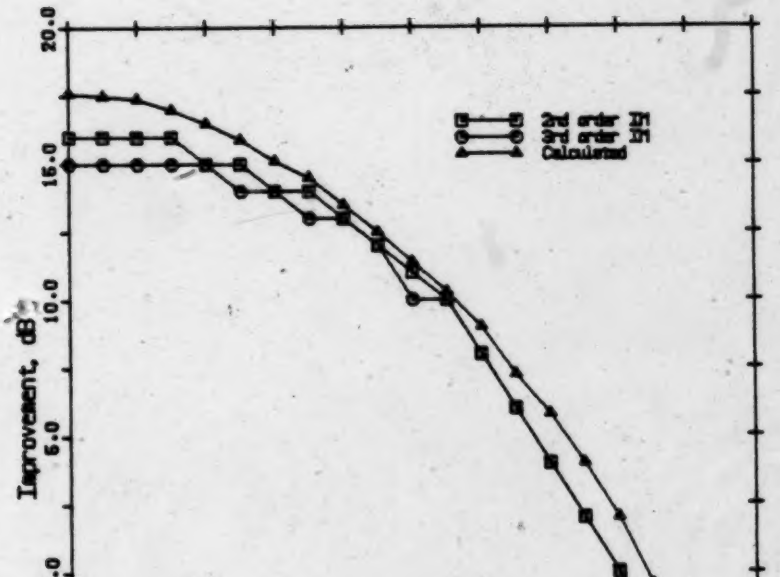

Figure 5.8 Calculated and observed reduction in IM distortion as a function of frequency f_1 (with Δf=0.1 MHz).

are the observed values of $\Delta IM(f_2-f_1)$ and $\Delta IM(2f_2-f_1)$ for f_1 varying between 0 and 17 MHz, The frequency separation Δf is kept constant at 0.2 MHz and the LD modulation current is 17 mA p-p.

The observed reduction in the second- and third order IM distortion are almost identical, in agreement with (5.5). In addition, the plots of $\Delta IM(2f_2-f_1)$ match very closely the calculated plot, except that they are shifted slightly to the left. Such a shift to the left would occur if the measured phase shifts of the loop gain $\beta A(f)$ were in error by about 7°. The frequency at which feedback has no effect on $IM(f_2-f_1)$ and $IM(2f_2-f_1)$ is equal to 16.0 MHz which is in good agreement with the calculated value of 16.8 MHz.

The measurements of $\Delta IM(f_2-f_1)$ and $\Delta IM(2f_2-f_1)$ were made for a fixed value of frequency separation, Δf=0.2 MHz, and for a fixed LD modulation current of 17 mA p-p. It was found, though, that the values of $\Delta IM(f_2-f_1)$ and $\Delta IM(2f_2-f_1)$ remained the same even as Δf and the LD modulation current were varied over a certain range. In Fig. 5.9, $\Delta IM(f_2-f_1)$ and $\Delta IM(2f_2-f_1)$ are plotted as a function of Δf. Frequency f_1 was fixed at 3.0 MHz while f_2 was varied between 3.01 and 6.0 MHz. Hence Δf varies between 0.01 and 3.0 MHz. It is seen that both $\Delta IM(f_2-f_1)$ and $\Delta IM(2f_2-f_1)$ remain constant at 16 dB and 15 db, respectively, over this range of Δf. The lower limit of 0.01 MHz is imposed by the frequency resolution of the spectrum analyzer.

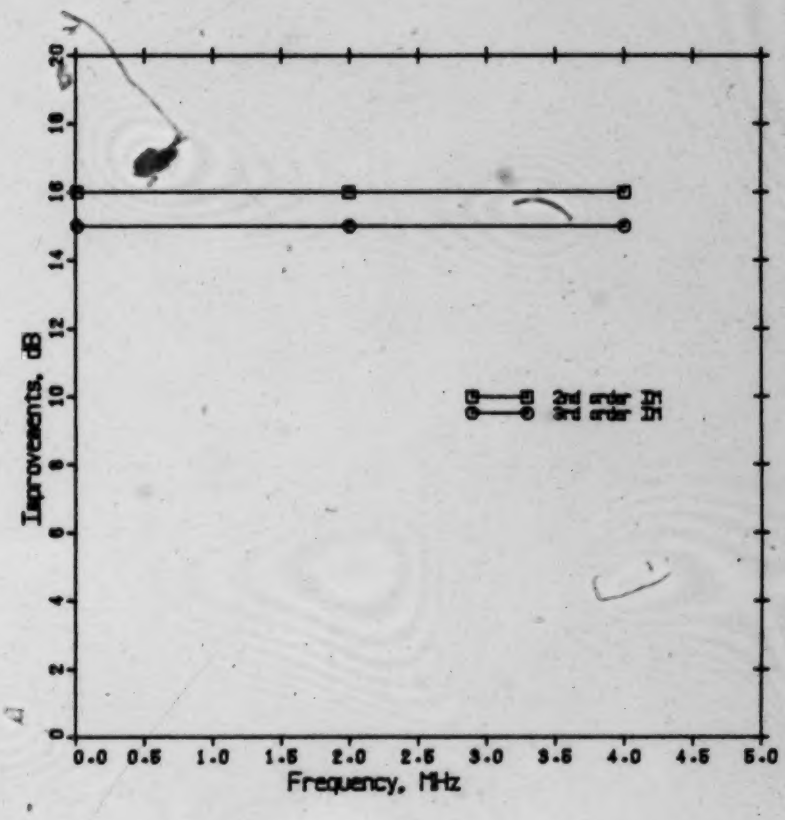

Figure 5.9 Variation of $\Delta IM(f_2-f_1)$ and $\Delta IM(2f_2-f_1)$ with Δf (with f_1=3.0 MHz).

In Fig. 5.10, $\Delta IM(f_2-f_1)$ is plotted as a function of the peak-to-peak LD modulation current for a two-tone input signal at frequencies f_1=3.0 MHz and f_2=3.2 MHz. The values of $\Delta IM(2f_2-f_1)$ are not plotted since they could not be measured for small values of modulation current. The value of $\Delta IM(f_2-f_1)$ remains constant at 16 dB for a modulation current of up to 20 mA p-p. For modulation currents larger than this, the gain of the LD driver starts decreasing. Thus, as explained in section 5.1, feedback becomes less effective in reducing IM distortion and there is a gradual decrease in $\Delta IM(f_2-f_1)$. A modulation current greater than 30 mA p-p results in the laser diode current dropping below the threshold value during part of each cycle. The consequent clipping and severe degradation of the output signal results in a rapid decline in $\Delta IM(2f_2-f_1)$. The reduction in third order IM distortion, $\Delta IM(2f_2-f_1)$, also declines in much the same manner as $\Delta IM(f_2-f_1)$ for modulation currents above 20 mA p-p.

The opto-electronic feedback scheme investigated in this section has provided significantly better results than the previous feedback scheme because of the use of inexpensive wideband amplifiers with low phase shifts in the feedback loop. The reductions in IM distortion obtained are at least 4 dB greater than that obtained in the previous scheme. In addition, the present scheme is effective in reducing distortion for frequencies up to 16 MHz as compared to only 10.8 MHz for the previous scheme.

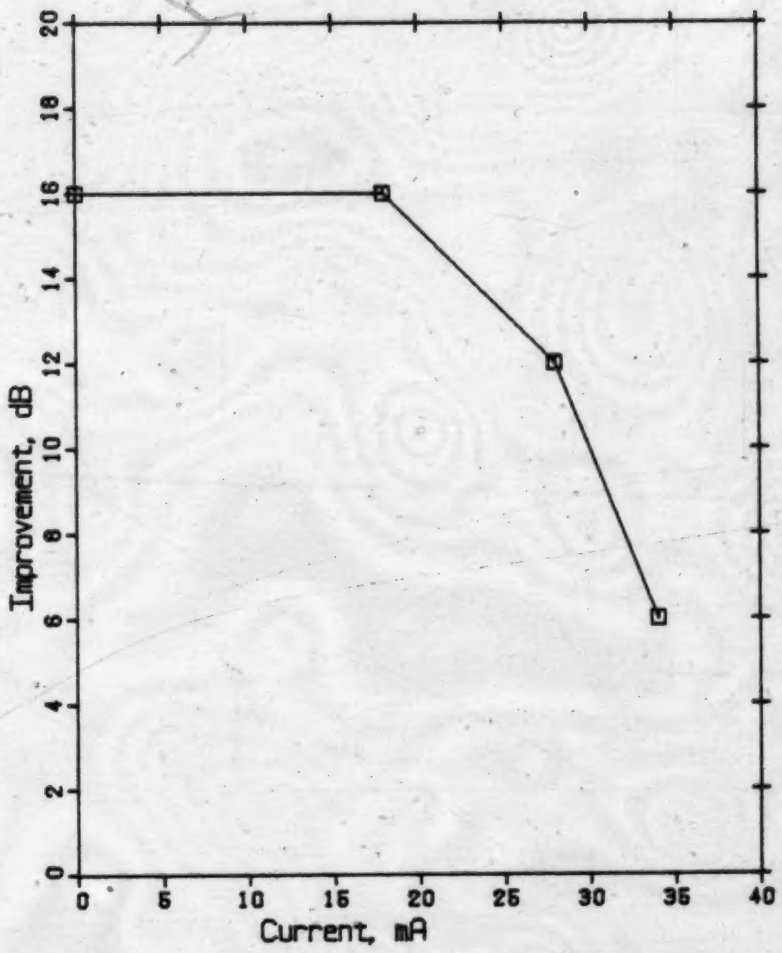

Figure 5.10 Plot of $\Delta IM(f_2-f_1)$ versus p-p laser diode modulation current.

D. Summary

Two opto-electronic feedback schemes were tested for their effectiveness in linearising the light-current characteristic of a laser diode. Reductions in second- and third order IM distortion of 12 dB and 11 dB, respectively, were obtained for frequencies up to 5 MHz with the first technique. As well, smaller improvements could be obtained for frequencies up to 10.8 MHz.

Significantly better results were obtained with the second technique by using inexpensive wideband amplifiers with low phase shifts. Second and third order IM improvements of 16 dB and 15 dB, respectively, were obtained for frequencies up to 5 MHz and improvements of more than 10 dB were obtained for frequencies up to 11 MHz. Smaller improvements were obtained for frequencies up to 16 MHz. This technique is therefore useful in the transmission of baseband video signals.

The Nyquist plots of the feedback amplifiers proved to be useful tools in evaluating the opto-electronic feedback schemes. The stability of the feedback amplifiers, the range of frequencies over which reductions in IM distortion could be obtained and the magnitude of the IM improvements at each frequency can all be calculated from the Nyquist plot.

The maximum frequency at which feedback is effective in reducing IM distortion is limited by the time delay around the feedback loop. The wideband amplifiers used in the second feedback scheme had a phase shift of only -15° at 16

MHz which represents a delay of only 2.6 ns. The time delay introduced by the LD driver, fiber pigtail, and optical receiver is much greater than this and is the main reason why the effectiveness of the feedback scheme is limited to frequencies less than 16 MHz.

A reduction of 5 ns in the time delay around the feedback loop could possibly be obtained through the use of a laser diode with a built-in monitoring photodiode. Such a decrease would mean that the feedback amplifier would not enter the region of positive feedback until the frequency reached 30 MHz. The opto-electronic feedback scheme would then be effective in reducing distortion for frequencies up to 30 MHz. This technique would then be useful in the transmission of about four or five video signals.

VI. DETERMINATION OF LASER DIODE CHARACTERISTICS

In this chapter, the static and dynamic light-current characteristics of the laser diode are determined. The dynamic characteristic is found at a modulation frequency high enough that thermal effects are small. The dynamic characteristic will be used in the succeeding chapter to determine the distortion characteristics of the laser diode.

A. Static Light-Current Characteristic

The static L-I characteristic of the laser diode (Laser Diode Labs, Model LCW-10F) is determined with the laser diode mounted on a heat sink and maintained at a constant temperature. By measuring the laser diode light output at various forward currents, the characteristic of Fig. 6.1 is obtained. Also shown in Fig. 6.1, as a dotted line, is an extrapolation of the linear section of this characteristic. The intersection of this line with the horizontal axis gives the threshold current which, for this laser diode, is 70 mA.

For forward currents less than 65 mA the light output consists entirely of spontaneous emission and the L-I characteristic of the laser diode is linear. Between 65 mA and 75 mA, the onset of stimulated emission causes the light-current characteristic to become strongly superlinear. The characteristic is approximately linear after this until the high radiance region is encountered at an optical output of approximately 1.5 mW. The L-I characteristic exhibits

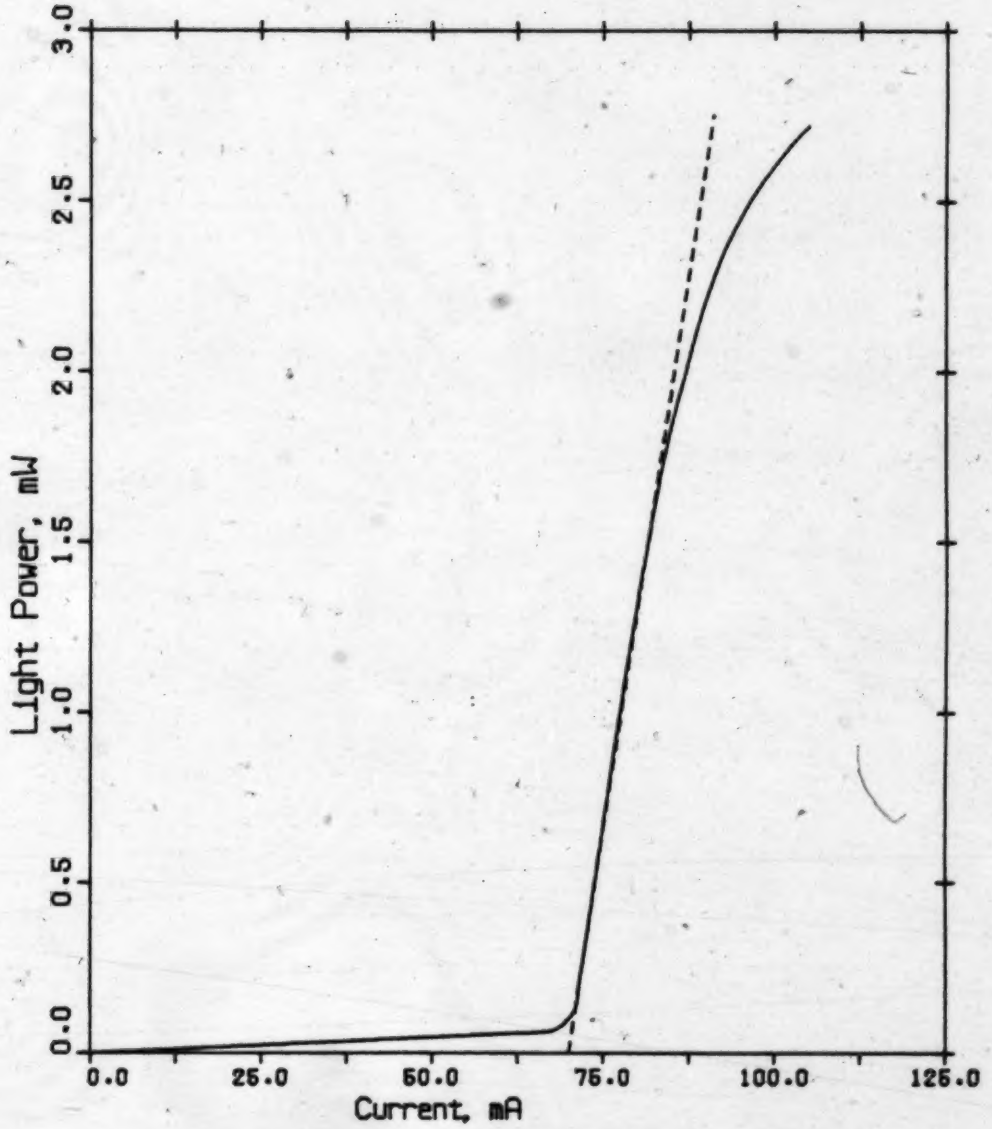

Figure 6.1 Static light-current characteristic of laser diode.

strong sublinearity in the high power region due to the effects of junction heating. No "kinks" were evident in the static L-I characteristic of this laser diode.

B. Dynamic Light-Current Characteristic

For modulation frequencies between d.c. and a few hundred Hertz, the transfer characteristic of the laser diode is given by the static L-I characteristic. Clearly, a large optical output at these frequencies would contain considerable amounts of distortion due to the nonlinearity of the static characteristic. But, for modulation frequencies in the megahertz range, the transfer characteristic of the laser diode is given by its dynamic L-I characteristic, which is normally more linear than the static characteristic. This is because the period of such a high frequency signal is smaller than the thermal time constant of the diode; hence the junction temperature does not vary with the input level as it does for low frequency signals.

The dynamic characteristic can be determined by using the circuit shown in Fig. 6.2. A triangular input signal, V_i, is connected to the non-inverting terminal of the laser driver. The output, V_o, of the optical receiver and the input, V_i, are then of opposite polarity. A wideband operational amplifier subsequently sums the two signals to produce the error signal V_e. This procedure, where the operational amplifier is used as a summer rather than as a

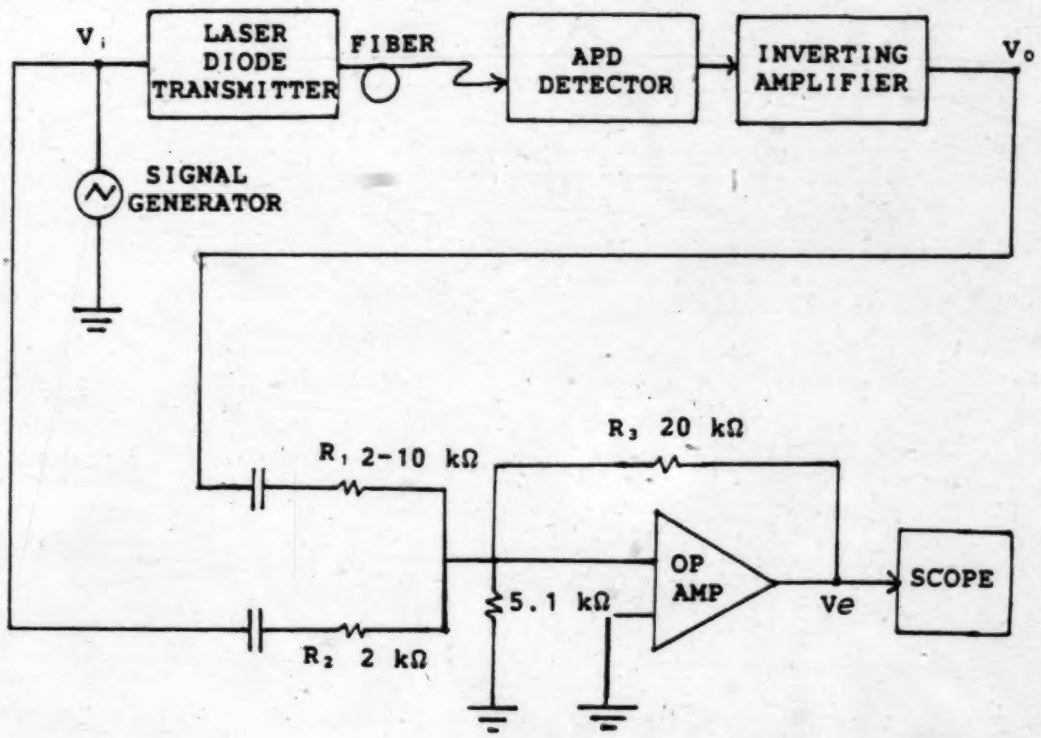

Figure 6.2 Circuit used to determine the dynamic light-current characteristic of the laser diode.

differential amplifier, eliminates problems that can arise due to the decrease in the common mode rejection ratio seen at high frequencies (i.e. > 100 kHz).

The error signal Ve is given by

$$Ve = -(R_3/R_2)[V_i+(R_2/R_1)V_o]$$
$$= -10[V_i+(R_2/R_1)V_o] \qquad (6.1)$$

Since V_o is larger than V_i (by a factor of between 3 and 4) it has to be scaled down to the same size as V_i. This is done by varying resistor R_1 until the error signal Ve, as observed on the oscilloscope, is minimized.

If V_o, properly scaled, is exactly the same as V_i then the error signal Ve would equal zero. If V_o is equal to zero then the error signal Ve would equal $-10\ V_i$. Thus the percentage deviation of the dynamic transfer characteristic of the laser diode from that of a linear characteristic can be calculated if the waveforms $Ve(t)$ and $V_i(t)$ are known. The percentage deviation is given by

$$\% = (Ve/10V_i) \times 100 \qquad (6.2)$$

The error waveform possesses mirror symmetry since the input signal also does. However, this mirror symmetry is seen to break down at frequencies greater than a few hundred kilohertz. This is due to delay between V_o and V_i and to the introduction of frequency dependent distortion and

attenuation by the operational amplifier at these higher frequencies. Under these circumstances, the error waveform $V_e(t)$ can no longer be used to determine the dynamic transfer characteristic of the laser diode.

The highest frequency at which the error waveform still possesses good mirror symmetry is 350 kHz. A section of the error voltage waveform, $V_e(t)$, is shown in Fig. 6.3(a). Since the input waveform, $V_i(t)$, is a triangular waveform, the laser diode current varies linearly with time during each half-cycle. Hence the horizontal axis has been calibrated in terms of the laser diode current. The portion of the error waveform shown corresponds to a laser diode current between 76 mA and 96 mA. The laser diode modulation has been kept small to minimize the distortion introduced by the laser driver circuitry and by the receiver amplifier. Consequently, the L-I characteristic of the laser diode and the transfer characteristic of the transmitter-receiver combination are approximately identical.

To determine the variation of the laser characteristic with frequency, the error waveform for a very low modulation frequency is also obtained. The transfer function of the optical receiver-amplifier stage has a zero at s=0 and hence introduces large phase shifts at very low frequencies. The lowest laser diode modulation frequency for which a good error voltage waveform is obtained is 15 kHz. A section of this waveform corresponding to a laser diode current ranging between 76 mA and 96 mA is shown in Fig. 6.3(b). The

(a)

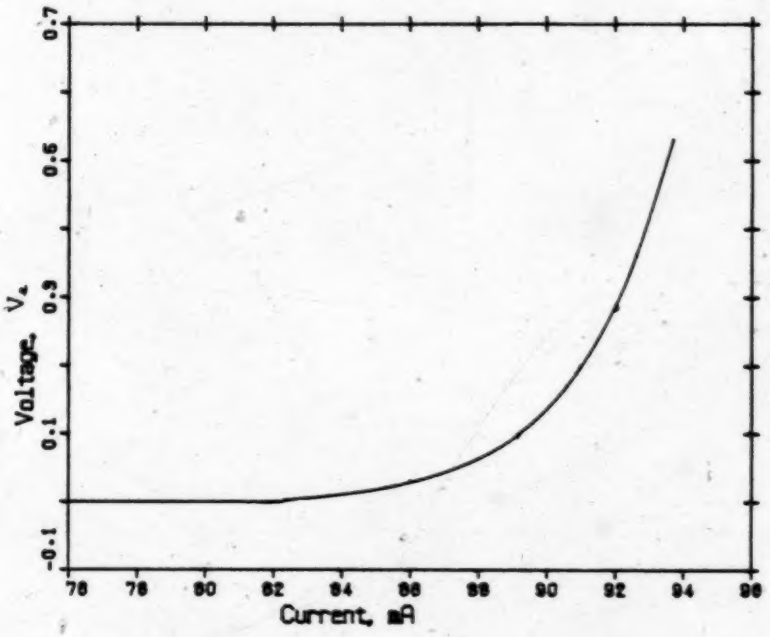

(b)

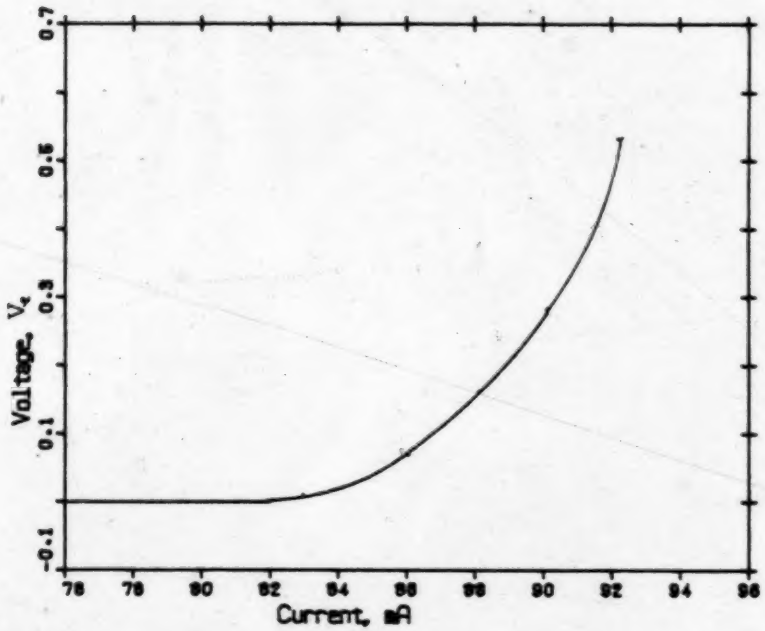

Figure 6.3 The error voltage waveform $V_e(t)$ for a laser diode modulation frequency of (a) 350 kHz and (b) 15 kHz.

horizontal and the vertical scales are the same as in 6.3(a). The error voltage is noticeably greater at a modulation frequency of 15 kHz than at 350 kHz.

From a knowledge of the error voltage waveform, $V_e(t)$, the percentage deviation of the dynamic transfer characteristic of the laser diode from that of an ideal linear characteristic can be found from equation (6.2). Figure 6.4 plots these percentage deviations for laser diode currents between 74 mA and 96 mA and for modulation frequencies of 15 kHz and 350 kHz.

Knowing that the slope of the linear section of the laser diode L-I characteristic is 0.13 mW/mA and that the threshold current is 70 mA, the dynamic transfer characteristics of the laser diode can be plotted at different modulation frequencies by making use of Fig. 6.4. The dynamic transfer characteristic for modulation frequency of 15 kHz and 350 kHz, the static characteristic and the linear extrapolation are all plotted in Fig.6.5. The high radiance region where the sublinearity of the characteristics is evident is shown in more detail in Fig. 6.6.

At the threshold current (70 mA @ 25°C) the characteristics exhibit severe superlinearity due to the onset of stimulated emission. Above 74 mA, the characteristics have an approximately linear region of 10mA. A magnification of the error voltage waveform in this linear region reveals that the L-I characteristic is actually

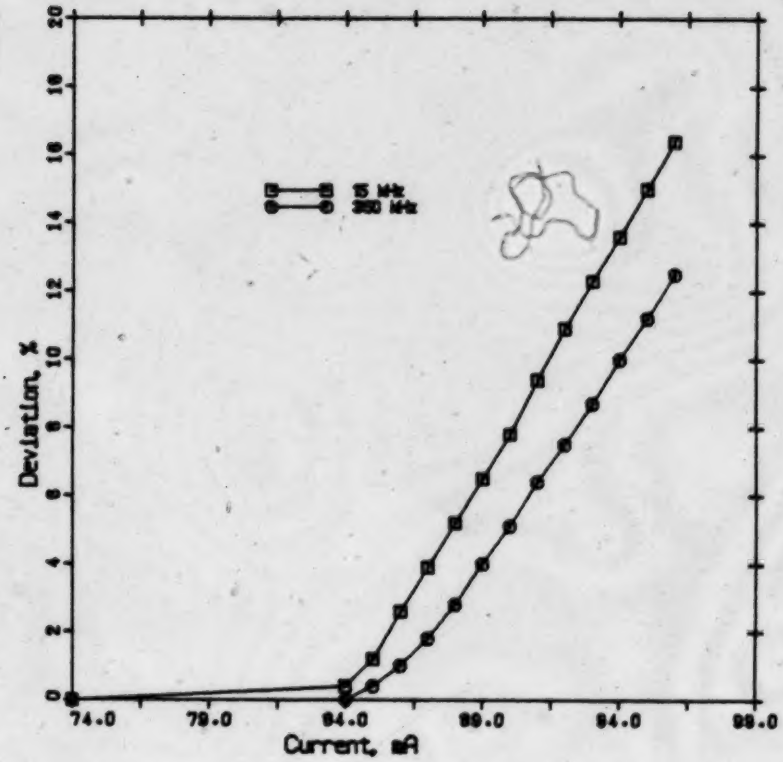

Figure 6.4 Percentage deviation of the dynamic characteristic of the laser diode from that of an ideal linear characteristic at modulation frequencies of 15 kHz and 350 kHz.

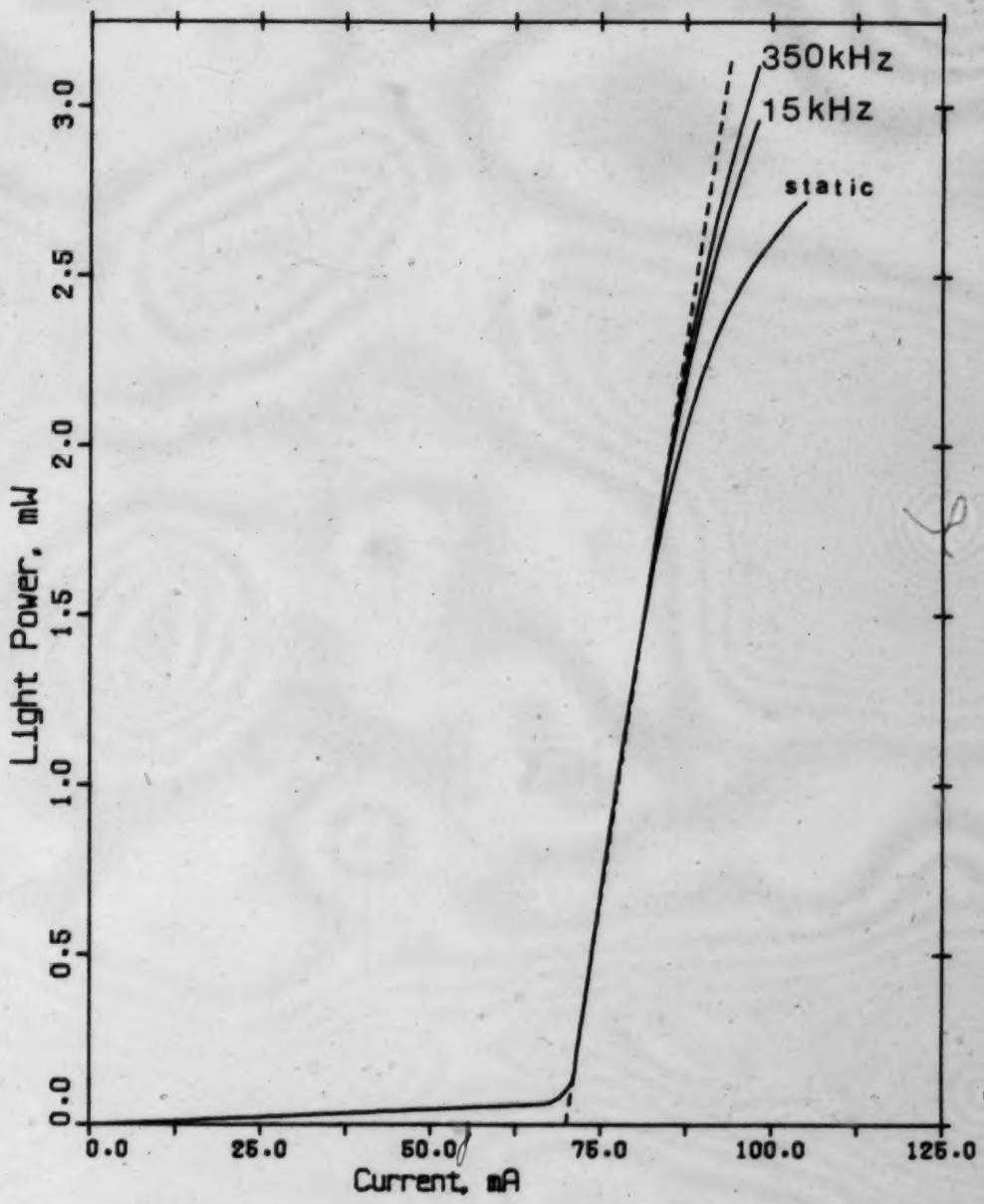

Figure 6.5 Static and dynamic light-current characteristics of laser diode.

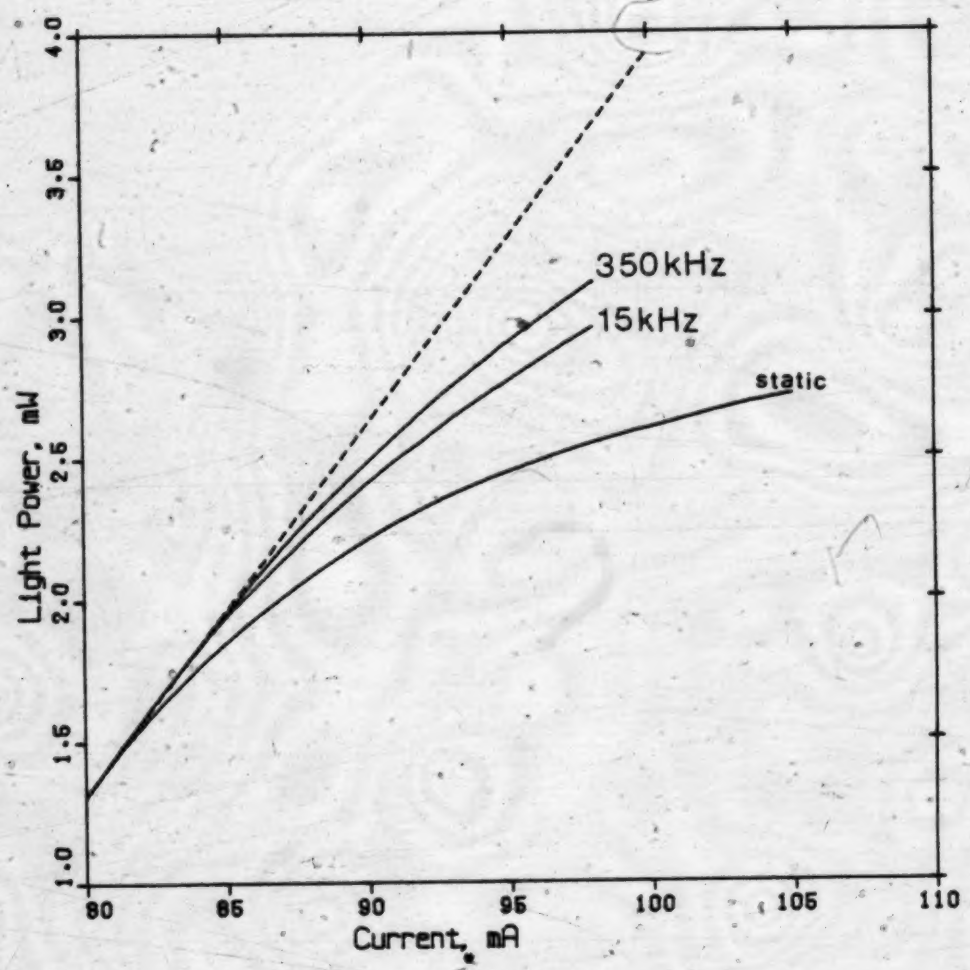

Figure 6.6 Sublinearity of the static and dynamic light-current characteristics in the high radiance region.

slightly superlinear. The deviation from linearity, however, is very small; the IM distortion if the LD is modulated in this region is less than -45dB. This is less than or equal to the distortion introduced by other components in the experimental setup. Therefore, the deviation from linearity in this region is negligible and this region of the L-I characteristic will be modelled by a straight line. The slope of this line is the same as that of the static characteristic shown in Fig. 6.1, namely 0.13 mW/mA.

At higher optical outputs a point is reached when the characteristic switches from being superlinear to being sublinear. The position of this inflection point depends on the laser diode modulation frequency. For the static transfer characteristic the inflection point occurs at a current of 81 mA. This shifts to 83 mA for a modulation frequency of 15 kHz and 84 mA for a modulation frequency of 350 kHz. The sublinearity of the static characteristic above its inflection point is much more severe than is the case for a modulation frequency of 350 kHz or even 15 kHz. Still, from Fig. 6.4, it can be seen that the percentage deviation of the transfer characteristic (at 350 kHz) from a linear characteristic exceeds 10% in the very high radiance region. Consequently, large-signal modulation of the laser diode will result in the distortion exceeding -30 dB.

The transfer characteristic corresponding to a modulation frequency of 15 kHz shows more sublinearity than the characteristic corresponding to a modulation frequency

of 350 kHz. Hence, thermal effects are significant in the frequency range between 15 kHz and 350 kHz. The sublinearity of the static characteristic is much more pronounced than that of the characteristic corresponding to a 15 kHz modulation frequency. This shows that thermal effects are most severe at frequencies less than 15 kHz.

C. Summary

The dynamic L-I characteristic of the laser diode was determined for a modulation frequency of 350 kHz. This was done by finding the deviation of the dynamic characteristic from a perfectly linear characteristic and then amplifying this small signal using an operational amplifier.

To determine the effect of junction heating on the laser characteristic, the dynamic L-I characteristic at a modulation frequency of 15 kHz and the static characteristic (i.e., modulation frequency of zero) were also found. It was verified that the nonlinearity of the characteristics became increasingly severe at lower frequencies. While some change in the nonlinearity of the characteristics was noticed between 15 kHz and 350 kHz, it was seen that thermal effects are most severe at frequencies less than 15 kHz.

It is concluded that thermal effects are small at frequencies higher than 350 kHz. The change in the transfer characteristic for modulation frequencies between 200 KHz and 350 KHz was observed to be slight. The dynamic characteristic obtained at this frequency will therefore be

used in the next chapter to determine the distortion characteristics of the laser diode at much higher frequencies.

VII. ANALYSIS OF LASER DIODE DISTORTION

The light-current characteristic of laser diodes designed for use in optical fiber communications is virtually independent of modulation frequency within the approximate range 1-100 MHz. At higher frequencies, harmonics of the modulation signal approach the resonance frequency of the laser diode with a consequent degradation of LD linearity. At frequencies lower than 1 MHz, active layer heating causes severe sublinearity of the laser characteristic at high optical outputs. The excess distortion resulting from both these phenomena are frequency dependent and hence represent a nonlinearity with memory. For modulation frequencies within the range ≃ 1-100 MHz, however, a laser diode behaves like a simple nonlinearity without memory [84],[88]; i.e., the LD's distortion and input-output characteristics are independent of frequency. The LD distortion characteristics can then be determined by modelling the dynamic L-I characteristic by a polynomial power series. The coefficients of the power series are constants independent of frequency or time, since the LD's nonlinearity is memory-free.

Two such methods are examined in this chapter: one where the LD characteristic is modelled by a simple polynomial curve and another where a polynomial spline model is employed. The IM distortions and their variation with LD bias current and modulation depth are theoretically

calculated using these models and compared with the observed data.

A. Single Polynomial Model

In this section, a fourth degree polynomial will be fitted to the dynamic light-current characteristic of the laser diode using an univariate curvilinear regression model. Expressions for the intermodulation products will be derived from this model. The behaviour of the intermodulation distortion as the LD bias current is varied is calculated and compared to experimental results. In the next section, these results will be compared to those from the case where the light-current characteristic is modelled by a polynomial spline.

Formulas for Intermodulation Distortion

The derivation of the laser diode intermodulation distortion is now described. Let x denote the deviation of the laser diode current from its quiescent value and y the deviation of the laser diode light output from its quiescent value. A section of the light-current characteristic around the quiescent point x=0, y=0, can then be modelled by a polynomial curve. The best fitting polynomial (in the mean square sense) is found using the univariate curvilinear regression subroutine RLFOR from the IMSL library). A fourth degree polynomial is used for curve fitting even though only terms of order three or less are used to calculate the

second- and third order intermodulation products. The polynomial approximation is of the form

$$y = a_1x + a_2x^2 + a_3x^3 + a_4x^4 \qquad (7.1)$$

If the laser diode is modulated by the two-tone signal

$$x(t) = A\cos(\omega_1 t) + B\cos(\omega_2 t) \qquad (7.2)$$

then, from equation 7.1, the light output is given by

$$\begin{aligned} y(t) = {} & \text{dc term} \\ & + (a_1A + 3a_3A^3/4 + 3a_3AB^2/2)\cos(\omega_1 t) \\ & + (a_1B + 3a_3B^3/4 + 3a_3A^2B/2)\cos(\omega_2 t) \\ & + (a_2A^2/2)\cos(2\omega_1 t) + (a_2B^2/2)\cos(2\omega_2 t) \\ & + a_2AB[\cos(\omega_1+\omega_2)t + \cos(\omega_1-\omega_2)t] \\ & + (a_3A^3/4)\cos(3\omega_1 t) + (a_3B^3/4)\cos(3\omega_2 t) \\ & + (3a_3A^2B/4)[\cos(2\omega_1+\omega_2)t + \cos(2\omega_1-\omega_2)t] \\ & + (3a_3B^2A/4)[\cos(2\omega_2+\omega_1)t + \cos(2\omega_2-\omega_1)t] \end{aligned} \qquad (7.3)$$

The dc term is due to the fact that the light output is not symmetrical about y=0 because of the sublinearity of the light-current curve. The first two terms after that are the fundamental tones at frequencies f_1 and f_2; the next two are second harmonics at frequencies $2f_1$ and $2f_2$; and the fifth and sixth terms are the second order intermodulation products at frequencies f_2-f_1 and f_2+f_1. The seventh and

eighth terms of equation 7.3 are the third harmonics and the last four terms represent the third order intermodulation products. Note that if the modulation coefficients A and B are functions of time rather than constants then the fundamental terms in equation 7.3 indicate that there has been a transfer of modulation from one carrier to the other (resulting in cross-modulation distortion). The coefficients of the cross-modulation terms are a_3AB^2 and a_3A^2B. Hence, cross-modulation distortion disappears if $a_3 = 0$. Note also that the second order distortion terms vanish if $a_2 = 0$ and that the third order distortion terms vanish if $a_3 = 0$.

For simplicity, the case of an equal amplitude two-tone signal is considered,

$$x(t) = A[\cos(\omega_1 t) + \cos(\omega_2 t)] \tag{7.4}$$

From (7.3), the peak power in any of the third order intermodulation distortion terms is equal to $3|a_3|A^3/4$, the peak power in either of the second order intermodulation distortion terms is equal to $|a_2|A^2$, and the peak power in either of the two fundamental tones is equal to $|a_1|A$. The second- and third order IM distortions are thus given by

$$\begin{aligned} IM(f_2-f_1) &= |a_2/a_1|\ A \\ IM(2f_2-f_1) &= 3|a_3/a_1|\ A^2/4 \end{aligned} \tag{7.5}$$

respectively. Expressed in terms of decibels, these

equations become

$$IM(f_2-f_1) = -12 + 20\log(|a_2/a_1|) + 20\log(M) \qquad (7.6)$$
$$IM(2f_2-f_1) = -24 + 20\log(|3a_3/4a_1|) + 40\log(M)$$

where M, the peak-to-peak modulation current, is equal to 4A.

By performing a polynomial interpolation of different sections of the L-I characteristic, the IM distortion for any given LD bias current and modulation level can be calculated using (7.6).

Distortion versus Bias Current

The behavior of the second- and third order IM distortion as a function of the laser diode bias current is now calculated by performing a single polynomial interpolation at different points of the light-current characteristic. The calculations are performed assuming a constant laser diode current modulation of 4mA p-p for the bias currents 70 mA, 84 mA, 88 mA, 92 mA and 96 mA. The computer program that performs the polynomial interpolation and calculates the second- and third order intermodulation distortion is given in Appendix I.

An unweighted, univariate curvilinear regression analysis using orthogonal polynomials is carried out using the IMSL routine RLFOR. The input to the program is a set of nine points (x_i,y_i) lying on the laser diode light-current

characteristic. The points span a segment of the dynamic light-current characteristic that is centered at the laser diode bias current and extends 2 mA on either side. The interpolation polynomial is that fourth degree polynomial that minimizes the mean square error between itself and the nine data points. Polynomials of any other degree can also be used in the interpolation process. By increasing the degree of the interpolating polynomial, arbitrarily small mean square errors can be obtained. However, the intermodulation distortion levels calculated from this polynomial would be in error: the reason for this is that such an interpolation would not be sufficiently "smooth". As an extreme case, if the degree of the interpolating polynomial is greater than or equal to the number of data points then the mean square error is zero (since the polynomial goes through all the data points) but the polynomial oscillates about the data points. Since nine data points are being used it is found that an interpolating polynomial of degree four strikes the proper balance between degree of smoothness and minimal mean square error.

The calculated values of second- and third order IM distortion for laser diode bias currents of 70 mA, 84 mA, 88 mA, 92 mA and 96 mA and for a constant modulation current of 4 mA p-p are plotted in Fig. 7.1 and Fig. 7.2, respectively. Fig. 7.1 also shows the observed values of IM(f_2-f_1). The values of IM($2f_2$-f_1) were too small to be measured at this modulation level. The measurements were made using a

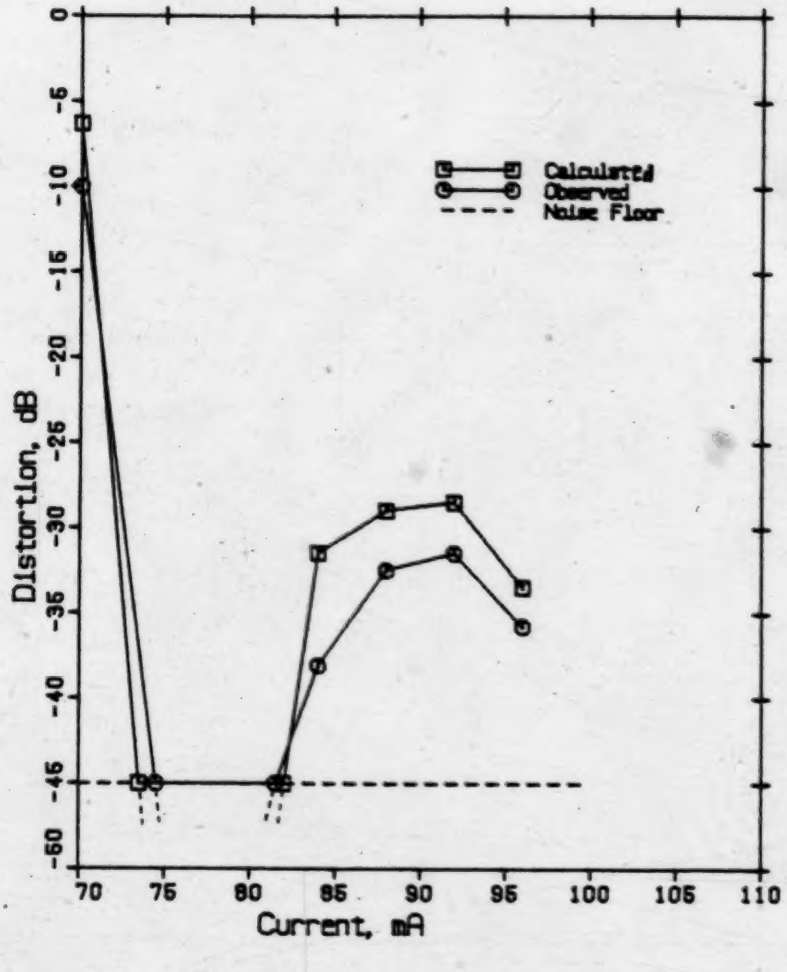

Figure 7.1 Calculated and measured values of IM(f_2-f_1) as a function of LD bias current (with f_1 = 10.0 MHz, f_2 = 10.2 MHz, and modulation current = 4mA p-p).

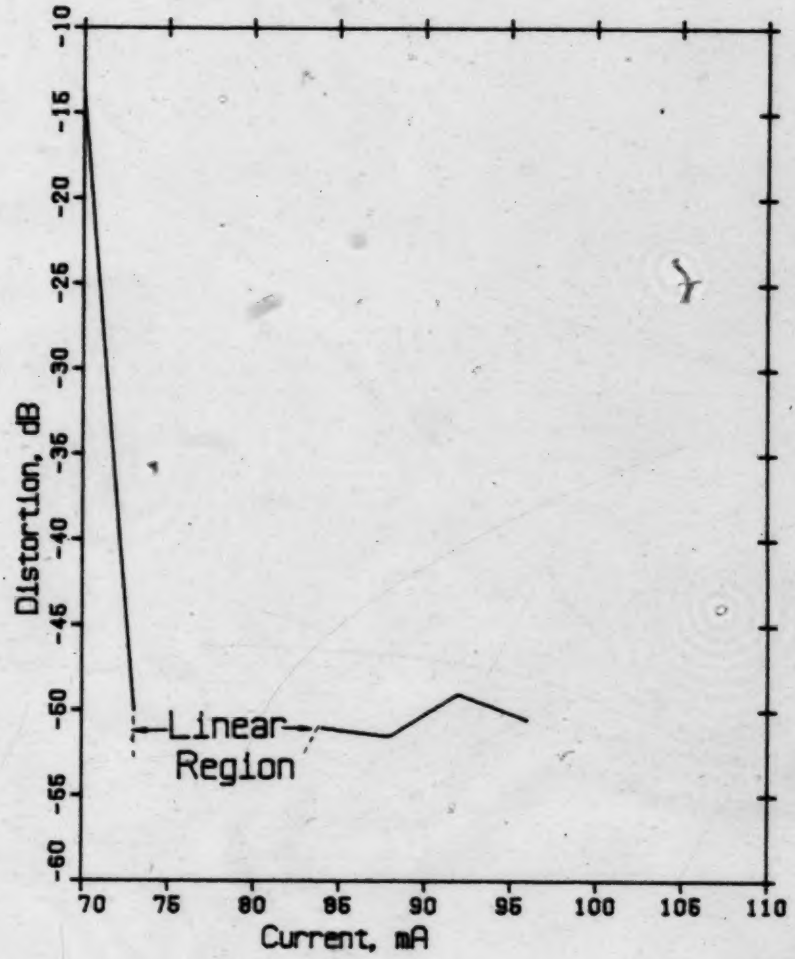

Figure 7.2 Calculated values of IM($2f_2$-f_1) as a function of LD bias current (for a modulation current of 4 mA p-p).

two-tone input signal at fundamental frequencies f_1 = 10.0 MHz and f_2 = 10.2 MHz. The measured values were found to be virtually independent of frequency as long as the two fundamental frequencies were between 1 MHz and the upper bandwidth of the LD transmitter. This is due to the fact that the nonlinearity of the laser diode is memory free in this frequency range.

This frequency independence of $IM(f_2-f_1)$ and $IM(2f_2-f_1)$ is illustrated in Fig. 7.3. The observed values of $IM(f_2-f_1)$ and $IM(2f_2-f_1)$ are plotted as a function of frequency f_1, with Δf constant at 0.1MHz. The laser diode bias current is 84 mA and the modulation current is 12 mA p-p. It can be seen that the values of the second- and third order IM distortion change by less than 1 dB over the frequency range 1 MHz to 40 MHz.

From Fig. 7.1 it can be seen that $IM(f_2-f_1)$ decreases rapidly as the bias current is increased beyond the threshold current of the laser diode (70 mA). When the modulation is entirely in the linear region of the light current characteristic, the second order IM distortion is less than -45 dB and lies below the noise floor of the spectrum analyzer. As the laser diode bias current is increased, the region of modulation of the laser diode encroaches more and more into the sublinear section of the light-current characteristic, resulting in a sharp rise in intermodulation distortion. In the high radiance region above 92 mA, however, the intermodulation distortion

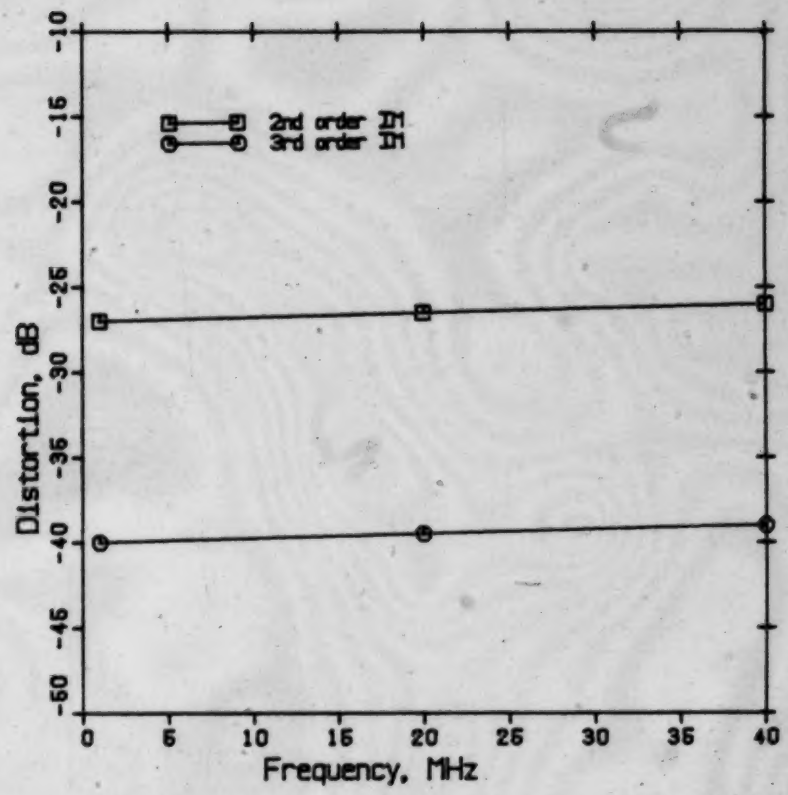

Figure 7.3 Observed variation of IM(f_2-f_1) and IM($2f_2$-f_1) with frequency f_1 (with Δf=0.1 MHz, LD bias current = 84 mA, and LD modulation current = 12 mA p-p).

actually starts decreasing. This can be explained by the fact that the slope of the light current characteristic is changing at a slower rate in the high radiance region than in the region between 85 mA and 90 mA. Thus, modulation by a small signal (such as 4 mA p-p) will result in less distortion in the high radiance region than in the region between 85 mA and 90 mA.

The plot of the calculated values of second order IM distortion, illustrated in Fig. 7.1, shows roughly the same behaviour as the plot of the measured values. The calculated values are within 3 dB of the measured values except in a neighbourhood of 85 mA where the values are anomalously high (6 dB higher than the measured values). The calculated value of $IM(2f_2-f_1)$ at 84 mA is also anomalously high; it predicts that the distortion at 84 mA is greater than that at 88 mA whereas in actuality the values of both $IM(f_2-f_1)$ and $IM(2f_2-f_1)$ are known to increase between 84mA and 88 mA.

The reason that the calculated values of $IM(f_2-f_1)$ and $IM(2f_2-f_1)$ are more inaccurate in a neighbourhood of the inflection point at 84 mA than in other regions of the light-current characteristic could be that this point is the boundary between two distinct regions. To the left of this point, the second derivative is almost zero and the curve is quite linear. To the right of this point the second derivative takes an almost disontinuous jump in the negative direction and the curve becomes sublinear. It is not possible for a polynomial to be perfectly linear in one

region and sublinear in another. Thus interpolation of both these regions by a single fourth degree polynomial results in a mean square error that is much larger than if the interpolation was performed in only one of these regions. The mean square error can be made small of course by using an interpolating polynomial of much higher degree; but such a polynomial tends to oscillate about the data points, as mentioned earlier.

B. Polynomial Spline Model

For laser diode bias currents between 83 mA and 87 mA, much better correlation between calculated and measured values of IM distortion can be obtained by using two polynomials to model the light-current characteristic; one polynomial (a straight line) for the region to the left of 84 mA and another polynomial for the sublinear region to the right of 84 mA.

Formulas for Intermodulation Distortion

As in the previous section, let x denote the deviation of the LD current from its quiescent value (@ 84 mA) and y the deviation of the LD light output from its quiescent value. The region to the left of the quiescent point ($x<0$) is modelled by a straight line. In the previous sction, the slope of this line segment was found to be 0.131 mW/mA. In the region to the right of the quiescent point ($x>0$) a polynomial interpolation is performed. The same IMSL routine

(RLFOR) is used as in the previous section but with two differences. Firstly, the interpolation is only performed in the region x>0 instead of on both sides of the quiescent point. Secondly, two additional constraints are imposed on the interpolating polynomial; that its constant term be zero, and that the coefficient of its first degree term be 0.131 mW/mA. The first condition ensures that the polynomial goes through the origin x=0, y=0. The second condition allows the polynomial spline to be written as the sum of a straight line of slope 0.131 mW/mA and some higher order perturbation terms. Thus the polynomial spline model is of the form

$$y = \begin{cases} 0.131x & \text{for } x<0 \\ 0.131x + a_2x^2 + \beta_3x^3 & \text{for } x>0 \end{cases} \qquad (7.7)$$

If the laser diode is modulated by the two-tone signal

$$x(t) = A\,[\cos(\omega_1 t) + \cos(\omega_2 t)] \qquad (7.8)$$

then, from equations 7.3, 7.7, and 7.8, the laser diode light output is given by

$$y(t) = \begin{cases} 0.131\,A\,[\cos(\omega_1 t) + \cos(\omega_2 t)] & \text{if } x(t)<0 \end{cases} \qquad (7.9)$$

$$0.131\ A\ [\cos(\omega_1 t) + \cos(\omega_2 t)]$$
$$+a_2A^2\cos(\omega_2-\omega_1)t + (3a_3A^3/4)\cos(2\omega_2-\omega_1)t$$
$$+ \text{ other terms} \qquad \text{if } x(t)>0$$

where "other terms" denotes components at frequencies $2f_1$, $2f_2$, f_1+f_2, $2f_1+f_2$, etc..., which do not affect the calculation of $IM(f_2-f_1)$ and $IM(2f_2-f_1)$.

Equation 7.9 can be rearranged and written as

$$y(t) = 0.131\ A[\cos(\omega_1 t) + \cos(\omega_2 t)] + y_2(t) + y_3(t) + \text{other terms} \qquad (7.10)$$

where

$$y_2(t) = \begin{cases} a_2A^2\cos(\omega_2-\omega_1 t) & \text{whenever } x(t)>0 \\ 0 & \text{whenever } x(t)<0 \end{cases} \qquad (7.11)$$

and

$$y_3(t) = \begin{cases} (3a_3A^3/4)\cos(\omega_2-\omega_1)t & \text{whenever } x(t)>0 \\ 0 & \text{whenever } x(t)<0 \end{cases} \qquad (7.12)$$

The signal $x(t)$ varies sinusoidally with period $T_1 = 2/(f_1+f_2)$ and has a beat frequency of period $T_2 = 1/(f_2-f_1)$. The signal $y_2(t)$ represents the sinusoid $a_2A^2\cos(\omega_2-\omega_1)t$ sampled every T_1 seconds using a gating pulse of width $T_1/2$. Similarly, the signal $y_3(t)$ represents the sinusoid

$(3a_3A^3/4)\ \cos(2\omega_2-\omega_1)t$ sampled every T_1 seconds using a gating pulse width $T_1/2$.

By calculating the Fourier coefficients of $y_2(t)$ and $y_3(t)$, equations 7.11 and 7.12 can be rewritten as

$$y_2(t) = \text{dc term} + (a_2A^2/2)\cos(\omega_2-\omega_1)t + c_2\cos 2(\omega_2-\omega_1)t + c_3\cos 3(\omega_2-\omega_1)t + \ldots \quad (7.13)$$

and

$$y_3(t) = \text{dc term} + (3a_3A^3/8)\cos(2\omega_2-\omega_1)t + d_2\cos 2(2\omega_2-\omega_1)t + d_3\cos 3(2\omega_2-\omega_1)t + \ldots \quad (7.14)$$

where c_i and d_i are the Fourier coefficients of $y_2(t)$ and $y_3(t)$, respectively.

From equations 7.10, 7.13, and 7.14, the peak power in either of the two fundamental tones is equal to 0.131 A, the peak power in the second order IM distortion product at frequency f_2-f_1 is $|a_2A^2/2|$, and the peak power in the third order IM distortion product at frequency $2f_2-f_1$ is $|3a_3A^3/8|$. The second- and third order IM distortions are thus given by

$$IM(f_2-f_1) = |a_2/2(0.131)|\ A \quad (7.15)$$

and

$$IM(2f_2-f_1) = |3a_3/8(0.131)|\ A^2 \quad (7.16)$$

respectively. Expressed in terms of decibels these become

$$IM(f_2-f_1) = -12 + 20\log|a_2/2(0.131)| + 20\log(M) \quad (7.17)$$

$$IM(2f_2-f_1) = -24 + 20\log|3a_3/8(0.131)| + 40\log(M) \quad (7.18)$$

where the peak-to-peak modulation current, M, is equal to 4A.

By performing the required polynomial interpolation in the region x>0 and substituting the polynomial coefficients and the value of the LD modulation current into equations 7.17 and 7.18, the second- and third order IM distortion are found. The computer program used to calculate the IM distortion (for a current modulation of 4 mA p-p and a bias current of 84 mA) using the polynomial spline model is listed in Appendix II.

If the interpolation is done on the data points (x_i,y_i) there is no assurance that the interpolation polynomial will satisfy the conditions that its constant term be zero and its first degree term be 0.131x. Therefore, a new set of points (z_i) is defined by the transformation

$$z_i = (y_i - 0.131x_i)/x_i^2 \quad (7.19)$$

A straight line interpolation is then performed on the points (x_i,z_i) in the x-z plane. Suppose the best fitting straight line to the points (x_i,z_i) is

$$z = a + bx \tag{7.20}$$

Then, from equation 7.19, the best fitting polynomial through the points (x_i, y_i) is the polynomial

$$y = 0.131x + ax^2 + bx^3 \tag{7.21}$$

This polynomial clearly passes through the origin and has 0.131 as the first order coefficient.

Distortion Versus Bias Current

Graphs of the calculated values of $IM(f_2-f_1)$ and $IM(2f_2-f_1)$ as a function of the laser diode bias current are given in Fig. 7.4 and Fig. 7.5, respectively. The polynomial spline model has been used to calculate the values of distortion in the region around the inflection point at 84 mA. The values of $IM(f_2-f_1)$ and $IM(2f_2-f_1)$ for the bias currents 88 mA, 92 mA, and 96 mA are the same as in figures 7.1 and 7.2 since for these bias currents the region of modulation is entirely in the sublinear region of the light-current characteristic.

The plot of $IM(2f_2-f_1)$ in Fig. 7.5 does not show the anomalous behavior in the region between 83 mA and 87 mA that was seen in Fig. 7.2. The third order IM distortion increases gradually as the LD quiescent point enters the sublinear region of the light-current characteristic and then decreases slightly in the high radiance region.

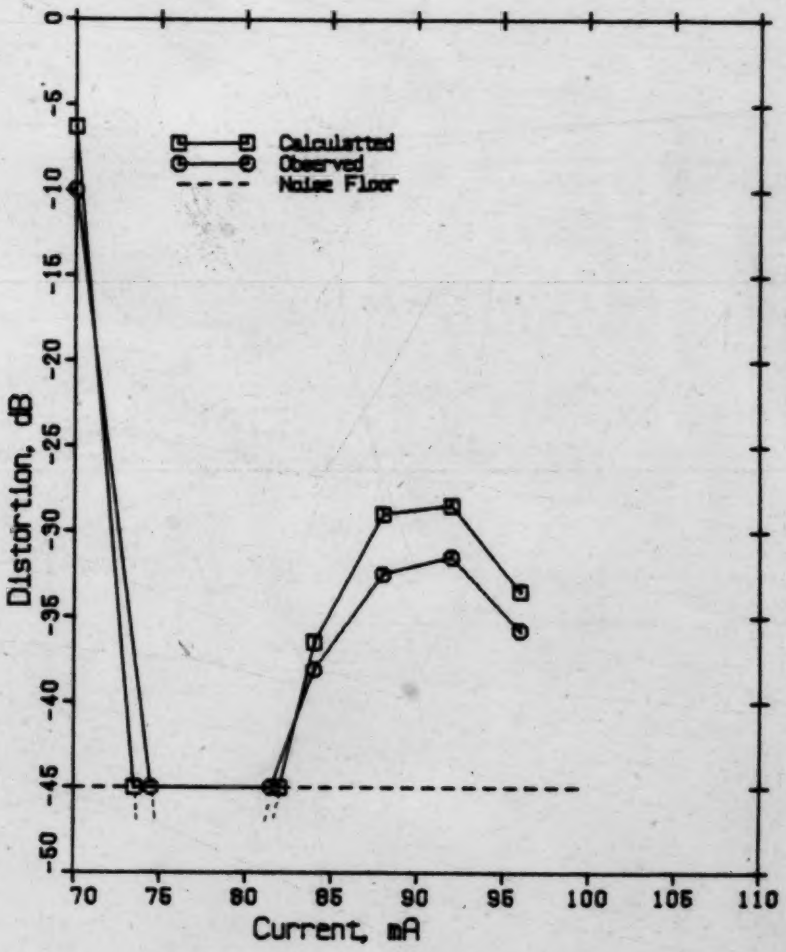

Figure 7.4 Calculated values of IM(f_2-f_1) versus LD bias current using the polynomial spline model, and measured values (for f_1 = 10.0 MHz, f_2 = 10.2 MHz, and LD modulation current = 4 mA p-p).

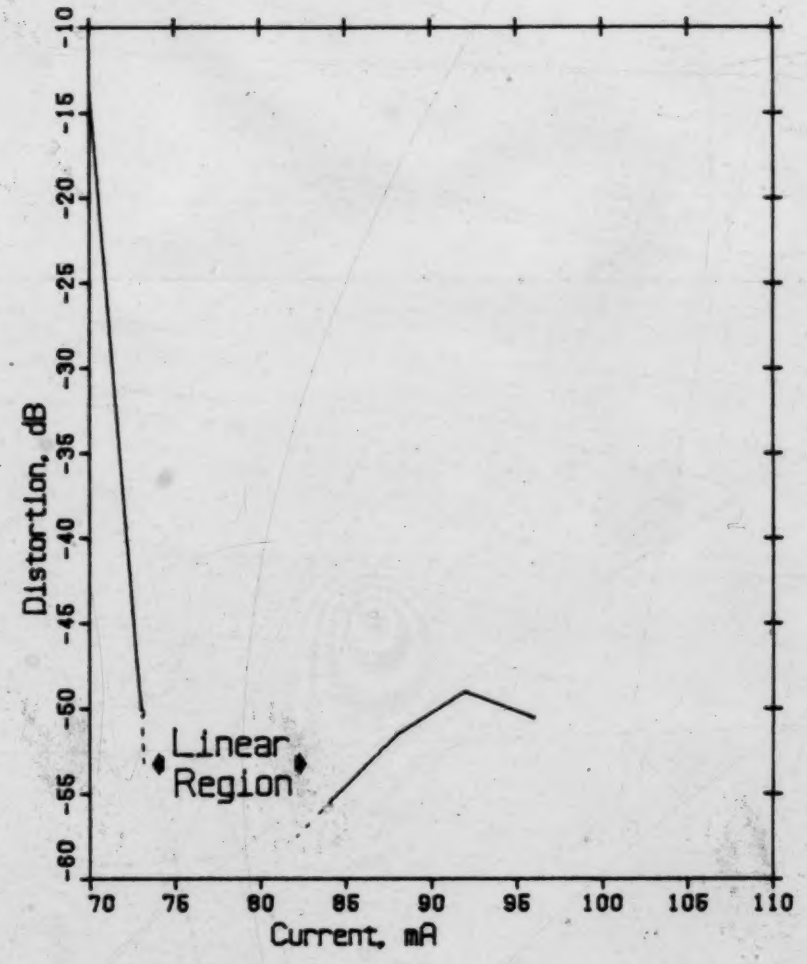

Figure 7.5 Calculated values of IM($2f_2$-f_1) versus LD bias current using the polynomial spline model (for a LD modulation current of 4 mA p-p).

In Fig. 7.4, the calculated values are compared with the measured values of IM(f_2-f_1) (for frequencies f_1 = 10.0 MHz and f_2 = 10.2 MHz, and a modulation current of 4 mA p-p). The correlation between calculated and measured values is much better than when a single polynomial interpolation was performed. The two curves are separated by less than 3 dB at all bias currents where IM(f_2-f_1) could be measured. The plot of the calculated values is very similar in shape to that of the measured values except that it is generally displaced vertically by about 2 dB to 3 dB. There may be two reasons for this. Firstly, the dynamic L-I characteristic of the laser diode at a modulation frequency of 350 KHz was used in the calculation of IM distortion; the actual dynamic L-I characteristic for frequencies above 1 MHz could be slightly more linear. Secondly, the interpolation polynomial used in the calculation of the IM distortion does not go through the data points with the same degree of smoothness as the actual light-current characteristic. Both these circumstances would result in a calculated value of IM distortion that is higher than is actually the case.

Distortion Versus Modulation Current

Finally, by performing the polynomial spline interpolation over a larger and larger region of the light-current characteristic, the behavior of the intermodulation distortion as a function of the LD modulation current can be calculated. Second and third order

intermodulation distortion for a bias current of 84 mA and for LD modulation currents of 12 mA p-p, 20 mA p-p, and 28 mA p-p were calculated using the same RLFOR program as in Appendix II.

The calculated and measured values of $IM(f_2-f_1)$ and $IM(2f_2-f_1)$ are plotted in Fig. 7.6 and Fig. 7.7, respectively. For the reasons given before, the calculated values of IM distortion are higher than the measured values by about 2 dB to 3 dB. But, except for this, the calculated and measured values are in excellent agreement. The slope of the plot of $IM(f_2-f_1)$ is 20 dB/decade for low modulation levels and rises to 30 dB/decade for modulation levels greater than 20 mA p-p. Similarly, the slope of the plot of $IM(2f_2-f_1)$ is 40 dB/decade for low level modulation and increases to 51 dB/decade for modulation levels greater than 20 mA p-p. This increase in slope at high modulation levels is due to the large difference between the slope of the light-current characteristic in the high radiance region and in the linear region.

C. Summary

By finding the best fitting polynomial spline (in the mean square sense) to the laser diode's dynamic characteristic, the intermodulation distortions resulting from a two-tone modulation of the laser diode were calculated. In this method, the dynamic characteristic was partitioned into two distinct regions: a linear region and a

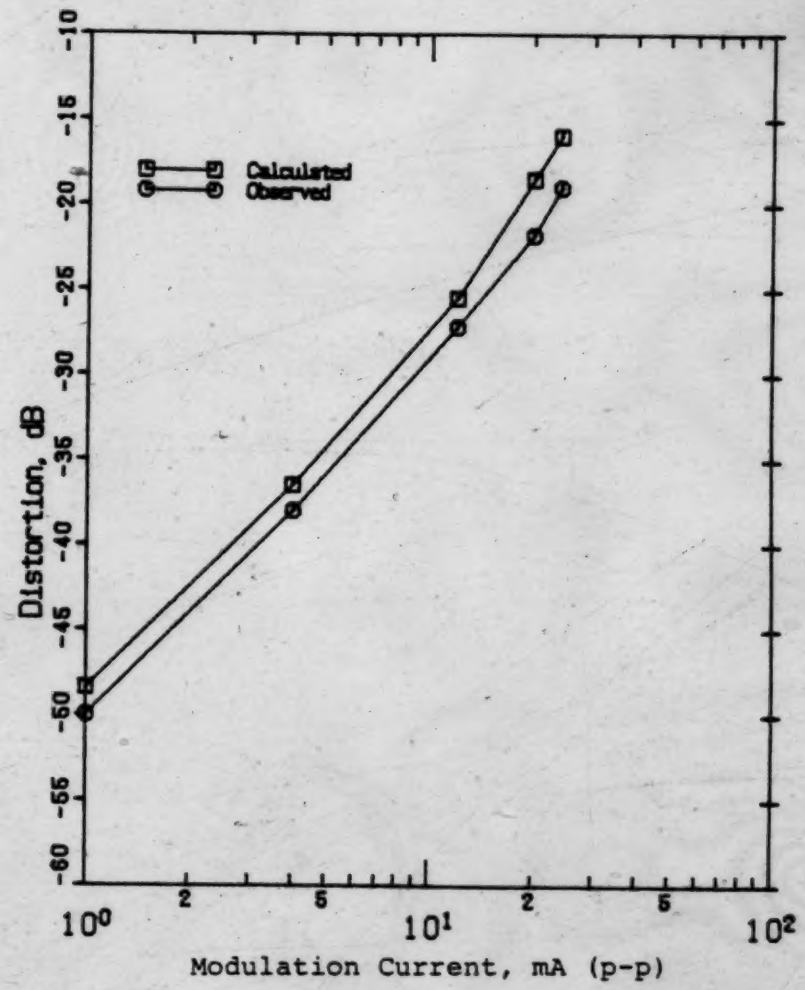

Figure 7.6 Calculated values of $IM(f_2-f_1)$ versus LD modulation current using the polynomial spline model, and measured values (for f_1 = 10.0 MHz, f_2 = 10.2 MHz, and LD bias current = 84 mA).

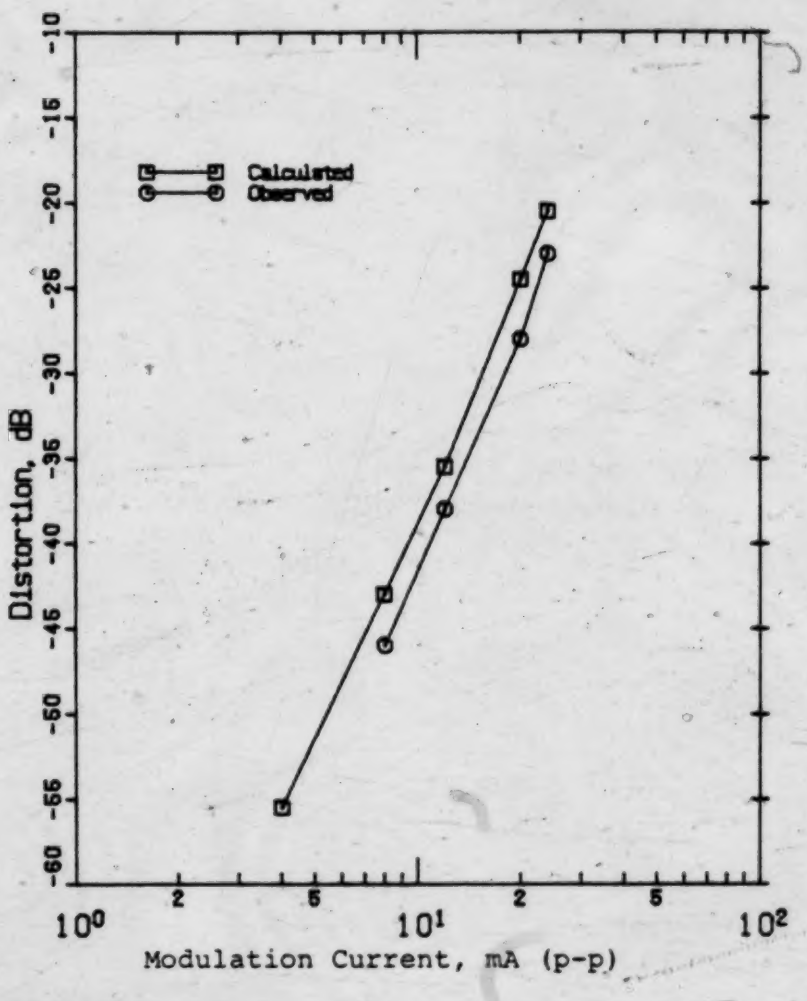

Figure 7.7 Calculated values of IM($2f_2$-f_1) versus LD modulation current using the polynomial spline model, and measured values (for f_1 = 10.0 MHz, f_2 = 10.2 MHz, and LD bias current = 84 mA).

sublinear region. Interpolation by a fourth degree polynomial was then performed in both these regions. Formulas for the IM distortion were then derived as a function of the polynomial coefficients and the amplitude of the modulation current. By performing the interpolation at different points on the laser diode characteristic, the behavior of the IM distortion as a function of the laser diode bias current was calculated. The behavior of the IM distortion as a function of the LD modulation current was also calculated.

These calculated values of IM distortion were found to be in good qualitative agreement with the experimentally observed values. The polynomial spline model gave results that were in much better agreement with experimentally measured values than the results from an alternate model where a single polynomial interpolation of the laser diode characteristic was performed. In addition, it was found that the IM distortion were virtually independent of frequency for frequencies between 1 MHz and 40 MHz (the upper bandwidth of the LD transmitter). This is in agreement with the hypothesis that a laser diode possesses a nonlinearity without memory at frequencies between roughly 1 to 200 MHz.

It is concluded therefore, that the nonlinearity of a laser diode can be accurately characterized (for frequencies where the LD has a simple nonlinearity without memory) by determining the dynamic light-current characteristic of the laser diode and approximating it with polynomial functions.

VIII. A PREDISTORTION COMPENSATION TECHNIQUE

In this chapter, a laser diode linearisation technique is examined that has the potential of improving laser diode linearity over a much larger frequency range than is possible using opto-electronic feedback. This technique involves the introduction of complementary distortion in the drive circuitry to compensate for the distortion that is generated by the laser diode.

In principle, linearisation of the light-current characteristic can be achieved over the entire frequency range in which the laser diode nonlinearity is memory free. In practice, the frequency range over which linearisation can be achieved is limited by the bandwidth of the drive circuitry, while the degree of linearisation that can be obtained is limited by how well the nonlinearities of the laser diode and the predistortin circuitry can be matched.

A. Description of the Predistortion Technique

The nonlinearity of the laser diode used in this experiment is due to the sublinearity of its light-current characteristic above its inflection point at 84mA. The predistortion technique presented here involves the introduction of a nonlinear circuit into the LD transmitter described in chapter IV. The transfer characteristic of this nonlinear circuit is superlinear (i.e., the second derivative of the characteristic is positive). The

interaction of this superlinearity with the sublinearity of the LD light/current characteristic results in an overall transfer characteristic that is more linear than the light-current characteristic of the LD.

The circuit schematic of the predistortion scheme is shown in Fig. 8.1. The transistor Q3 is the nonlinear addition to the basic LD transmitter. Except for this addition, the rest of the circuit is identical to the LD transmitter shown in Fig. 4.1. Neglecting the effect of Q3 the LD quiescent current is equal to $I_1+(I_2/2)$. Defining $x = I_{C_2} - (I_2/2) = I_{C_2} - 20$ mA, the diode current can be written as $I_d = I_1 + (I_2/2) + x = 84$ mA + x. Thus x represents the deviation of the LD current from its quiescent value. Since x varies linearly with V_1, so does I_d. Thus the transfer characteristic of the LD transmitter (defined as the plot of the LD light output versus x) has the same shape as the dynamic light-current characteristic of the LD. The transistor Q3 is biased in such a manner that it draws an additional predistortion current, $I\rho(x)$, above the inflection point of the LD. The laser diode current is thus equal to $I_d = 84$ mA + x + $I\rho(x)$. This predistortion current varies superlinearly with x.

The current x can vary between -20 mA and +20 mA. When x = -20 mA, the voltage V_{C_1} is equal to zero, Q3 is off, and $I\rho = 0$. As x increases, V_{C_1} increases and at a point determined by resistors R_1 and R_2, Q3 turns on. No discontinuity is introduced in the slope of the transfer

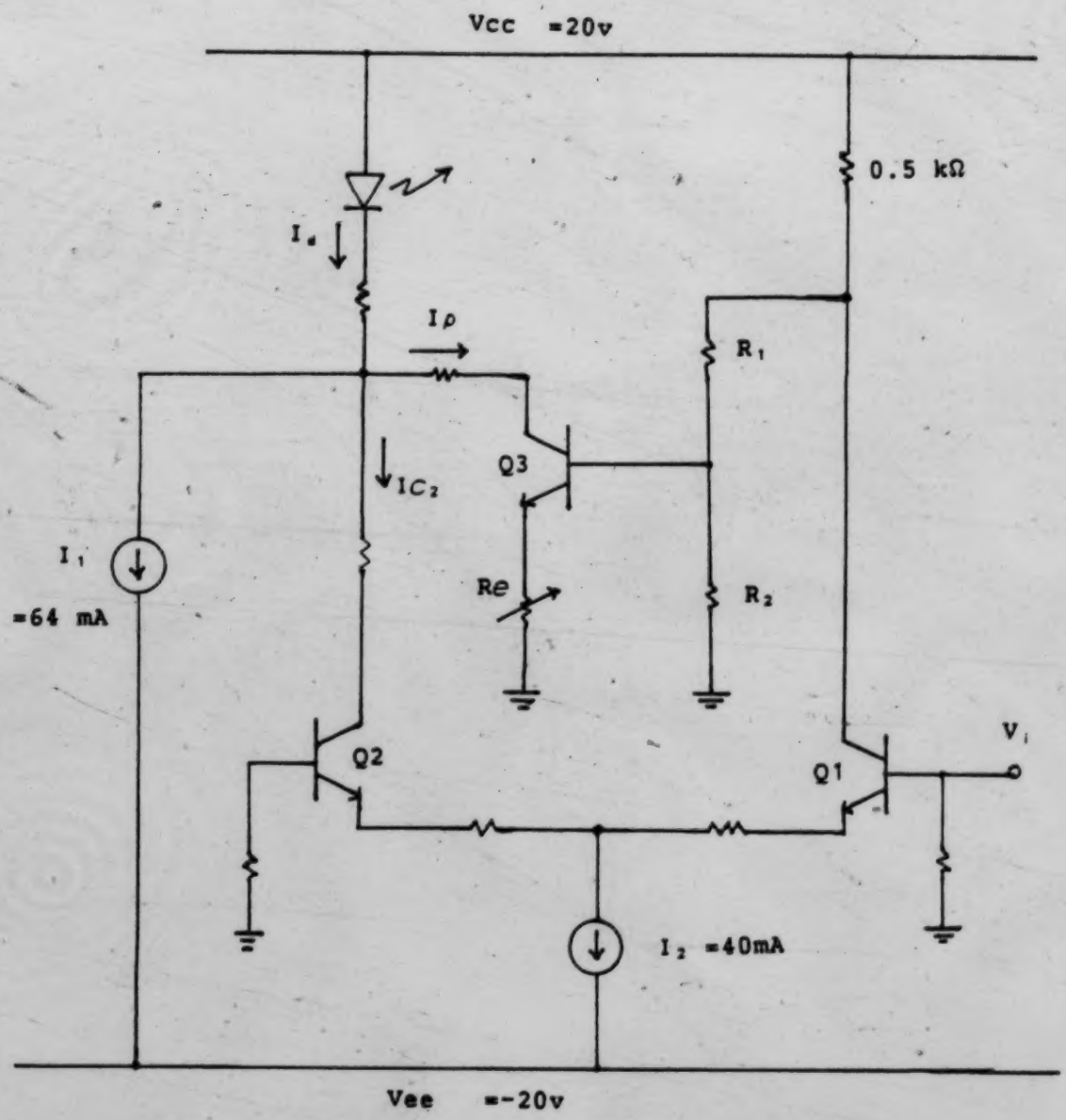

Figure 8.1 Schematic of laser diode transmitter with predistortion.

characteristic, since Q3 turns on gradually. Since the LD is biased at 84 mA, which is where the sublinear region of the LD light-current characteristic begins, the resistors R_1 and R_2 are chosen so that Q3 turns on when $x = 0$. Thus I_ρ is zero for $x \leq 0$ and is positive for $x > 0$.

The magnitude of I_ρ after Q3 starts to conduct is determined by the variable resistor R_e. As the emitter resistance R_e is decreased, the magnitude of I_ρ increases, the superlinearity of I_ρ also increases (for $x \geq 0$), and the sublinearity of the overall transfer characteristic decreases. If R_e becomes too small, however, the transfer characteristic becomes superlinear. Furthermore, care must be taken so that I_ρ never becomes large enough that the laser diode current exceeds its maximum safe value.

In principle, more transistors can be added to turn on or off at different points on the characteristic. The additional transistors could supply either more or less current to the laser diode than would otherwise be the case. By using a number of such transistors, very low values of distortion could be obtained. Laser diodes manufactured presently for the purpose of optical communication have outputs that are free of kinks and usually exhibit a single inflection point in their light-current characteristic. For such laser diodes, it is demonstrated that good linearity can be achieved with single transistor compensation.

B. Predicted Improvements in Intermodulation Distortion

In this section, the transfer characteristic of the compensated LD transmitter is derived for several values of emitter resistance, R_e. The transfer characteristic is a plot of the LD light output versus the modulation current x. From these transfer characteristics the intermodulation distortion products can be calculated using the polynomial spline model. The distortion of the uncompensated LD transmitter has been calculated in Section 7.2; hence, the reductions in $IM(f_2-f_1)$ and $IM(2f_2-f_1)$ due to the application of predistortion can be determined as a function of R_e.

To determine the transfer characteristic of the linearised LD transmitter, it is first necessary to find the predistortion current, $I_\rho(x)$. The laser diode current $I_d(x)$ is then also known. The LD light output as a function of x is then easily found from the LD dynamic light-current characteristic diode that was found in chapter VI (Fig. 6.6).

The predistortion current $I_\rho(x)$ is equal to the collector current of Q3. By using a nonlinear transistor model, this current has been plotted as a function of x in Fig. 8.2. for several values of R_e.

Given $I_\rho(x)$, it is a simple matter to plot $I_d(x) = 84mA + x + I_\rho(x)$. This has been done in Fig. 8.3. It can be seen that the curves exhibit superlinearity due to the predistortion current $I_\rho(x)$ and that the severity of the

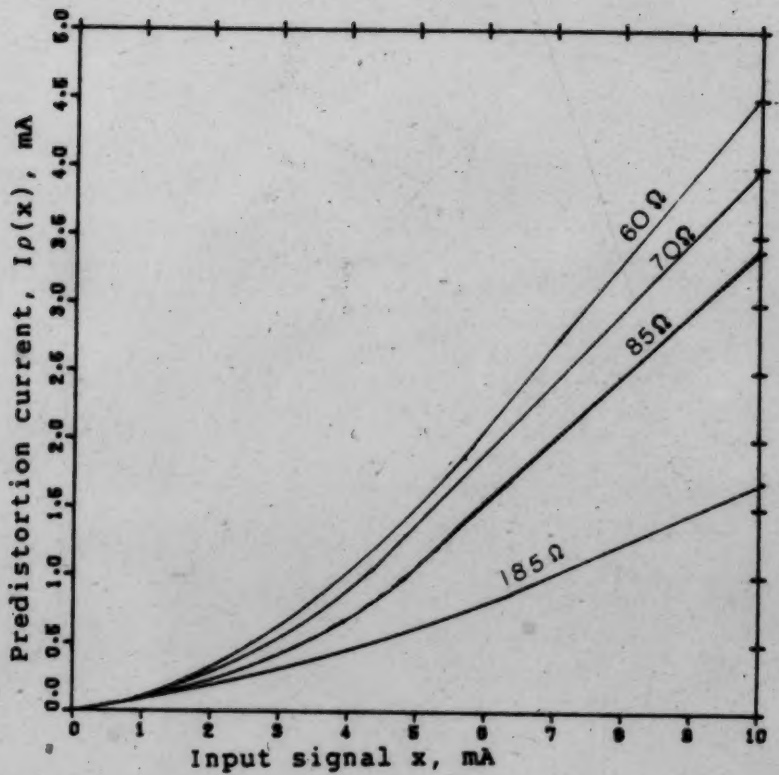

Figure 8.2 Calculated predistortion current, Iρ(x), for several values of Re.

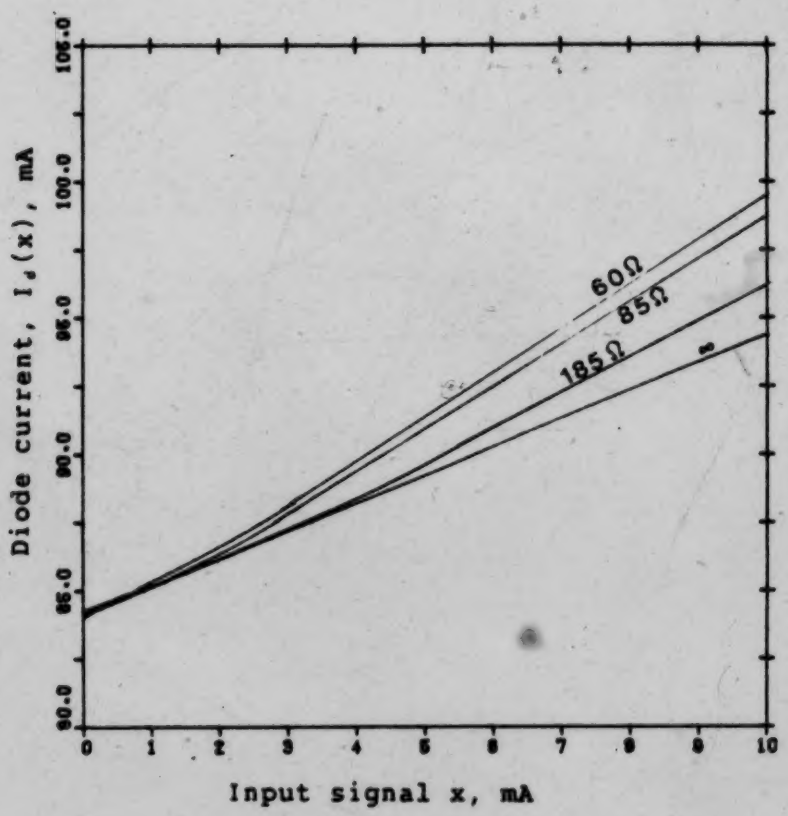

Figure 8.3 Calculated laser diode current, $I_d(x)$, illustrating the superlinearity due to predistortion.

superlinearity increases as the emitter resistance R_e decreases.

Knowing the laser diode current I_d as a function of x, the transfer characteristic of the compensated LD transmitter is found graphically from Fig. 6.6. These transfer characteristics are plotted in Fig. 8.4 for several values of R_e. Clearly, the superlinearity of the LD current has partly counteracted the sublinearity of the LD characteristic resulting in a more linear transfer characteristic. When R_e is infinite, the predistortion current is equal to zero and the transfer characteristic is identical to the LD dynamic characteristic. The transfer characteristic becomes more linear as R_e is decreased; but for values of R_e less than 85 Ω, overcompensation causes the transfer characteristic to become superlinear.

By approximating each of these characteristics by a polynomial spline model and using the techniques of chapter VII, a plot of the reductions in second- and third order IM distortion versus R_e is obtained (for a LD modulation current of 8 mA p-p). This plot is shown in Fig. 8.5. The computer program used and the results obtained are contained in Appendix III. It is seen that the greatest degree of linearisation occurs for R_e = 85 Ω. This is also readily apparent from the plots of the transfer characteristics shown in Fig. 8.4. For this value of emitter resistance, reductions in second- and third order IM distortions of 13.6 dB and 11.5 dB, respectively, are predicted.

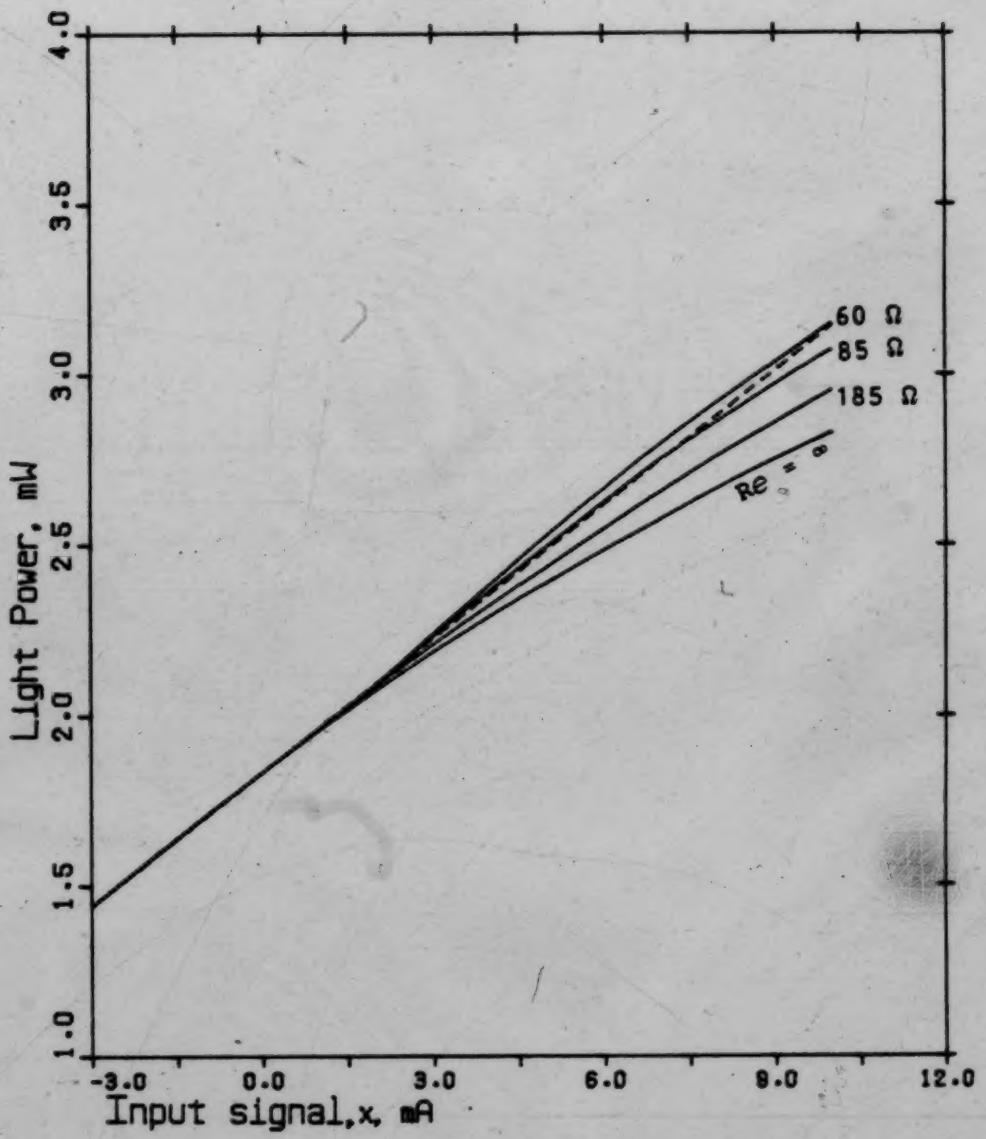

Figure 8.4 Transfer characteristic of the compensated laser diode transmitter for several values of *Re*.

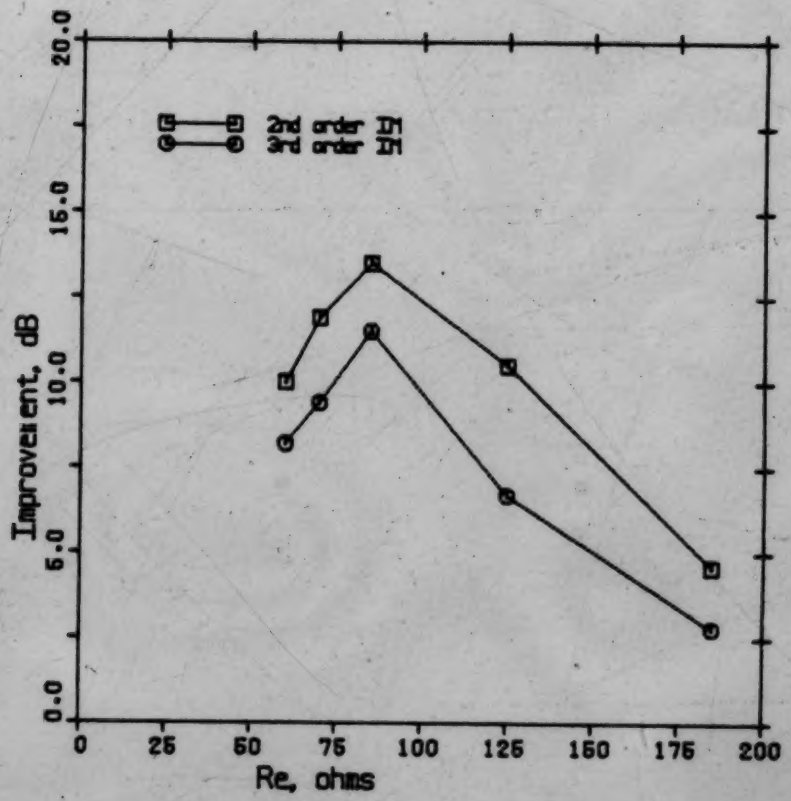

Figure 8.5 Predicted improvements in second- and third order IM distortion as a function of R_e (for a LD modulation current of 8 mA p-p).

The 2nd (3rd) order IM distortion increases at an almost constant slope of 20 dB/decade (40 dB/decade) with increasing modulation current (up to a certain level) for both the compensated and uncompensated LD transmitter. Hence, the reductions in the IM distortion, $\Delta IM(f_2-f_1)$ and $\Delta IM(2f_2-f_1)$, should ideally be independent of the modulation current, at least at low modulation levels.

C. Observed Improvements in Intermodulation Distortion

The predicted performance of the predistortion scheme is compared with experimental results in this section. For a LD modulation current of 8 mA p-p, the experimentally observed reductions in IM distortions, $\Delta IM(f_2-f_1)$ and $\Delta IM(2f_2-f_1)$, are plotted in Fig. 8.6 and Fig. 8.7, respectively. The measurements were made for a two-tone input signal with f_1 = 29 MHz and f_2 = 30 MHz. The results are almost independent of frequency in the frequency range from 1 MHz to 30 MHz.

For comparison, the theoretical values of $\Delta IM(f_2-f_1)$ and $\Delta IM(2f_2-f_1)$ are also included in the appropriate figures. The observed reductions in both the second- and third order IM distortions are a maximum at R_e = 80 Ω, rather than at R_e = 85 Ω as calculated. Thus the plots of measured reductions in IM distortions are displaced slightly to the left relative to the calculated plots. Also, the peak values of IM distortion reductions are observed to be 15 dB for second order IM distortion and 11 dB for third order IM

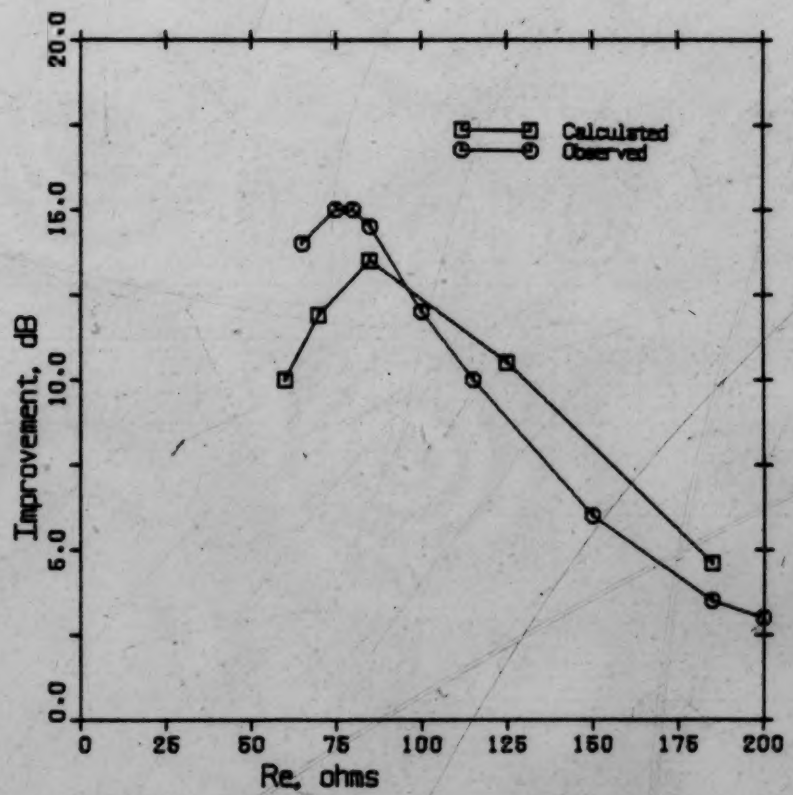

Figure 8.6 Calculated and observed values of $\Delta IM(f_2-f_1)$ (for a LD modulation current of 8 mA p-p and using a two-tone signal f_1 = 29 MHz, f_2 = 30 MHz).

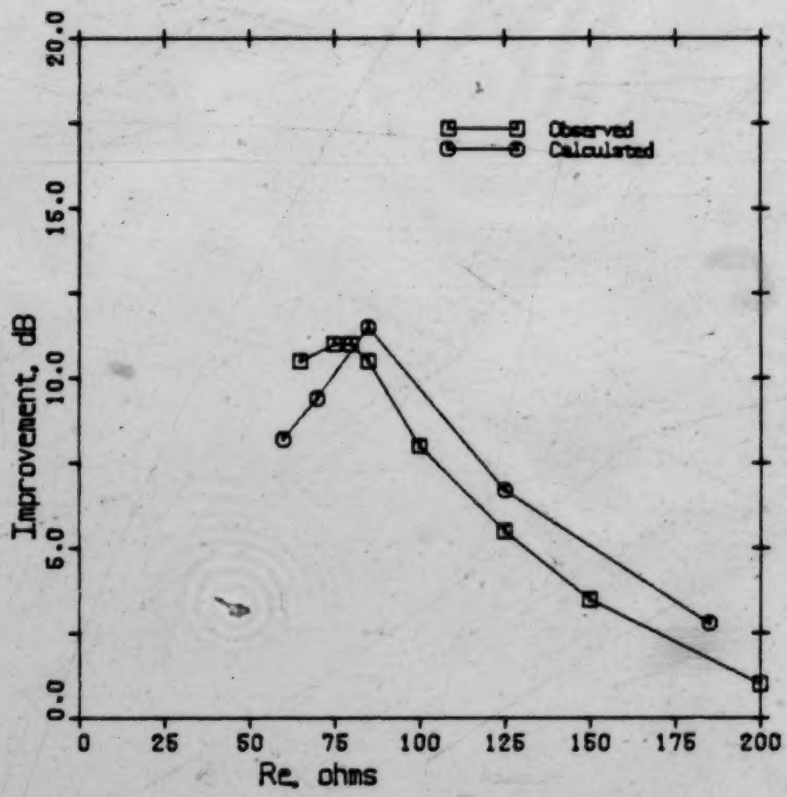

Figure 8.7 Calculated and observed values of $\Delta IM(2f_2-f_1)$ (for a LD modulation current of 8 mA p-p and using a two-tone signal f_1 = 29 MHz, f_2 = 30 MHz).

distortion. This compares well with the calculated values of 13.6 dB and 11.5 dB, respectively. The calculated plots of $\Delta IM(f_2-f_1)$ and $\Delta IM(2f_2-f_1)$ are thus in excellent agreement with the experimentally observed performance of the predistortion scheme; in fact, the calculated plots are within 3 dB of the observed plots for values of R_e greater than 60 Ω. No measurements were made for values of R_e less than 60 Ω since the resulting large values of predistortion current could damage the laser diode.

As the LD modulation current is increased beyond 8 mA p-p, the maximum values of $\Delta IM(f_2-f_1)$ and $\Delta IM(2f_2-f_1)$ that are observed still occurs for a value of R_e = 80 Ω, but this maximum value is now a function of the modulation current.

This is illustrated in Fig. 8.8 where $\Delta IM(f_2-f_1)$ and $\Delta IM(2f_2-f_1)$ are plotted as a function of the peak-to-peak modulation current (with R_e = 80 Ω, f_1 = 29 MHz, and f_2 = 30 MHz). The reductions in IM distortion for modulation currents less than 6 mA (p-p) could not be observed as the intermodulation distortion disappeared beneath the noise floor of the spectrum analyzer when predistortion was applied at such small modulation levels. For modulation currents between 6 mA (p-p) and 16 mA (p-p) the second (third) order IM reduction was constant at 15 dB (11 dB). In Fig. 8.9 the observed reductions in IM distortions are shown for a LD modulation current of 16 mA (p-p). It is seen that, without predistortion compensation, the values of IM distortions are $IM(f_2-f_1)$ = -26 dB and $IM(2f_2-f_1)$ = -31 dB

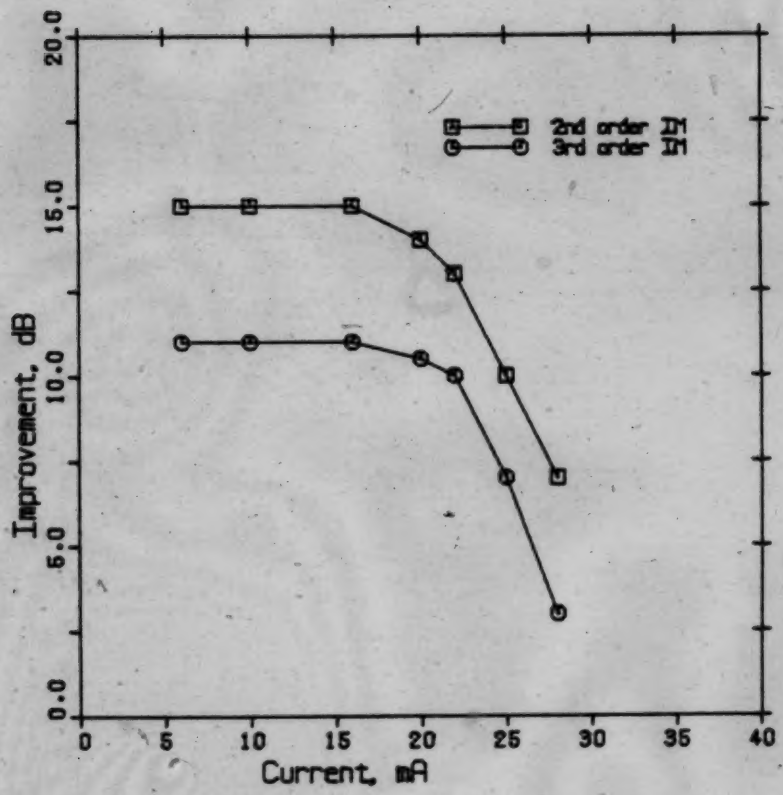

Figure 8.8 Observed values of $\Delta IM(f_2-f_1)$ and $\Delta IM(2f_2-f_1)$ versus LD modulation current (for R_e = 80 ohms and f_1 = 29 MHz, f_2 = 30 MHz).

(a)

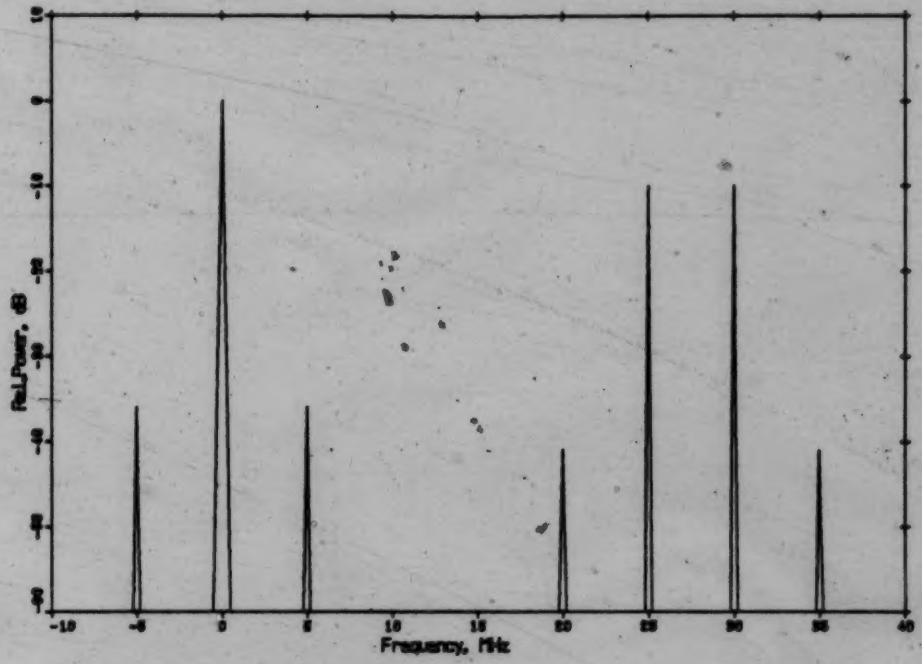

(b)

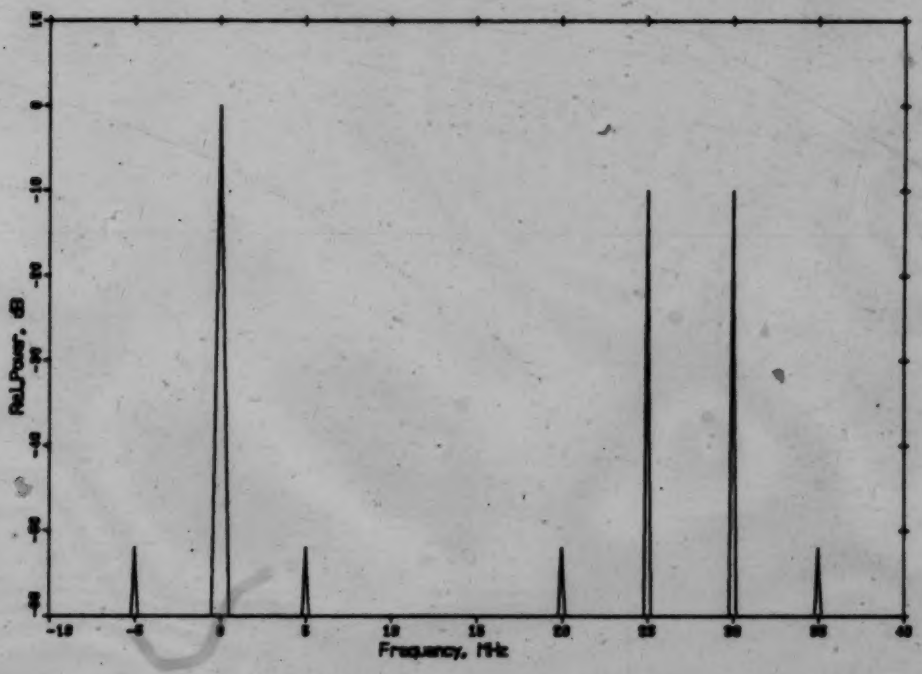

Figure 8.9 Intermodulation distortion present in laser diode output (a) without predistortion and (b) with predistortion for a two-tone signal (f_1 = 25 MHz, f_2 = 30 MHz) and a LD modulation current of 16 mA (p-p).

for f_1 = 25 MHz and f_2 = 30MHz. With predistortion compensation, the IM distortions are reduced to $IM(f_2-f_1)$ = -42 dB and $IM(2f_2-f_1)$ = -42 dB. Hence, the reductions in IM distortions are $\Delta IM(f_2-f_1)$ = 15 dB and $\Delta IM(2f_2-f_1)$ = 11 dB.

For LD modulation currents greater than 16 mA (p-p) the reductions in IM distortions were observed to decrease. The reason for this behavior can be deduced from Fig. 8.4. The transfer characteristic corresponding to R_e = 85 Ω is extremely linear for currents up to x = 8 mA (i.e., in the region between the threshold current and 92 mA); but for values of x greater than 8 mA the characteristic becomes sublinear. Hence, maximum linearisation is obtained for modulation currents less than 16 mA (p-p). The degree of linearisation obtained by this predistortion technique diminishes for current modulation above this value. It is possible to extend the region of maximum linearisation by incorporating another transistor into the predistortion circuitry that would turn on and draw additional predistortion current for laser diode currents larger than 92 mA. This is not attempted, however, as the additional complexity introduced by having a second circuit to optimize makes it impractical.

An important advantage of linearisation by predistortion, rather than by opto-electronic feedback, is that the reductions in IM distortions are independent of frequency. This is shown in Fig. 8.10 where $\Delta IM(f_2-f_1)$ and $\Delta IM(2f_2-f_1)$ are plotted as a function of the frequency f_1

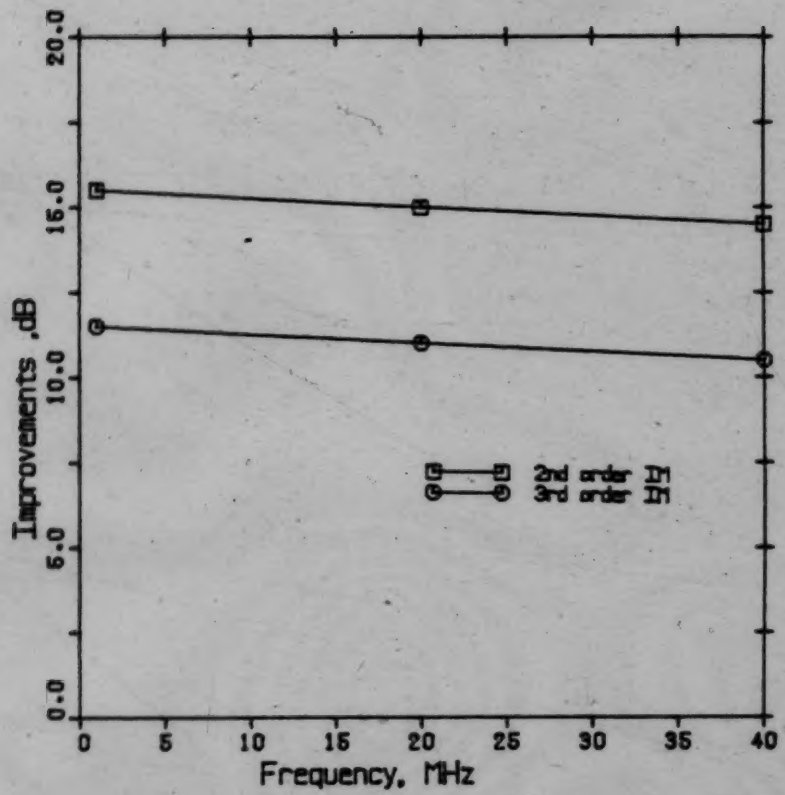

Figure 8.10 Observed variations of $\Delta IM(f_2-f_1)$ and $\Delta IM(2f_2-f_1)$ with frequency f, (with Δf = 0.1 MHz, R_e = 80 ohms and LD modulation current = 12 mA p-p).

while keeping Δf fixed at 0.1 MHz. The IM reductions are almost independent of frequency over the entire bandwidth of the laser diode transmitter. This predistortion technique could thus prove useful for transmission of broadband signals such as multichannel video.

D. Summary

In a previous chapter (chapter V), reduction in intermodulation distortion for frequencies up to 16 MHz was demonstrated using opto-electronic feedback. This bandwidth is sufficient for transmission of a baseband signal or one FM video channel. For a broadband signal containing, for example, twenty or more TV channels, linearisation over a bandwidth of more than 100 MHz is needed. Linearisation by predistortion does not suffer from the inherent bandwidth limitations that opto-electronic feedback does; in theory, linearisation over bandwidths well over 100 MHz should be possible using predistortion.

In this chapter, a predistortion circuit was incorporated into the LD transmitter of chapter IV. It was shown that the introduction of predistortion resulted in a reduction of second- and third order IM distortion of 15 dB and 11 dB, respectively. In addition, the degree of linearisation obtained was independent of frequency over the entire bandwidth of the laser diode transmitter (a range of over 40 MHz).

The predistortion circuit consists of a single transistor and associated resistors to control the turn-on point and the collector current of the transistor (Fig. 8.1). The nonlinearity of the laser diode is due to the sublinearity of its light-current characteristic above its inflection point at 84 mA. The predistortion circuitry is therefore adjusted so that the transistor turns on and draws an additional quantity of predistortion current above the inflection point of the laser diode. This predistortion current is a nonlinear function of the driving voltage; in fact, it varies superlinearly with the input voltage. The interaction of this superlinearity with the sublinearity of the LD light-current characteristic results in a transmitter whose overall transfer characteristic is more linear than that of the uncompensated transmitter.

Knowing the transfer characteristics of the predistortion circuitry and the laser diode, it was possible to derive the transfer characteristic of the compensated LD transmitter for various values of emitter resistances (of the predistortion transistor). It was seen (Fig. 8.4) that the best degree of linearisation would be achieved by using an emitter resistance of 85 Ω. By fitting polynomial splines to the calculated transfer characteristics it was also possible to derive the expected IM reductions for various emitter resistances. It was again found (Fig. 8.5) that the greatest degree of linearisation would occur for a emitter resistance of 85 Ω and that the reductions in the second-

and third order IM distortion for this value of emitter resistance would be 13.6 dB and 11.5 dB, respectively.

Fig. 8.6 and Fig. 8.7 show the results of the predistortion experiment. The maximum 2nd (3rd) order IM reduction was 15 dB (11 dB) at an emitter resistance of 80 Ω. This is in very good agreement with the calculated values. Moreover, these IM reductions were virtually independent of frequency over the entire bandwidth of the laser diode transmitter (Fig. 8.10). The feasibility of predistortion for transmission of broadband signals has thus been demonstrated.

IX. AN ADAPTIVE PREDISTORTION STRATEGY

Predistortion techniques, while capable of linearising LED or LD transmitters over a wide frequency range, have a major drawback that has precluded their use in LD transmitters until recently. The drawback is that laser diodes have light-current characteristics that change with aging or with temperature changes. Predistortion techniques that are optimized for a particular LD characteristic, such as the one described in the previous chapter, only work under controlled laboratory conditions and are not practical for general commercial use. The lifetime and reliability of laser diodes have been vastly improved over the last decade due to continuing advances in laser diode technology. It is probable that, in the near future, laser diodes with characteristics that age as slowly as present day LEDs will be fabricated [89],[90]. However, temperature dependent changes in the light-current characteristics are an inherent property of laser diodes. Consequently, any predistortion technique for LD transmitters, to be feasible, must incorporate adaptive schemes that measures the nonlinearity of the transmitter and corrects it in real time. Such a scheme is demonstrated in this chapter.

Also in this chapter, the construction of a highly linear LD transmitter suitable for high quality transmission of a single video channel (either baseband or FM) is described. The transmitter incorporates both opto-electronic

feedback and adaptive predistortion to achieve very low values of distortion.

A. Introduction

A recent publication [67] has described the successful use of adaptive predistortion for broadband applications. In this predistortion technique, the predistorted driving signal to the laser diode consists of the (undistorted) input signal plus its (weighted) second- and third order harmonics. By careful manipulation of the weighing coefficients, the predistortion of the driving signal is made complementary to the distortion introduced by the laser diode. The authors report 2nd and 3rd order IM reductions of 18 dB and 13 dB, respectively. This technique is made adaptive through the use of a sinusoidal pilot tone in an unused frequency band. A monitoring photodiode detects the pilot tone and its residual harmonics in the laser diode output. These residual 2nd and 3rd order harmonics are measured by mixing the feedback signal with the pilot generators harmonics. Low pass filtering of these signals yields error signals; the gradients of the error signals, found by differentiation, are used in the adjustment strategy of the weighing coefficients. The authors report that this technique of adaptive adjustment by correlation was successfully tested in a purely electronic simulation (i.e., with the laser diode removed from the circuit).

The adaptive technique to be demonstrated in this chapter also uses a pilot tone in an unused frequency band to yield an error signal to be used for adaptive adjustments; however, the adjustment strategy is much simpler. The technique mentioned above requires several frequency converters, integrators, differentiators, and square and cube law devices; in contrast, the technique to be presented here performs real time linearity corrections utilizing only a low bandwidth differential amplifier and a variable resistance FET.

Compensating for Threshold Current Changes

Studies have shown that the major effects of temperature changes and aging on laser diode characteristics are a change in the threshold current and the differential quantum efficiency [89]-[92]. The adaptive adjustment strategy must therefore be able to compensate for at least some degree of change in these two factors.

A LDs threshold current is exponentially dependent on temperature with a constant, positive coefficient of approximately 1.5% per °C. Thus the threshold current can increase by almost 50% if the device temperature increases by 35 C°. Aging also results in an increase in the threshold current. The main degradation mechanisms are facet erosion, thermal impedance aging, and bulk degradation at the facet [73],[74]. Facet erosion is caused by photo-oxidation of the facet in the high optical flux. Thermal impedance aging is

caused by interdiffusion of gold and indium resulting in the formation of voids and intermetallic compounds which increase resistance to heat flow. Bulk degradation is due to the formation of nonradiative centers in the crystal near the facet due to point defect motion. Due to these effects, it has been found that the threshold current increases and that this increase is proportional to the square root of time [90].

Mean times to failure of almost 10^5 hours are now common for DH GaAlAs laser diodes [89],[90],[92]. The system independent definition of end-of-life used by most manufacturers is that point at which the lasing threshold has increased by 50% of its initial value. An adaptive predistortion technique must therefore be able to compensate for changes up to 50% in the threshold current of the laser diode.

Suppose that the threshold current of the laser diode used in this experiment changes by an amount ΔI_t but that otherwise the shape of the light-current characteristic remain unchanged. Then for the predistortion scheme shown in Fig. 8.1 to continue to be effective, the bias current through the laser diode must also be increased by the amount ΔI_t. This could be done by using a monitoring photodiode coupled to a low bandwidth feedback circuit that would adjust the current drawn by current source I_t from 64mA to 64mA + ΔI_t. The problem of adaptively establishing the bias current at a value required to maintain the light output of

a laser diode constant is one that is common to all laser diode transmitters and many techniques for doing this have been published in thee literature [93],[94]. Therefore, we shall go on to the more difficult task of compensating for changes in the laser diode's differential quantum efficiency.

Compensating for Changes in Quantum Efficiency

The second major effect of aging is a decrease in the differential quantum efficiency caused by the introduction of non radiative recombination centers into the active region of the laser diode. The percentage change in the differential quantum efficiency is, however, much smaller than the change in the threshold current. A recent study on DH GaAlAs laser diodes showed that, other than a translation of the curve and a change in slope, the shape of the characteristics remained substantially unchanged even after 50,000 hours [90].

Over the lifetime of a DH GaAlAs laser diode, its threshold current can change up to 50% but the slope of its characteristic will probably change by only 10% to 20%. An adaptive strategy to compensate for such changes in slope must therefore be devised.

B. Description of Adaptive Predistortion Circuitry

A change in the differential quantum efficiency means that the degree of sublinearity of the laser diode characteristic also changes (usually for the worse). Therefore the amount of predistortion current drawn by transistor Q3 in Fig. 8.1 must be made adjustable. This can be done by replacing emitter resistor R_e by a variable resistance JFET. The drain resistance of the FET can then be varied using an error signal obtained from a monitoring photodiode coupled to a feedback circuit.

The proposed scheme is shown in Fig. 9.1. The predistortion technique of the previous chapter is made adaptive through the use of a sinusoidal pilot tone of frequency 0.3 MHz that is added to the input signal. The input signal lies in frequency bands above 1 MHz. A monitoring photodiode and a 1 MHz low pass filter extracts the pilot tone and its residual distortion from the laser diode output. This signal is subtracted from the original (undistorted) pilot tone to yield a waveform whose polarity indicates whether the transfer characteristic of the LD transmitter is sublinear or superlinear and whose magnitude is a measure of the severity of the nonlinearity. A 1 KHz low pass filter integrates this waveform and provides a slowly varying error voltage that is used to control the amount of predistortion current drawn by transistor Q3 of Fig. 8.1. This control is effected by replacing the emitter resistor of Q3 by a variable resistance JFET; the error

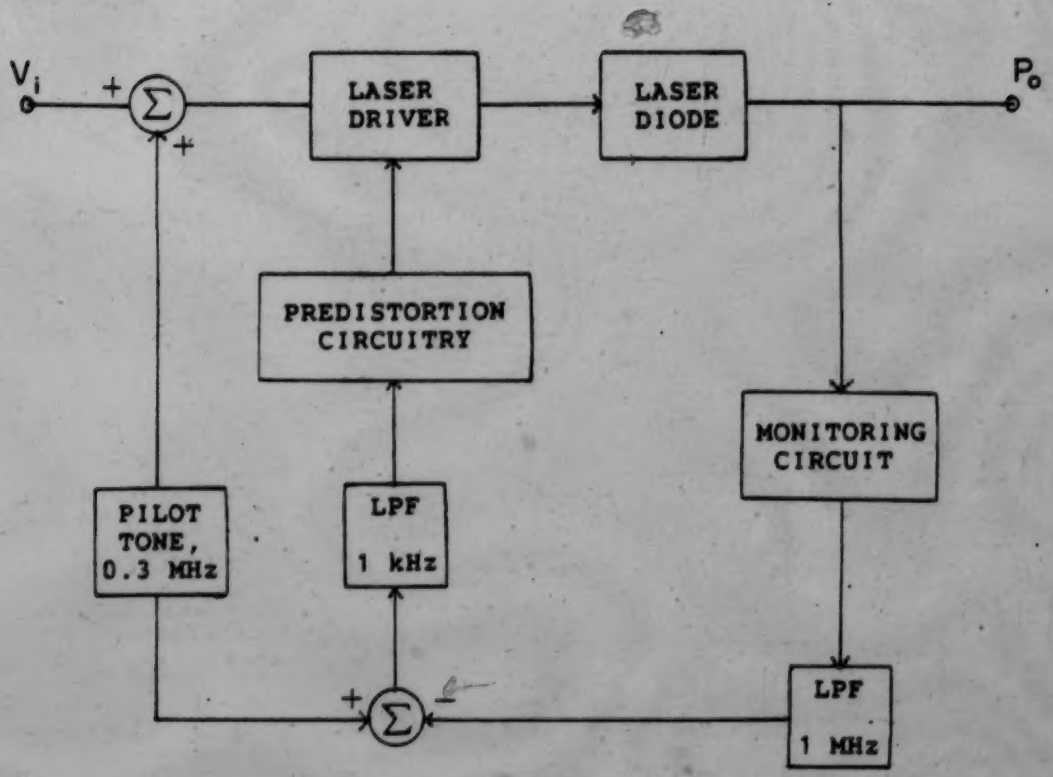

Figure 9.1 A linearised laser diode transmitter using adaptive predistortion.

voltage provides the gate-source bias voltage for the JFET and hence determines the drain-source resistance of the FET.

The monitoring photodiode and associated feedback circuitry are shown in Fig. 9.2. The emitter resistance of Q3 consists of the resistor R_e and the drain-source resistance of the parallel combination of the two JFETs. The gate-source voltages of both FETs are provided by the error signal obtained by integrating the difference between the detected pilot signal and the original pilot tone.

The drain-source resistance of the JFET is 60 Ω when the gate-source voltage, V_{gs}, equals zero and approaches tens of kΩ as V_{gs} approaches the pinch-off value of V_p=-8v. By using a parallel combination of two JFETs the net drain resistance can be varied from 30 Ω (@ V_{gs}=0v) to several hundred Ω (@ V_{gs}=-6v). The fact that the emitter resistance of transistor Q3 can be adaptively adjusted over this extended range of resistance values means that the predistortion technique will remain effective even if there is a large percentage change in the slope of the laser diode characteristic.

C. Experimental Results

The effectiveness of the adaptive predistortion technique can be tested by removing the laser diode from the circuit and using purely electrical means to check the performance of the feedback circuitry [67]. In this experiment, however, the effectiveness of the adaptive

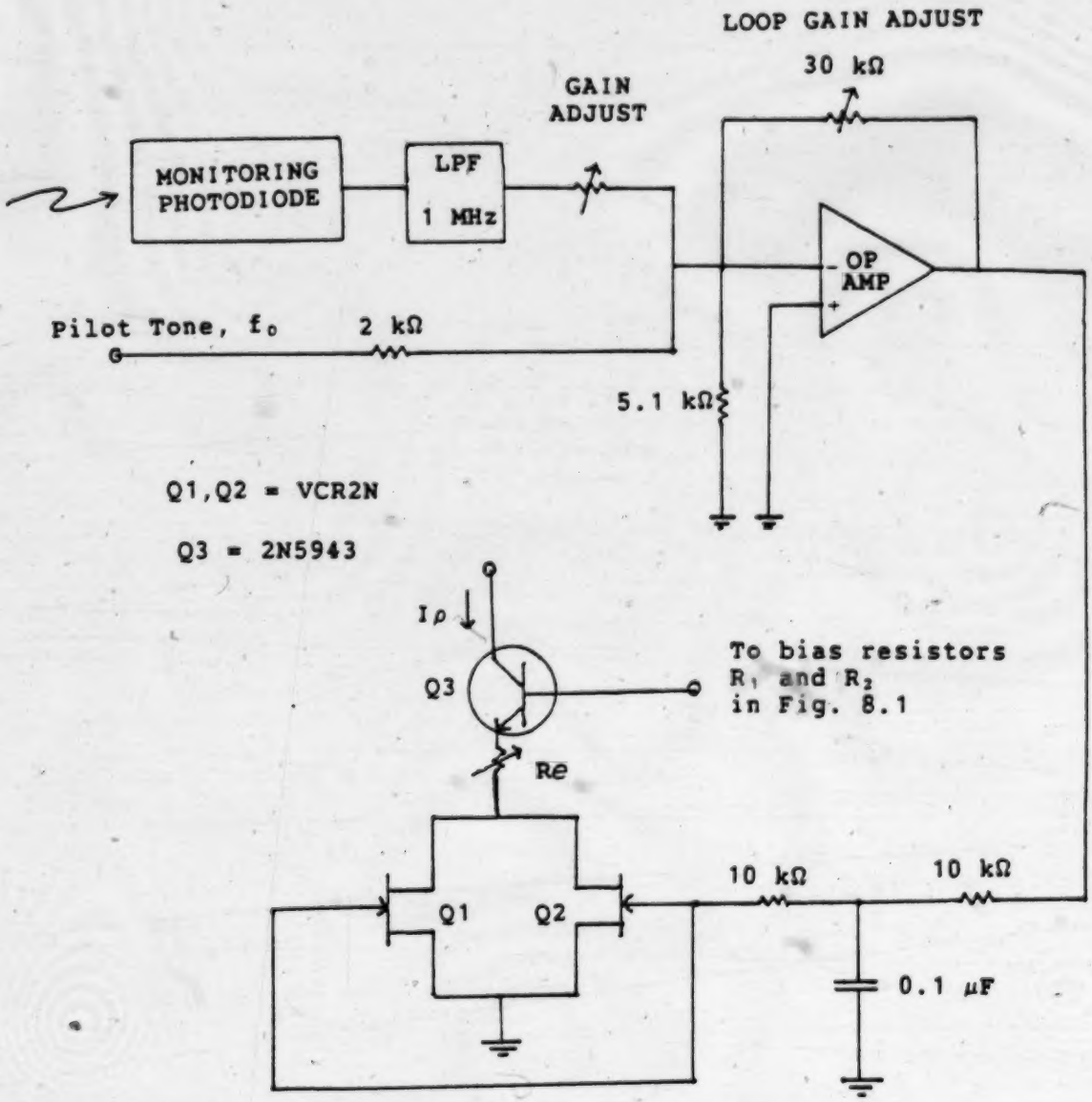

Figure 9.2 Adaptive predistortion circuitry.

predistortion strategy was tested directly by altering the transfer characteristic of the LD transmitter. This can be done by varying the resistor R_e in Fig. 9.2. From Fig. 8.4 it can be seen that varying R_e has the effect of changing the slope of the transfer characteristic.

Initially, R_e was set to zero Ω with the feedback loop open. In order to obtain maximum linearization it is necessary to make the FET drain resistance equal to 80 Ω (see Fig. 8.6 and Fig. 8.7). This can be done by adjusting the offset dc voltage of the differential amplifier in Fig. 9.2 to -2.9v. For this value of V_g, the drain resistance of the FET combination is 80 Ω and 2nd (3rd) order IM reduction of 15 dB (11dB) was obtained.

If R_e is increased above zero Ω (with the feedback loop still open) then, since the FET drain resistance remains fixed at 80 Ω, the observed IM improvements will fall off in the manner shown in figures 8.6 and 8.7. If R_e is varied with the feedback loop closed, however, the FETs drain resistance should adaptively adjust to compensate for the change in R_e (and hence the change in the slope of the transfer characteristic); the IM improvements should remain constant over at least some range of resistance values.

For the FETs to act as variable resistors, they must be operated in the ohmic region of the FET characteristic. A necessary condition for this is that the drain-source voltage v_{ds} be less than $(V_g - V_p)$. The offset voltage and gain of the differential amplifier are such that $(V_g - V_p)$ is

greater than 2v while $v_{s.}$, an a.c quantity, is less than 1v. Hence the FETs are always operated in their ohmic region. The gain of the differential amplifier is large enough so that Vg, can be varied between the two extremes of 0v and -6v. Achieving this large gain in the feedback loop is not a problem due to the small loop bandwidth.

The IM improvements obtained as *Re* is increased from 0 to 100 Ω with the feedback loop closed are shown in Fig. 9.3 and Fig. 9.4. For this test no input signal was applied to the circuit. Instead the pilot signal itself was observed at the LD output. Also, in order to observe intermodulation distortion instead of harmonic distortion, the pilot signal consisted of two tones (f_1 = 0.3 MHz, f_2 = 0.35 MHz, and LD modulation current = 12 mA p-p). The adjustment strategy is unaffected by the use of a two-tone pilot signal instead of a single tone as it is independent of the shape of the pilot signal.

Also shown in Fig. 9.3 and Fig. 9.4 are the observed second- and third order IM improvements when *Re* is varied with the feeedback loop open. It is seen that without adaptive adjustment, the IM improvements are greatly diminished when the transfer characteristic deviates from that characteristic for which the predistortion technique is optimized. With the feedback loop closed, however, the IM improvements remain constant as *Re* is varied from 0 to 52 Ω and then decrease for higher values of *Re*. It is more informative to plot the IM improvements as a function of a

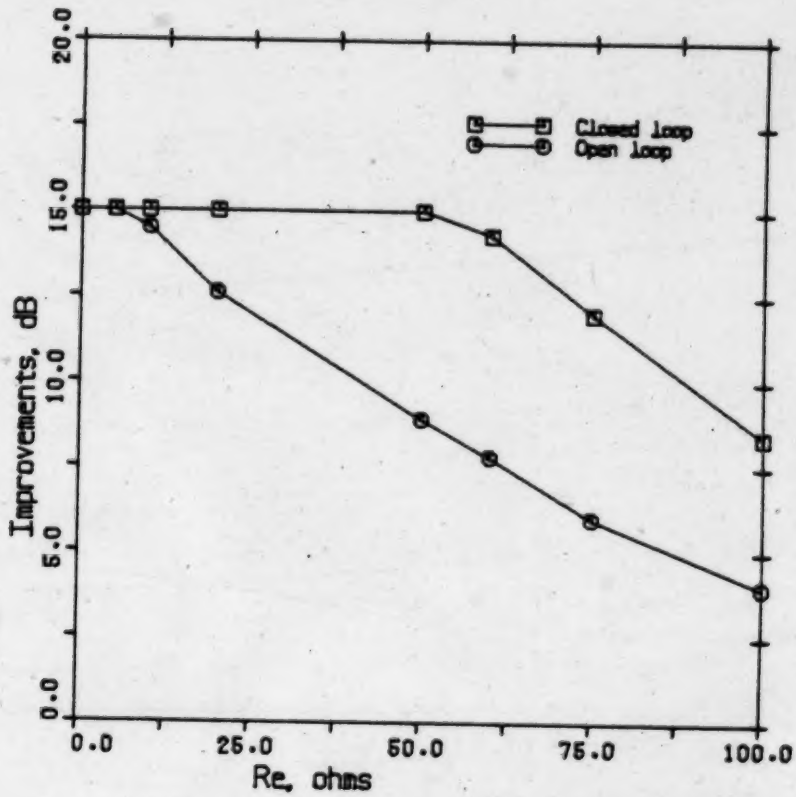

Figure 9.3 Second order IM improvement as a function of Re for two cases; namely, adaptive feedback loop (a) closed and (b) open.

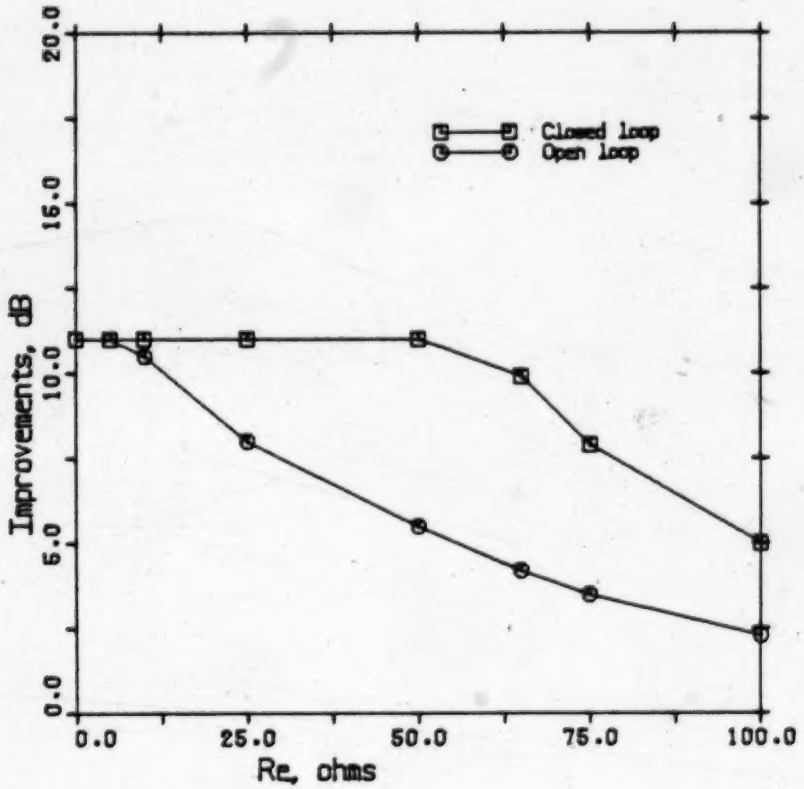

Figure 9.4 Third order IM improvement as a function of Re for two cases; namely, adaptive feedback loop (a) closed and (b) open.

physically significant quantity such as the percentage variation in the slope of the LD characteristic. From Fig. 8.4 (which shows the transfer characteristic for various values of R_e), the percentage change in the slope of the transfer characteristic (above the inflection point) can be found for various values of R_e. Then, from Fig. 9.3 and Fig. 9.4, the IM improvements can be found as a function of the percentage change in the slope of the transfer characteristic. This has been done in Fig. 9.5. In this figure, 'slope' refers to the slope of the laser characteristic in the sublinear region (between 90 mA and 94 mA) and 'percentage variation' is with respect to the uncompensated characteristic shown in Fig. 6.6.

As the sublinearity of the LD characteristic in the high radiance region becomes increasingly worse with time, the predistortion circuitry has to compensate by increasing the amount of predistortion current drawn. Fig. 9.5 shows that variations in slope up to -40% in the high radiance region can be compensated for by the adaptive circuitry. The circuitry also can compensate in case the sublinearity of the LD becomes less severe (an ulikely event). In this case, the predistortion circuitry must adapt by decreasing the predistortion current. Variations in slope up to +33% in the high radiance region (resulting in an almost linear laser characteristic) can be compensated for by the adaptive circuitry.

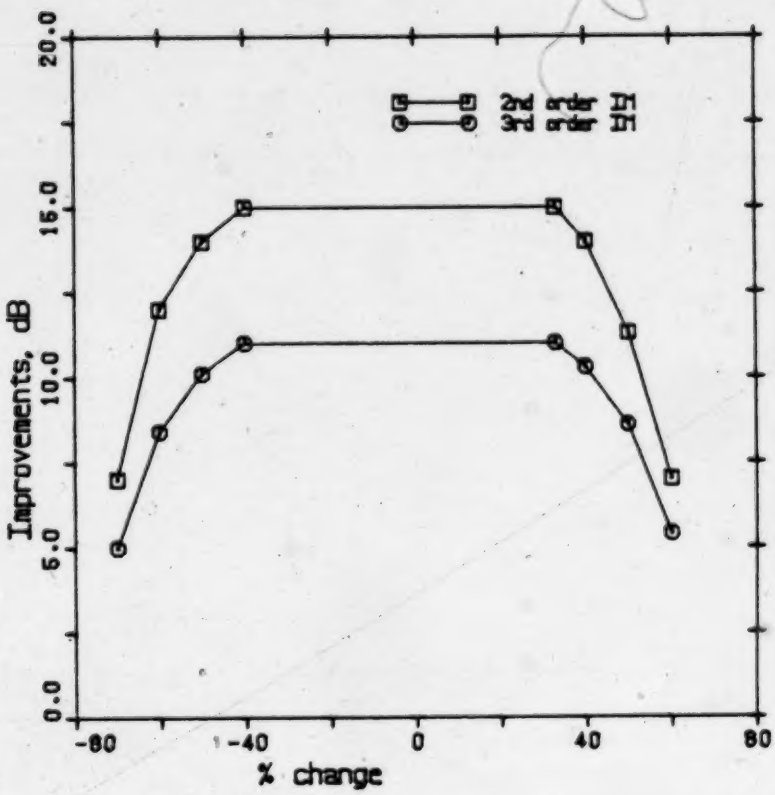

Figure 9.5 Second and third order IM improvements as a function of the percentage variation in slope (with the adaptive feedback loop closed).

The adaptive predistortion technique demonstrated in this section is able to compensate for changes in the laser characteristic anticipated over the entire useful lifetime of the laser diode (defined as the time until the threshold current has increased by 50% or until kinks form in the laser characteristic). It is therefore feasible to use a LD transmitter utilizing this scheme for the high quality transmission of analog broadband signals.

D. Simultaneous Use of Adaptive Predistortion and Opto-Electronic Feedback

Linearisation of the LD transmitter using adaptive predistortion has yielded improvements of 15 dB and 11 dB in the second- and third order intermodulation distortion, respectively. However, the linearity of the laser diode used in this experiment is sufficiently severe that, even with the use of predistortion, significant levels of distortion occur at high optical power. For example, when the laser diode is modulated so that its maximum rated power output is obtained (2.8 mW p-p) then the second- and third order IM products are -40 dB and -41 dB, respectively (with predistortion employed). This is because predistortion using a single nonlinear element cannot linearise the laser diode characteristic over the entire operating region.

The residual nonlinearity that remains even after predistortion has been applied can be greatly reduced if opto-electronic feedback is also employed. This is more

advantageous than the alternative of backing off the output until the desired distortion levels are obtained. Intermodulation products well below -50 dB should be be obtainable by using both adaptive predistortion and opto-electronic feedback. The disadvantage is in reduced bandwidth; the opto-electronic feedback scheme described in chapter V, for example, would be effective in reducing the residual distortion only for frequencies up to 16 MHz.

In those circumstances where extremely high quality transmission of a signal video channel is required, a LD transmitter linearised by the use of both adaptive predistortion and opto-electronic feedback could provide the necessary degree of linearity. The schematic diagram of such a transmitter is shown in Fig. 9.6.

The monitoring photodiode forms a part of two distinct feedback loops. The first loop has a very low loop bandwidth (1 kHz) and is used for adaptive control of the predistortion circuitry as described earlier in this chapter. The second loop has a high loop bandwidth and is used for the opto-electronic feedback scheme described in chapter V. The IM improvements resulting from the use of opto-electronic feedback are constants (at each fixed frequency) that are not affected by the use of predistortion. Thus one would expect the IM improvements (in dB's) resulting from the application of predistortion and opto-electronic feedback simultaneously to be approximately the sum of the IM improvements due to either one applied

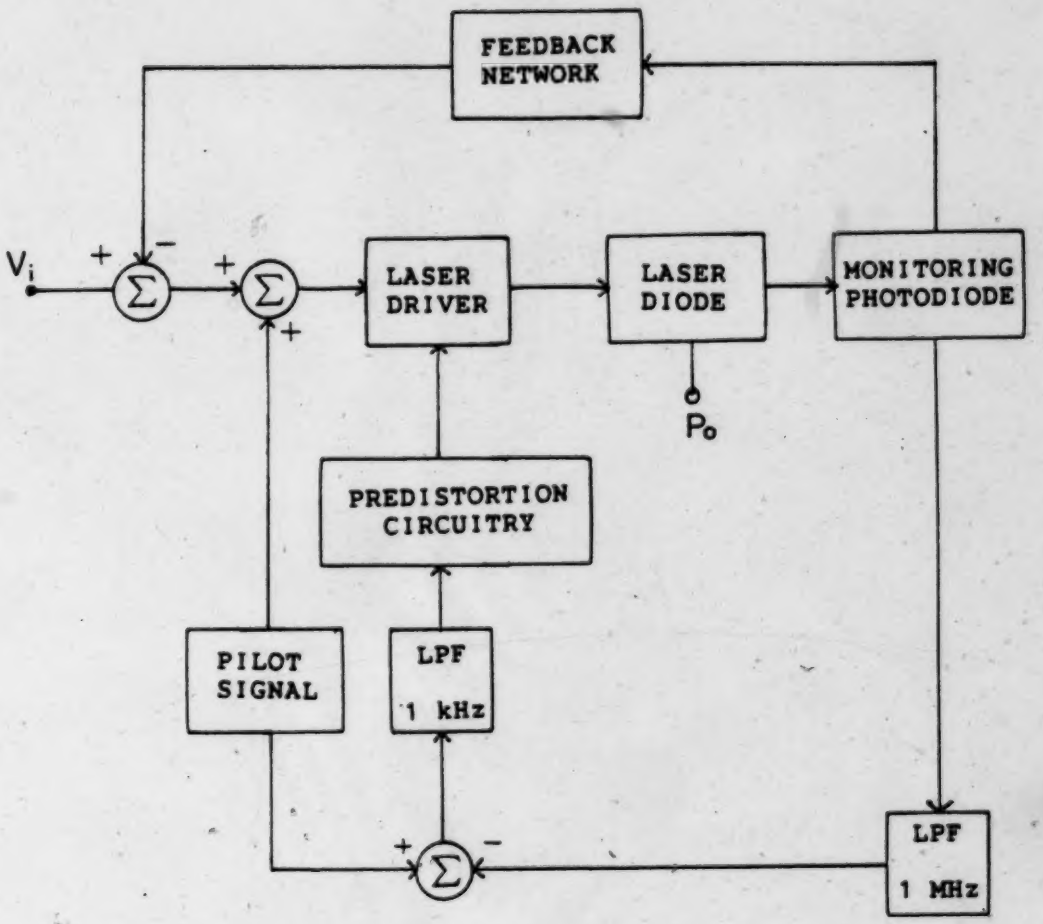

Figure 9.6 A linearised LD transmitter using both opto-electronic feedback and adaptive predistortion.

separately. For example, at frequencies below 1 MHz a 2nd (3rd) order IM improvement of 16 dB (15 dB) is obtained from opto-electronic feedback and an improvement of 15 dB (11 dB) is obtained from predistortion. Thus second- and third order IM improvements of 31 dB and 26 dB, respectively, should be attainable at these frequencies if both linearisation techniques are used together.

The linearised transmitter of Fig. 9.6 was modulated by a two-tone test signal (f_1 = 300 KHz, f_2 = 320 KHz); Fig. 9.7 shows the third order intermodulation distortion (a) when no linearisation technique is employed (i.e., both feedback loops are open) and (b) when adaptive predistortion and opto-electronic feedback are both used. In both cases the LD output was 3.0 mW p-p. The LD was modulated slightly over its rated output in order that the full extent of the IM improvement could be measured. The third order IM distortion is seen to decrease from -26 dB to -51 dB; an improvement of 25 dB. This is close to the expected improvement of 26 dB. The observed improvement in second order IM distortion was approximately 30 dB.

At frequencies above 1 MHz, the IM improvements start decreasing due to the reduced effectiveness of opto-electronic feedback. In Fig. 9.8 the IM improvements are plotted as a function of frequency f_1 (with Δf fixed at 0.1 MHz). Second and third order IM improvements of greater than 25 dB and 20 dB, respectively, were obtained for frequencies up to 11 MHz.

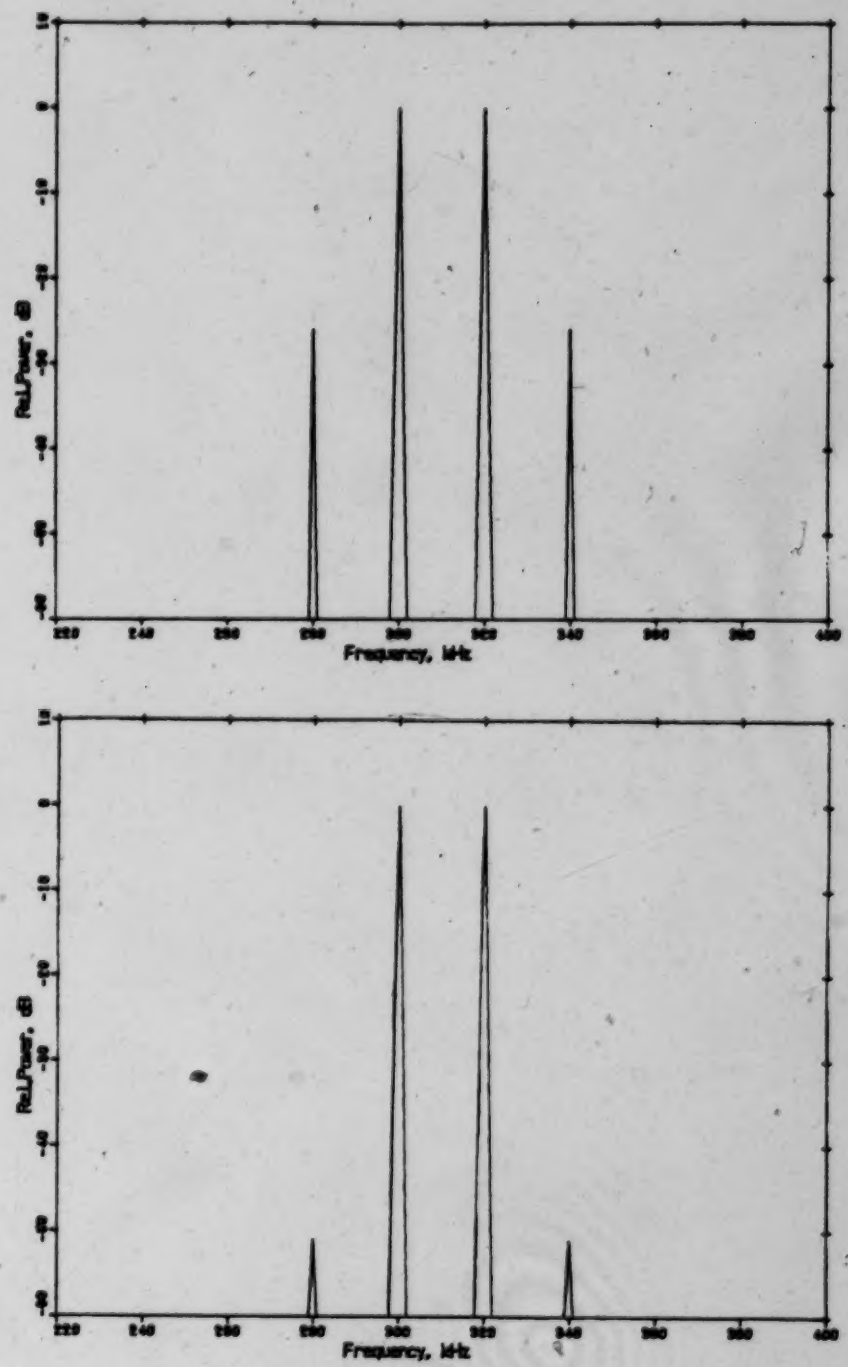

Figure 9.7 Third order IM distortion (for a LD output of 3.0 mW p-p): (a) with no linearisation, and (b) with opto-electronic feedback and adaptive predistortion.

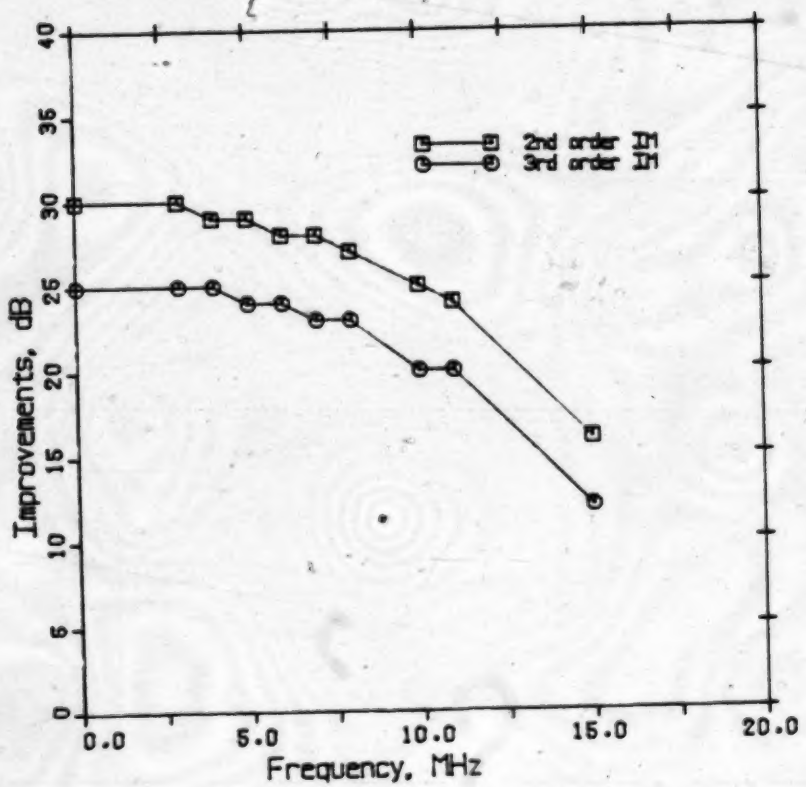

Figure 9.8 IM improvements as a function of frequency f, when both opto-electronic feedback and adaptive predistortion are used.

It is demonstrated therefore that even a laser diode with an appreciably nonlinear characteristic, such as the one used in this experiment, can be used for good quality transmission of a video signal if the transmitter is linearised using adaptive predistortion and opto-electronic feedback. For example, the linearised transmitter of this section can couple 2 mW p-p of optical power to the fibre pigtail with IM distortion levels less than -50 dB.

E. Summary

An adaptive predistortion scheme that measures the nonlinearity of the laser diode transmitter and corrects it in real time has been described in this chapter. Without such an adaptive strategy the predistortion scheme of the previous chapter, which was optimized for a particular transfer characteristic, would become ineffective as this characteristic changed due to temperature variations or laser aging.

The major effects of temperature changes and aging on laser diode characteristics are a change in the threshold current and the differential quantum efficiency. To compensate for an increase in the threshold current, it is only necessary to increase the LD bias current by a corresponding amount; no changes are needed in the predistortion circuitry itself. Many techniques for doing this using simple feedback circuitry are known. A change in the slope of the characteristic, however, means that the

predistortion circuitry itself must be modified to allow for adaptive control. An adaptive strategy was demonstrated whereby a pilot signal in an unused frequency band was used to obtain an error signal which was proportional to the deviation of the transfer characteristic from linearity. This error signal was then used to control the amount of predistortion current drawn by the predistortion circuitry. This strategy was tested by deliberately altering the slope of the transfer characteristic in the high radiance region. It was observed that the IM improvements did not decrease appreciably even when the slope of the characteristic was varied by a wide margin (from -40% to +33% of its normal values). These results were obtained under the condition that the characteristic changed smoothly. It is concluded that the addition of adaptive circuitry makes predistortion a feasible method of linearising LD transmitters for broadband analog communication.

Also in this chapter, it was shown that the simultaneous use of opto-electronic feedback and adaptive predistortion resulted in very high values of IM improvements. A disadvantage is that these improvements are over a smaller bandwidth than that obtainable with predistortion alone. By using both opto-electronic feedback and adaptive predistortion, second- and third order IM improvements of greater than 25 dB and 20 dB, respectively, were obtained for frequencies up to 11 MHz. High quality single-channel video transmission is therefore possible with

this linearised transmitter.

X. SUMMARY AND DISCUSSION

In this thesis, mathematical techniques involving interpolation of the dynamic light-current characteristic of a laser diode by polynomial splines have been used to determine the distortion characteristics of a laser diode. As well, the effectiveness of opto-electronic feedback and adaptive predistortion in linearising the LD light-current characteristic at video frequencies was investigated. A linear, broadband, LD transmitter was constructed; the use of these linearisation techniques resulted in reductions of both second- and third order distortion of greater than 20 dB over a frequency bandwidth large enough to prove useful for single- and multi- channel video transmission.

The mathematical technique consists of modelling the L-I characteristic of the laser diode by a polynomial power series. This technique is only valid if the laser diode has a nonlinearity without memory, in which case the distortion characteristics of the laser diode are frequency independent. It is known that, for modulation frequencies less than 100 kHz, active layer heating causes a 'floating' value of threshold current and a sublinearity in the static L-I characteristic of the laser diode. At frequencies of several hundred MHz, on the other hand, harmonics of the modulation frequency approach the resonance frequency of the laser diode. Both of these effects introduce frequency dependent distortion and hence represent a nonlinearity with

memory. In the intermediate frequency range of roughly 1-200 MHz, however, the LD nonlinearity is memory free. The mathematical techniques presented in this thesis are valid over this frequency range.

The characterization of LD nonlinearity begins with the determination of the LD dynamic L-I characteristic at a frequency large enough to escape thermal effects. A method was devised (Fig. 6.2) whereby the dynamic characteristic was determined at a modulation frequency of 350 kHZ by finding its deviation from a perfectly linear characteristic. The dynamic characteristic is approximately linear in the region immediately above the threshold current, but exhibits significant sublinearity at higher optical outputs. Determination of the dynamic characteristic at other frequencies showed that the nonlinearity became much worse at frequencies less than 15 kHz (Fig. 6.5).

For a given value of LD bias current, the region of the dynamic characteristic in a neighborhood of this point is modelled by a polynomial spline of degree four using an univariate curvilinear regression model. For a two-tone modulation of the laser diode, the formulas for the second- and third order IM distortions were calculated from this model (Equation 7.6). By performing these calculations at different regions on the dynamic characteristic, graphs of the calculated second- and third order IM distortions were found as a function of LD bias and modulation current (Figures 7.4 to 7.7). These results were found to be in good

agreement with observed values. The results from the polynomial spline model were in better agreement with observed values than an alternate model where interpolation by a single polynomial was performed.

For the purpose of testing linearisation techniques, a linear LD transmitter was constructed that had a bandwidth of 40 MHz (Fig. 4.1). The use of current sources allowed for the precise and independent control of the LD bias and modulation currents. The LD transmitter was first linearised using an opto-electronic feedback technique (Fig. 5.5). The stability of the feedback scheme and the expected reduction in distortion were calculated from the Nyquist diagram of the feedback amplifier (Fig. 5.6). This technique resulted in improvements of better than 15 dB in both the 2nd and 3rd order IM distortion in the frequency range 0-5 MHz; IM improvements greater than 10 dB were obtained for frequencies up to 11 MHz and a smaller reduction in distortion was seen for frequencies up to 16 MHz. These results were in excellent agreement with the calculated values. This opto-electronic feedback scheme would be useful in the transmission of baseband video signals.

The maximum frequency at which opto-electronic feedback is effective in reducing distortion is limited by the time delay around the feedback loop. The wideband amplifiers used in the feedback scheme had a phase shift of only -15° at 16 MHz which represents a delay of only 2.6ns. The time delay introduced by the LD driver, fiber pigtail, and optical

receiver was much greater than this and was the main reason why the effectiveness of the feedback scheme was limited to frequencies less than 16 MHz.

If a reduction of even 5 ns in the loop delay could be obtained (for example, by using a laser diode with a built-in monitoring photodiode) then it was calculated that the effectiveness of the feedback scheme would extend to frequencies up to approximately 30 MHz. The technique could then be used in the transmission of about four or five video signals.

The other linearisation technique investigated in this thesis was predistortion. This technique involves the deliberate introduction of complementary distortion in the drive circuitry to compensate for the distortion that is generated by the laser diode. This was done by introducing a controlled current source into the LD driver circuitry which would draw an additional amount of 'predistortion current' through the laser diode in the region above the inflection point of the LD dynamic characteristic (Fig. 8.1). The cut-in point of the controlled current source and the magnitude of the predistortion current that it drew were adjusted to obtain the best degree of linearisation possible.

In principle, linearisation of the L-I characteristic can be achieved over the entire frequency range (≃ 1-200 MHz) where the LD nonlinearity is memory free. In practice, the frequency range over which linearisation can be achieved

is limited by the bandwidth of the driver circuitry; as well, the degree of linearisation that can be obtained is limited by how well the nonlinearities of the laser diode and the predistortion circuitry can be matched.

Matching of nonlinearities is, in general, a difficult task. In principle, a very high degree of linearisation can be obtained by the use of more controlled current sources; these additional current sources could either withhold current or supply extra current to the laser diode at different points on the characteristic. However, matching of nonlinearities is made easier by the fact that many types of laser diodes have L-I characteristics that are smooth (i.e., free of kinks) and which possess a single inflection point above which the curve become sublinear. It was demonstrated that the use of a single controlled current source still resulted in a good degree of linearisation.

The predistortion technique was effective in reducing second- and third order IM distortion by 15 dB and 11 dB, respectively. These IM improvements did not vary appreciably over the entire bandwidth of th LD transmitter (40 MHz) and only decreased at very high modulation levels (Fig. 8.8 and Fig. 8.10).

The effect of predistortion is to linearise the overall transfer characteristic of the LD transmitter. By analyzing the predistortion circuitry, the compensated characteristics for several values of predistortion drive levels were calculated in Section 8.2 (Fig. 8.4). By modelling both the

compensated and uncompensated characteristics by polynomial splines, it was possible to theoretically calculate the improvements in IM distortion resulting from predistortion. The calculated and observed values agree closely (Fig. 8.5 and Fig. 8.6).

A predistortion technique that is optimized for a particular LD characteristic is not suitable for general commercial use since the L-I characteristic of a laser diode changes with aging or temperature variations. To be useful, a predistortion technique must incorporate an adaptive scheme that will measure the nonlinearity of the LD transmitter and perform real-time corrections.

The major effects of temperature changes and aging on LD characteristics are a change in the threshold current and differential quantum efficiency (slope). If only the threshold current changes, the predistortion scheme described above is not affected as long as the LD bias current is changed by a similar amount. Many techniques for the adaptive control of LD bias current are known; hence, an adaptive scheme that could adjust to changes in the slope of the LD characteristic was tested (Fig. 9.1 and Fig. 9.2).

In this technique, a 'pilot tone' of frequency 0.3 MHz is added to the input signal. The input signal is constrained to lie in the frequency band above 1 MHz. A monitoring photodiode and a 1 MHz low pass filter extracts the pilot tone and its residual distortion from the LD output. This signal is then subtracted from the original

(undistorted) pilot tone to yield a waveform whose polarity indicates whether the transfer characteristic of the transmitter is sublinear or superlinear and whose magnitude is a measure of the severity of the nonlinearity. A 1 kHz low pass filter integrates this waveform and provides a slowly varying error voltage that is used to control the amount of predistortion current drawn. This control is effected by using a variable resistance JFET.

The adaptive strategy outlined above was tested by changing the slope of the transfer characteristic (of the LD transmitter) and observing the effect on the IM improvements. The slope of the transfer characteristic can be changed by altering the L-I characteristic of the laser diode itself (by subjecting it to elevated temperatures, for example). This was not attempted as the laser diode could be damaged by this procedure. Instead, it was found that the slope of the transfer characteristic could be varied by purely electrical means (by adjusting a variable resistor). It was observed that, in the absence of adaptive feedback, the IM improvements decreased rapidly as the slope of the characteristic was changed. With the adaptive strategy employed, however, the IM improvements were observed to remain constant as the slope was varied over a certain interval; outside this interval the IM improvements dropped off (Fig. 9.3 and Fig. 9.4). It was found that the adaptive strategy was effective for percentage variations in slope between -40% and +30% (in the sublinear region of the

characteristic).

However, these results are valid only under the following conditions: (1) that the laser characteristic varies in a sufficiently 'smooth' manner (without the formation of kinks) and (2) that the difference between the threshold current and that current at which the laser characteristic deviates from its linear extrapolation remains constant with time. Almost all laser diodes manufactured presently for the purpose of analog communication would satisfy the first condition.

The second condition is due to the fact that no allowance was made to vary the turn-on point of the controlled current source. The current source always turns on at a point 14 mA above the threshold current (i.e. at 84 mA when the threshold current is 70 mA). The position at which the LD characteristic deviates from linearity may, however, change with time as the laser ages. In this case, the adaptive circuitry will not be able to maintain maximum IM improvements as the laser ages.

The limitation of the proposed adaptive scheme could be overcome if the turn-on point of the current source was also placed under adaptive control. This would require a means of determining where the laser characteristic deviates from linearity. By a slight modification of the adaptive technique, such information could indeed be obtained. In the present adaptive strategy, the error signal obtained by subtracting the detected pilot signal from the original

pilot signal is integrated and the resulting voltage used to control the amount of predistortion current drawn. However, the error signal contains additional information about the shape of the transfer characteristic. When the characteristic is linear, the error voltage is approximately zero; but when the characteristic deviates from linearity, the error voltage deviates from zero. By using a comparator circuit, it is possible to detect that point on the characteristic where it deviates from linearity. By replacing one of the bias resistors in the current source by a variable resistance FET, it should be possible to adaptively adjust the turn-on point of the current source so that it always starts conducting at that point on the characteristic where it deviates from linearity. Incorporation of these modifications would make the adaptive strategy effective in compensating for more general variations in the laser diode characteristic.

A second drawback of the proposed adaptive strategy is the power penalty resulting from the use of the pilot signal. The purpose of the pilot signal is to extract information about that region of the transfer characteristic where the input signal is being modulated. This could be done, for example, by using a pilot signal of the same amplitude as the input signal. The resulting power penalty of 3 dB is rather severe. It can mean a reduction of several kilometers in repeater spacing. A method needs to be devised therefore that will reduce the power penalty while still

obtaining information about the nature of the transfer characteristic throughout the region of operation.

One possibility is to use a pilot signal whose amplitude is small relative to the input signal but which lies in a frequency band above the input signal. The result is a small amplitude, but high frequency, pilot signal modulated onto the large amplitude, but lower frequency, input signal. As a result, the pilot signal traverses the entire operating region while at the same time the power penalty is small. It may be possible to completely eliminate the power penalty by using part of the input signal itself as the pilot signal. A signal obtained by band-pass filtering of the input signal could serve as the pilot signal. This can be done since the adaptive strategy does not require a pilot signal of any particular shape. An identical band-pass filter in the feedback loop would then provide the 'detected pilot signal'. In this manner the necessity of generating a pilot tone could be eliminated and as a result there would be no power penalty.

If the improvements suggested above are incorporated into the adaptive feedback circuitry, the predistortion technique described in this thesis would be a feasible and inexpensive method of linearising LD transmitters. Such techniques are needed in the CATV industry. The fiber trunks in the 20 or more fiber-optic CATV systems operating in North America presently can transmit a maximum of only 5 or 6 video channels per fiber (in a FDM format). This limit is

due to the nonlinearities in the system, of which the nonlinearity of the laser diode is a major component. Consequently, up to 10 fibers and their associated laser diode transmitters and photodetectors are required to replace a single coaxial cable capable of carrying up to 64 video channels. The use of more linear LD transmitters will mean that future trunks will carry more video channels per fiber, making fiber-optic CATV systems even more attractive from an economic viewpoint.

Finally, one last experiment was performed in which both the opto-electronic feedback technique (of Chapter V) and the adaptive predistortion technique (of Chapter IX) were used simultaneously to achieve a very high degree of linearisation (but over a smaller bandwidth than for predistortion by itself). Reductions in the second- and third order IM distortions of greater than 25 dB and 20 dB, respectively, were obtained for frequencies up to 11 MHz. This technique could prove useful in applications where baseband video transmission is employed. Examples of such applications are teleconferencing, remote monitoring and surveillance.

BIBLIOGRAPHY

[1] E. Risberg, *A History of the Finnish Telegraph Administration 1855-1955*, General Direction of Posts and Telecommunication, 1955.

[2] A. G. Bell, "Apparatus for signalling and communicating, called Photophone," *U.S. Patent 235199*, Aug., 1880.

[3] D. Hondros and P. Debye, "Elektromagnetische wellen an dielectrischen draehten," *Ann. Phys.*, Vol 32, pp. 465-476, 1910.

[4] K. C. Kao and G. A. Hocklam, "Dielectric-fiber surface waveguides for optical frequencies," *Proc. IEE*, Vol 113, pp. 1151-1158, July, 1966.

[5] F. P. Kapron, D. B. Keck, and R. D. Maurer, "Radiation loses in glass optical waveguides," *Appl. Phys. Lett.*, Vol 17, pp. 423-425, Nov., 1970.

[6] T. Li, "Advances in optical fiber communications: An historical perspective," *IEEE J. Selected Areas in Comm.*, Vol SAC-1, pp. 356-372, April, 1983.

[7] H. Ishio, "Japanese field trials and applications in telephony," *IEEE J. Selected Areas in Comm.*, Vol SAC-1, pp. 404-412, April, 1983.

[8] E. Iwahashi, "Trends in long-wavelength single-mode transmission systems and demonstrations in Japan," *IEEE J. Quant. Elect.*, Vol QE-17, pp. 890-896, June, 1981.

[9] A. Moncalvo and F. Tosco, "European field trials and early applications in telephony," *IEEE J. Selected Areas in Comm.* Vol SAC-1, pp. 398-403, April, 1983.

[10] P. Matthijsse, "Essential data on optical fibre systems installed in various countries," *ITU*

Telecomm. J., Vol 12, pp.141-143, Feb., 1982.

[11] J. S. Cook and O.I. Szentesi, "North American field trials and early applications in telephony," *IEEE J. Selected Areas in Comm.*, Vol SAC-1, pp. 393-397, April, 1983.

[12] P. H. Chouinard et al, "Description and performance review of the Yorkville integrated serices fiber optic trial,"*Proc. Intnl. Conf. Comm.*, p. 28.3, June, 1979.

[13] J. R. Stauffer, "FT3C-A lightwave system for metropolitan and intercity applications," *IEEE J. Selected Areas in Comm.*, Vol SAC-1, pp. 413-419, April, 1983.

[14] J. W. Toy and C.R. Patisaul, "FT-4 trunking system field experiences" *Intnl. Conf. Comm.*, June, 1982.

[15] K. Nakagawa, "Second -generation trunk transmission technology," *IEEE J. Selected Areas in Comm.*, Vol SAC-1, pp. 387-393, April, 1983.

[16] P. H. Krawarik et al., "A winter olympic lightwave system," *Proc. FOC*, pp. 75-76, September, 1980.

[17] D. A. Pinnow, "Fiber optics for CATV trunking and subscriber distribution in the U. S., *Conf. on Opt. Fiber Comm.*, pp. 85-86, March, 1983.

[18] A. C. Deichmiller, "Progress in fibre optics transmission systems for cable television," *IEEE Trans. CATV*, Vol CATV-5, pp. 50-59, April, 1980.

[19] Optical Spectra News, "Fiber optics comes to big-city CATV," *Optical Spectra*, Vol 15, pp. 40-42,August, 1981.

[20] K. Y. Chang and E. H. Hara, "Fiber-optic broad-band integrated distribution Elie and beyond," *IEEE J. on Selected Areas in Comm.*, Vol SAC-1, pp. 439-444, April, 1983.

[21] J. Kanzow, "BIGFON: preparation for the use of optical fiber technology in the local network of the Deutsche Bundespost," *IEEE J. on Selected Areas in Comm.*, Vol SAC-1, pp. 436-439, April, 1983.

[22] K. Sakurai and Asatani, "A review of broad-band fiber system activity in Japan," *IEEE J. on Selected Areas in Comm.*, Vol SAC-1, pp. 428-435, April, 1983.

[23] M. Wenyon, "Pulse-frequency modulation for broad-band transmission", *Laser Focus*, Vol 17, pp. 170-173, June, 1981.

[24] M. Nyquil, "The wired city of Biarritz," *Optical Spectra*, Vol 15, pp. 38-40, August, 1981.

[25] G. Lentiez, "The fibering of Biarritz," *Laser Focus*, Vol 17, pp. 125-128, November, 1981.

[26] R. M. Dorward, "Aspect of the quantization noise associated with the digital coding of color-television signals," *Elec. Lett.*, Vol 6, pp. 5-7, January 8, 1970.

[27] L. Veerhoeven, "More aspect of quantisation noise asssociated with digital coding of color-television signals," *Elec. Lett.*, Vol 9, pp. 69-70, February, 8, 1973.

[28] G. Morgensen, "An overview of broad-band systems - applications and tradeoffs," *IEEE J. on Selected Areas in Comm.*, Vol SAC-1, pp. 420-427, April, 1983.

[29] G. Morgensen, "TV-Transmission on optical fibres," *13th Intnl. TV Symp.*, Montreaux, May 28-June 2, 1983.

[30] G. Morgensen, "Review, wide-band optical fibre local distribution systems," *Optical and Quantum Elec.*, Vol 12, pp. 353-381, September, 1980.

[31] A. Netravali and J. O. Limb, "Picture coding, a

review," *Proc. IEEE*, Vol 68, pp. 366-406, March, 1980.

[32] P. B. Lyons et. al, "Applications of optical fibers to analog telemetry delay lines and sensing systems," *IEEE J. on Selected Areas in Comm.*, Vol SAC-1, pp. 555-561, April, 1983.

[33] H. Melchior, "Optical-fiber multichannel video transmission using analog modulation and lasers with low noise and signal distortions," *4th Intnl. Conf. on Integrated Optics and Opt. Fiber Comm.*, pp. 324-325, Tokyo, 1983.

[34] A. Mainguy, "Fiber optic analogue video transmission for broadband distribution systems, *Department of Communications Report*, 1981.

[35] H. P. Berger et. al., "Multichannel TV-transmission over graded index fibers using analog modulation with low distortion and low noise," *7th European Conf. on Opt. Comm.*, pp. 16.3-1 to 16.3-4, September, 1981.

[36] K. Nagano et. al., "Optimizing optical transmitter and receiver for transmitting multi-channel broadcasting TV signals using laser diodes," *5th European Conf. on Opt. Comm.*, pp. 13.1-1 to 13.1-4, 1979.

[37] C. Baack et. al., "Analogue optical transmission of 26 TV signals," *Elect. Lett.*, Vol 15, pp. 300-301, May, 1979.

[38] T, Asai et. al., "VHF multichannel TV transmission using multimode fibers," *6th European Conf. on Opt. Comm.*, pp. 402-405, September, 1980.

[39] K. Asatani et. al., "Feasibility experiments on analog video transmission using a semiconductor laser diode," *5th European Conf. on Opt. Comm.*, pp. 16.8-1 to 16.8-4, September, 1979.

[40] K. Ito et. al., "Optical fiber transmission of ITV video signal by analog baseband modulation of laser

diodes," *5th European Conf. on Opt. Comm.*, pp. 16.9-1 to 16.9-4, September, 1979.

[41] O. I. Szentesi, "Fiber optic analog video transmission," *Proc. FOC*, pp. 144-148, September, 1979.

[42] H. B. Kim and J. Conradi, "A long wavelength LED based multichannel video transmission system using FM," *BNR Report*, 1981.

[43] T. T. Tjhung et. al., "Anaalogue optical link for multichannel frequency modulated television transmission," *Elec. Lett.*, Vol 19, pp. 106-107, February, 1983.

[44] F. P. Kapron et. al., *Introduction to Optical Communications*, BNR class notes., pp. 85-86.

[45] T. D. Michaelis, "Laser diode evaluation for optical analog link," *IEEE Trans. CATV*, Vol CATV-4, pp. 30-42, January, 1979.

[46] K. Petermann, "Nonlinear distortions and noise in optical communication systems due to fiber connectrors," *IEEE J. on Quantum Elec.*, Vol QE-16, pp. 761-770, July, 1980.

[47] K. Sato et. al., "Speckle noise reduction in fiber optic analog video transmission using semiconductor laser diodes," *IEEE Trans. Comm.*, Vol COM-29, pp. 1017-1024, 1981.

[48] K. Kikushima et. al., "Properties of harmonic distortion of laser diodes with reflected waves," *J. Opt. Comm.*, Vol 3, pp. 129-132, 1982.

[49] D. Kato, "Suppression of light feedback from an optical fiber into a diode laser," *Opt. Comm.*, Vol 26, pp. 335-338, 1978.

[50] K. Kobayashi et. al., "Unstable horizontal transverse modes and their stabilization with a new stripe structure," *IEEE J. Quantum Elec.*, Vol

QE-13, pp. 687-691, August, 1977.

[51] R. W. Dixon et. al., "Improved light-output linearity in stripe geometry double heterostructure AlGaAs lasers," *Appl. Phys. Lett.*, Vol 29, pp. 372-374, 1976.

[52] T. L. Paoli, "Non linearities in the emission characteristics of stripe geometry AlGaAs double-heterostructure junction lasers," *IEEE J. Quantum Elect.*, Vol QE-12, p. 770, 1976.

[53] W. T. Tsang et. al., "High power fundamental transverse-mode strip buried heterostructure lasers with linear light-current characteristics," *Appl. Phys. Lett.*, Vol 32, p. 311, 1978.

[54] G. H. B. Thompson et. al., "Deep Zn-diffused GaAlAs heterostructure stripe laser with twin transverse junctions for low threshold and kinkfree light characteristics," *IEEE J. Quantum Electron.*, Vol QE-15, p. 772-775, 1979.

[55] K. Asatani, "Nonlinearity and compensation of semiconductor laser diodes for analog intensity modulation systems," *IEEE Trans. Comm.*, Vol COM-28, pp. 297-300, February, 1980.

[56] M. Sekita, T. Kawamura, K. Ito, S. Fujita, M. IShii and V. Mirjake, "TV video transmission by analog baseband modulation of 1.3 um-band laser diode," *6th European Conf. Opt. Comm.*, pp. 394-396, York, 1980.

[57] Y. Ueno and M. Kajitani, "Color TV transmission using light emitting diodes," *NEC Res. Dev.*, No. 35, pp. 15-20, 1974.

[58] M. Nakamura, T. TAmura, and T. Ozeki, "Elimination of laser noise and distortion induced by reflected waves," *3rd Intnl. Conf. on Integrated Optics and Opt. Fiber Comm.*, pp. 34-35, San Fransisco, 1981.

[59] J. Strauss, A. J. Springthorpe, and O. I. Szentesi, Phase shift modulation technique for the

linearisation of analog optical transmitters," *Elec. Lett.*, Vol 13, pp. 149-150, March, 1977.

[60] R. W. Dawson, "Shunt diode extends linear range of LED," *Electronics*, Vol 50, pp. 119-120, November 10, 1977.

[61] K. Asatani and T. Kimura, "Linearisation of LED nonlinearity by predistortions," *IEEE Trans. Elec. Dev.*, Vol ED-25, pp. 207-212, February, 1978.

[62] K. Asatani and T. Kimura, "Nonlinear distortions and their compensations of light emitting diodes," *Intnl. Conf. on Integrated optics and Optical Fiber Comm.*, Tokyo, Japan, July, 1977.

[63] K. Asatani and T. Kimura, "Nonlinear phase distortion and its compensation in LED direct modulation," *Electron. Lett.*, Vol. 13, pp. 158-159, 1977.

[64] R. E. Patterson, J. Strauss, G. Blenman, and T. Witkowicz, "Linearisation of multichannel analog optical transmitters by quasi-feedforward compensation technique," *IEEE Trans. Comm.*, Vol-COM 27, pp. 582-588, March, 1979.

[65] J. Strauss and O. I. Szentesi, "Linearisation of optical transmitters by a quasifeedforward compensation technique," *Elect. Lett.*, Vol 13, pp. 158-159, 1977.

[66] H. S. Black, *U. S. Patent 1686792*, issued October 9, 1929.

[67] M. Bertelsmeier and W. Zschunke, "Linearisation of light emitting and laser diodes for analog broadband applications by adaptive predistortions," *4th Intnl. Conf. on Integrated Optics and Opt. Fiber Comm.*, pp. 378-379, June, 1983.

[68] Bell Telephone Laboratories, *Transmission Systems for Communications*, Western Electric Company Technical Publications, 1971.

[69] Y. Suematsu and K. Iga, *Introduction to Optical Fiber Communications*, John Wiley & Sons, New York, 1982.

[70] C. P. Sandbank, *Optical Fibre Communication Systems*, John Wiley & Sons, Chichester, 1980.

[71] C. K. Kuo, *Optical Fiber Systems*, McGraw-Hill, New York, 1982.

[72] H. Kressel and J. K. Butler, *Semiconductor Lasers and Heterostructure LEDs*, Academic Press, New York, 1977.

[73] H. Kressel: Editor, *Semiconductor Devices for Optical Communications*, Vol 39, Springer-Verlag, New York, 1980.

[74] G. H. B. Thompson, *Physics of Semiconductor Laser Devices*, John Wiley & Sons, Chichester, 1980.

[75] N. G. Basor, O. N. Kroklin and Y. M. Popov, "Production of negative temperature states in p-n junctions of degenerate semiconductors," *Sov. Phys. JETP*, 13, 1961.

[76] T. E. Bell, "Single frequency semiconductor lasers," *IEEE Spectrum*, Vol 20, pp. 38-45, December, 1983.

[77] K. Aiki et. al., "Transverse mode stabilized AlGaAs injection lasers with channeled substrate planar structures," *IEEE J. Quant. Elect.*, Vol QE-14, p. 89, 1978.

[78] D. Botez, "Single mode cw operation of "double-dovetailed" constricted dh (AlGa)As diode lasers," *Appl. Phys. Lett.*, Vol 33, pp. 872-874, November 1978.

[79] D. R. Scrifres et. al., "GaAs/GaAlAs diode lasers with angled pumping stripes," *IEEE J. Quant. Elec.*, Vol QE-14, pp. 223-227, April, 1978.

[80] G. H. B. Thompson et. al., "Kinks in the light/current characteristics and near field shifts in GaAlAs heterostructure stripe lasers and their explanation by the effect of self focusing on a built-in waveguide," *Solid State and Elec. Dev.*, Vol 2, pp. 12-30, January, 1978.

[81] N. Chinone, "Nonlinearity in power output-current characteristics of stripe-geometry lasers," *J. Appl. Phys.*, Vol 48, pp. 3237-3243, August, 1977.

[82] K. Stubkjaer and M. Danielson, "Nonlinearities of GaAlAs lasers -harmonic distortion," *IEEE J. Quant. Elec.*, QE-16, pp. 531-537, May, 1980.

[83] K. Asatani and T. Kimura, "Analysis of LED nonlinear distortions," *IEEE Trans. on Elec. Dev.*, ED-25, pp. 199-206, February, 1978.

[84] K. Stubkjaer, "Nonlinearity of dh GaAlAs lasers" *Elec. Lett.*, Vol 15, pp. 61-63, 1979.

[85] M. Maeda et. al., "Harmonic distortion in semiconductor injection lasers," *Proc. of 3rd European Conf. on Opt. Comm.*, pp. 120-122, 1977.

[86] T. Hong et. al., "Harmonic characteristics of laser diodes," *J. Opt. Comm.*, Vol 3, pp. 42-48, 1982.

[87] K. Asatani and T. Kimura, "Linearisation of LED nonlinearity by predistortions," *IEEE J. Solid State Circuits*, Vol SSC-13, pp. 133-138, February, 1978.

[88] K. Stubkjaer, "Distortion of light signals transmitted via multimode graded-index fibres," *Elec. Lett.*, Vol 15, pp. 797-799, November, 1979.

[89] M. Ettenberg and H. Kressel, "The reliability of (AlGa)As CW laser diodes," *IEEE J. Quant. Elec.*, Vol QE-16, pp. 186-196, February, 1980.

[90] A.R. Goodwin and R.G. Plumb, "Life testing of diode laser sources: A case study," *Laser Focus*, pp.

111-114, March, 1983.

[91] M. Dixon and B.A. Dean, "Aging of the light-current characteristic of proton-bombarded AlGaAs lasers operated at 30°C in pulsed conditions," *Intl. Conf. on Integrated Optics and Optical Fiber Comm.*, pp. 36-37, 1981.

[92] H. Kressel et al., "Accelerated step temperature aging of AlGaAs heterostructure laser diodes," *Appl. Phys. Lett.*, Vol 32, pp. 305-308, March, 1978.

[93] F.S. Chen, "Simultaneous feedback control of bias and modulation currents for injection lasers," *Elec. Lett.*, Vol 16, pp. 7-8, 1980.

[94] D.W. Smith and M.R. Matthews, "Laser transmitter design for optical fiber systems," *IEEE J. Selected Areas in Comm.*, Vol SAC-1, pp. 515-523, April, 1983.

APPENDIX I-IM DISTORTION VERSUS LD BIAS CURRENT

```
C ######################################################################
C THIS PROGRAM COMPUTES THE IM DISTORTIONS FOR LD BIAS
C CURRENTS OF 70, 84, 88, 92, AND 96 mA FOR A CONSTANT
C LD MODULATION CURRENT OF 4 mA P-P. THE SINGLE
C POLYNOMIAL MODEL IS USED.
C ######################################################################
C INITIALIZE THE PARAMETERS OF THE SUBROUTINE RLFOR.
      INTEGER N,IX,MDP(3)/4,4,0/,IB/7/,IER,
     #CUR(5)/70,84,88,92,96/
      N=9
      IX=9
      REAL XYW(9,7),RSQ/100./,ALPB(2)/2*0.05/,ANOVA(13),B(7,12)
      DOUBLE PRECISION WK(36)
C######################################################################
C READ IN (X,Y) VALUES.
      READ(5,100) (XYW(I,1),I=1,N)
100   FORMAT(10F8.5)
      DO 10 I=1,N
 10   XYW(I,3)=1.
      DO 20 J=1,5
      READ(5,100) (XYW(I,2),I=1,N)
C ######################################################################
C CALCULATE THE BEST FITTING POLYNOMIAL CURVE.
      CALL RLFOR(XYW,IX,N,RSQ,MDP,ALPB,ANOVA,B,IB,PRED,IP,WK,IER)
      WRITE(6,200)
200   FORMAT(55('#'))
      WRITE(6,300) CUR(J)
300   FORMAT('THE BEST FITTING POLYNOMIAL CURVE IN A ',
     #'NEIGHBORHOOD OF',/,'THE POINT I=',I2,' mA IS: ')
      WRITE(6,400) B(5,2),B(1,2),B(2,2),B(3,2),B(4,2)
400   FORMAT('Y  =  (',F7.4,')  +  (',F7.4,') X  +  (',F9.6,
     #') X**2',/,T6,'+ (',F9.6,') X**3  +  (',F10.7,
     #') X**4')
C ######################################################################
C CALCULATE THE INTERMODULATION DISTORTIONS.
      R2=20*ALOG10(ABS(B(2,2)/B(1,2)))
      R3=20*ALOG10(ABS(3*B(3,2)/(4.*B(1,2))))
      WRITE(6,500) R2
500   FORMAT('IM(F2-F1)  =  ',F5.1,
     #' DB   for a modulation of 4mA p-p.')
      WRITE(6,600) R3
600   FORMAT('IM(2*F2-F1)  =  ',F5.1,
     #' DB   for a modulation of 4mA p-p.')
      WRITE(6,200)
C ######################################################################
20    CONTINUE
      STOP
      END
C ######################################################################
```

```
C ######################################################################
C INPUT DATA FOR ABOVE PROGRAM.
C
-2.,-1.5,-1.,-.5,0.,.5,1.,1.5,2.,
-.032,-.0280,-.020,-.0120,0.,.0140,.029,.0945,.160,
-.262,-.1965,-.131,-.0665,0.,.0615,.123,.1815,.24,
-.218,-.1615,-.105,-.0525,0.,.0490,.098,.1455,.193,
-.182,-.1365,-.091,-.0455,0.,.0420,.084,.123,.162,
-.145,-.110,-.070,-.0355,0.,.0350,.068,.105,.139,
##########################################################
C OUTPUT OF THE COMPUTER PROGRAM.
C
THE BEST FITTING POLYNOMIAL CURVE IN A NEIGHBORHOOD OF
THE POINT I=70 mA IS:

Y  =  (-0.0028)  +  ( 0.0229) X  +  ( 0.011050) X**2
   + ( 0.006461) X**3  +  ( 0.0014662) X**4

IM(F2-F1)  =   -6.3 DB   for a modulation of 4mA p-p.
IM(2*F2-F1)  =  -13.5 DB   for a modulation of 4mA p-p.
##########################################################
THE BEST FITTING POLYNOMIAL CURVE IN A NEIGHBORHOOD OF
THE POINT I=84 mA IS:

Y  =  (-0.0010)  +  ( 0.1274) X  +  (-0.003434) X**2
   + (-0.000485) X**3  +  ( 0.0002331) X**4

IM(F2-F1)  =  -31.4 DB   for a modulation of 4mA p-p.
IM(2*F2-F1)  =  -50.9 DB   for a modulation of 4mA p-p.
##########################################################
THE BEST FITTING POLYNOMIAL CURVE IN A NEIGHBORHOOD OF
THE POINT I=88 mA IS:

Y  =  (-0.0004)  +  ( 0.1014) X  +  (-0.003618) X**2
   + ( 0.000354) X**3  +  ( 0.0001469) X**4

IM(F2-F1)  =  -28.9 DB   for a modulation of 4mA p-p.
IM(2*F2-F1)  =  -51.6 DB   for a modulation of 4mA p-p.
##########################################################
THE BEST FITTING POLYNOMIAL CURVE IN A NEIGHBORHOOD OF
THE POINT I=92 mA IS:

Y  =  (-0.0006)  +  ( 0.0877) X  +  (-0.003272) X**2
   + (-0.000424) X**3  +  ( 0.0002284) X**4

IM(F2-F1)  =  -28.6 DB   for a modulation of 4mA p-p.
IM(2*F2-F1)  =  -48.8 DB   for a modulation of 4mA p-p.
##########################################################
THE BEST FITTING POLYNOMIAL CURVE IN A NEIGHBORHOOD OF
THE POINT I=96 mA IS:

Y  =  ( 0.0001)  +  ( 0.0701) X  +  (-0.001510) X**2
   + ( 0.000286) X**3  +  ( 0.0001795) X**4

IM(F2-F1)  =  -33.3 DB   for a modulation of 4mA p-p.
IM(2*F2-F1)  =  -50.3 DB   for a modulation of 4mA p-p.
##########################################################
```

APPENDIX II-POLYNOMIAL SPLINE MODEL

```
C ###################################################################
C THIS PROGRAM COMPUTES THE INTERMODULATION DISTORTIONS NEAR
C THE INFLECTION POINT AT 84 mA FOR A LD MODULATION CURRENT
C OF 4 mA P-P. THE POLYNOMIAL SPLINE MODEL IS USED.
C ###################################################################
C INITIALIZE THE PARAMETERS OF THE SUBROUTINE RLFOR.
      INTEGER N,IX,MDP(3)/2,2,0/,IB/5/,IER
      N=4
      IX=4
      REAL XYW(4,5),RSQ/100./,ALPB(2)/2*0.05/,ANOVA(13),B(5,12)
      DOUBLE PRECISION WK(16)
      REAL U(4),Z(4)
C ###################################################################
C READ IN (X,U) VALUES WHERE U = 0.131X - Y.
      READ(5,100) (XYW(I,1),I=1,N)
      READ(5,100) U
100   FORMAT(10F8.5)
      DO 10 I=1,N
      Z(I)=U(I)/(XYW(I,1)**2)
      XYW(I,2)=Z(I)
 10   XYW(I,3)=1.
C###################################################################
C FIND BEST FITTING POLYNOMIAL IN THE SUBLINEAR REGION.
      CALL RLFOR(XYW,IX,N,RSQ,MDP,ALPB,ANOVA,B,IB,PRED,IP,WK,IER)
      WRITE(6,200) B(3,2),B(1,2),B(2,2)
200   FORMAT('Y  =  (0.131) X  -  (',F9.6,') X**2  -  (',F9.6,
     #') X**3',/,T5,'-  (',F10.7,') X**4')
C ###################################################################
C CALCULATE INTERMODULATION DISTORTIONS.
      R2=20*ALOG10(ABS(B(3,2)/(2*0.131)))
      R3=20*ALOG10(ABS(3*B(1,2)/(8*0.131)))
      WRITE(6,300) R2
300   FORMAT('IM(F2-F1)  =  ',F5.1,' DB  + 20 LOG A')
      WRITE(6,400) R3
400   FORMAT('IM(2*F2-F1)  =  ',F5.1,' DB  + 40 LOG A')
C ###################################################################
      STOP
      END
C ###########################################################
C INPUT DATA FOR ABOVE PROGRAM.
C
0.5,1.,1.5,2.,
0.0010,.0055,.009,.022,
C ###########################################################
C OUTPUT OF THE COMPUTER PROGRAM.
C
Y  =  (0.131) X  -  ( 0.004000) X**2  -  ( 0.000600) X**3
   -  (-0.0000000) X**4

IM(F2-F1)  =  -36.3 DB  + 20 LOG A
IM(2*F2-F1)  =  -55.3 DB  + 40 LOG A
C ###########################################################
```

APPENDIX III-IM DISTORTION OF PREDISTORTED TRANSMITTER

```
C ######################################################################
C THIS PROGRAM COMPUTES THE IM DISTORTIONS FOR VARIOUS VALUES
C OF PREDISTORTION DRIVE CURRENTS. THE PREDISTORTION CURRENTS
C ARE THOSE CORRESPONDING TO EMITTER RESISTANCES OF Re = 60,
C 70, 85, 125, AND 185 OHMS. THE LD BIAS CURRENT IS 84 mA AND
C THE LD MODULATION IS 8 mA P-P.
C ######################################################################
C INITIALIZE THE PARAMETERS OF THE SUBROUTINE RLFOR.
      INTEGER N,IX,MDP(3)/2,2,0/,IB/5/,IER,RE(5)/60,70,85,125,185/
      N=8
      IX=8
      REAL XYW(8,5),RSQ/100./,ALPB(2)/2*0.05/,ANOVA(13),B(5,12)
      DOUBLE PRECISION WK(32)
      REAL U(8),Z(8)
C ######################################################################
C READ IN (X,U) VALUES WHERE U = 0.131X - Y.
      REAL X1(8)/.5,1.,1.5,2.,2.5,3.,3.5,4./
      DO 20 J=1,5
      READ(5,100) U
  100 FORMAT(10F8.5)
      DO 30 I=1,N
      XYW(I,1)=X1(I)
      Z(I)=U(I)/(XYW(I,1)**2)
      XYW(I,2)=Z(I)
   30 XYW(I,3)=1.
C ######################################################################
C CALCULATE THE INTERPOLATION POLYNOMIAL.
      CALL RLFOR(XYW,IX,N,RSQ,MDP,ALPB,ANOVA,B,IB,PRED,IP,WK,IER)
      WRITE(6,150)
  150 FORMAT(55('#'))
      WRITE(6,175) RE(J)
  175 FORMAT('THE INTERPOLATION POLYNOMIAL FOR THE COMPENSATED ',
     #'CHARACTERISTIC',/,'CORRESPONDING TO Re = ',I3,' OHMS IS:')
      WRITE(6,200) B(3,2),B(1,2),B(2,2)
  200 FORMAT('Y = (0.131) X - (',F9.6,') X**2 - (',F9.6,
     #') X**3',/,T5,'- (',F10.7,') X**4')
C ######################################################################
C CALCULATE INTERMODULATION DISTORTIONS.
      R2=20*ALOG10(ABS(B(3,2)/(2*0.131)))
      R3=20*ALOG10(ABS(3*B(1,2)/(8*0.131)))
      WRITE(6,300) R2
  300 FORMAT('IM(F2-F1) = ',F5.1,' DB + 20 LOG A')
      WRITE(6,400) R3
  400 FORMAT('IM(2*F2-F1) = ',F5.1,' DB + 40 LOG A')
C ######################################################################
   20 CONTINUE
      STOP
      END
C ######################################################################
```

```
C ########################################################
C INPUT DATA FOR COMPUTER PROGRAM>
C
.000,.002,.0030,.002,-.008,-.015,-.021,-.028,
.000,.002,.004,.003,-.005,-.010,-.015,-.020,
.000,.002,.0020,.0030,-.001,-.006,-.008,-.010,
.0001,.0028,.0030,.0050,.006,.007,.010,.015,
.0003,.0045,.0070,.0085,.0120,.018,.025,.033,
########################################################
C OUTPUT OF COMPUTER PROGRAM
C
C ########################################################
THE INTERPOLATION POLYNOMIAL FOR THE COMPENSATED CHARACTERISTIC
CORRESPONDING TO Re =  60 OHMS IS:

Y  =  (0.131) X  -  ( 0.001276) X**2  -  (-0.000234) X**3
   - (-0.0001682) X**4

IM(F2-F1)  =  -46.3 DB  + 20 LOG A
IM(2*F2-F1)  =  -63.5 DB  + 40 LOG A
########################################################
THE INTERPOLATION POLYNOMIAL FOR THE COMPENSATED CHARACTERISTIC
CORRESPONDING TO Re =  70 OHMS IS:

Y  =  (0.131) X  -  ( 0.001029) X**2  -  ( 0.000206) X**3
   - (-0.0002315) X**4

IM(F2-F1)  =  -48.1 DB  + 20 LOG A
IM(2*F2-F1)  =  -64.6 DB  + 40 LOG A
########################################################
THE INTERPOLATION POLYNOMIAL FOR THE COMPENSATED CHARACTERISTIC
CORRESPONDING TO Re =  85 OHMS IS:

Y  =  (0.131) X  -  ( 0.000842) X**2  -  ( 0.000159) X**3
   - (-0.0001582) X**4

IM(F2-F1)  =  -49.9 DB  + 20 LOG A
IM(2*F2-F1)  =  -66.8 DB  + 40 LOG A
########################################################
THE INTERPOLATION POLYNOMIAL FOR THE COMPENSATED CHARACTERISTIC
CORRESPONDING TO Re = 125 OHMS IS:

Y  =  (0.131) X  -  ( 0.001201) X**2  -  ( 0.000279) X**3
   - (-0.0001049) X**4

IM(F2-F1)  =  -46.8 DB  + 20 LOG A
IM(2*F2-F1)  =  -62.0 DB  + 40 LOG A
########################################################
THE INTERPOLATION POLYNOMIAL FOR THE COMPENSATED CHARACTERISTIC
CORRESPONDING TO Re = 185 OHMS IS:

Y  =  (0.131) X  -  ( 0.002343) X**2  -  ( 0.000429) X**3
   - (-0.0001471) X**4

IM(F2-F1)  =  -41.0 DB  + 20 LOG A
IM(2*F2-F1)  =  -58.2 DB  + 40 LOG A
C ########################################################
```